WEAR AND MICROSTRUCTURE OF EUTECTOID STEELS

Daniel Danks
B.Sc. California Polytechnic State University,
San Luis Obispo, 1982
M.S. Oregon Graduate Center, 1985

A dissertation submitted to the faculty
of the Oregon Graduate Center
in partial fulfillment of the
requirements for the degree
Doctor of Philosophy
in
Materials Science and Engineering

March 1989

The dissertation "Wear and Microstructure of Eutectoid Steels" by Daniel Danks has been examined and approved by the following Examination Committee:

Paul Clayton, Thesis Advisor
Professor

Roger K. Steele, Association of
American Railroads

S Shankar, Assistant Professor

John L. Johnsen, Adjunct Professor
Assistant Professor, University of Portland

Acknowledgements

Thanks are due first and foremost to Paul, whose exacting standards are exceeded only by his patience. Next I'd like to express appreciation to the rest of the thesis committee, Roger, Shankar and John, for their care and guidance. The people of the Association of American Railroads and the Facility for Accelerated Service Testing deserve acknowledgement for their expertise, material and financial support. Finally, thanks to all the people at the Center for their continuous encouragement and tolerance.

For Bugs, Doodie, Boogar, Miss Piggy and PJ.

Table of Contents

List of Tables

List of Figures

ABSTRACT

The interaction between a railroad vehicle wheel flange and the gauge face of the rail causes incredible amounts of material displacement and loss creating significant economic and safety ramifications for railroads. At the same time, inter-modal competition has reduced margins for profit, which in turn has promoted the use of higher tonnage vehicles. The final result is ever increasing rail deterioration rates as present rail metallurgical technology is pushed to its limits. To aggravate the problem, there is no simple method of evaluating potential rail steels for possible revenue use.

Several laboratory test procedures with two machines (Amsler twin disk and a pin-on-disk) were evaluated as simulations of the wheel flange/gauge face wear system. Test conditions involved non-lubricated, steel-on-steel, sliding and sliding/rolling wear. Based on relative wear rates, surface damage mechanisms and surface topographical features, the Amsler machine produced the best simulation with test conditions of high contact pressure and a high slide/roll ratio. The laboratory results were compared to accurately documented performances of four rail steels in trials conducted at the Transportation Test Center Facility for Accelerated Service Testing.

A complete range of pearlitic eutectoid microstructures was produced with isothermal heat treatments and their relative wear resistances ranked with the laboratory test procedure. Microstructures were judged based on pearlite interlamellar spacing, hardness and tensile strength. Relative wear resistances were judged according to

deformation and wear characteristics.

The wheel flange/gauge face wear mechanism was identified as one of third body abrasion, with the abrasive particles being rail and wheel debris carried into the contact zone, after being generated from previous encounters.

It was found that for the range of interlamellar spacings and hardnesses tested, 118 to 472 nm and 322 to 205 BHN respectively, both wear resistance and deformation resistance increased with reducing spacing. Wear rate/spacing relationships were developed based on the data generated. In addition it was confirmed that interlamellar spacing and hardness are closely related.

Introduction

JUSTIFICATION

Gauge face rail wear (Fig. 1) has always been a costly reality for railroads. As has been the case with most materials applications, rail is ultimately used for more severe conditions than it was originally designed for. This overuse accelerates the cost to maintain the lines as present rail technology is stretched to its limits. The objective of this program was, in a broad sense, to contribute to present rail wear understanding.

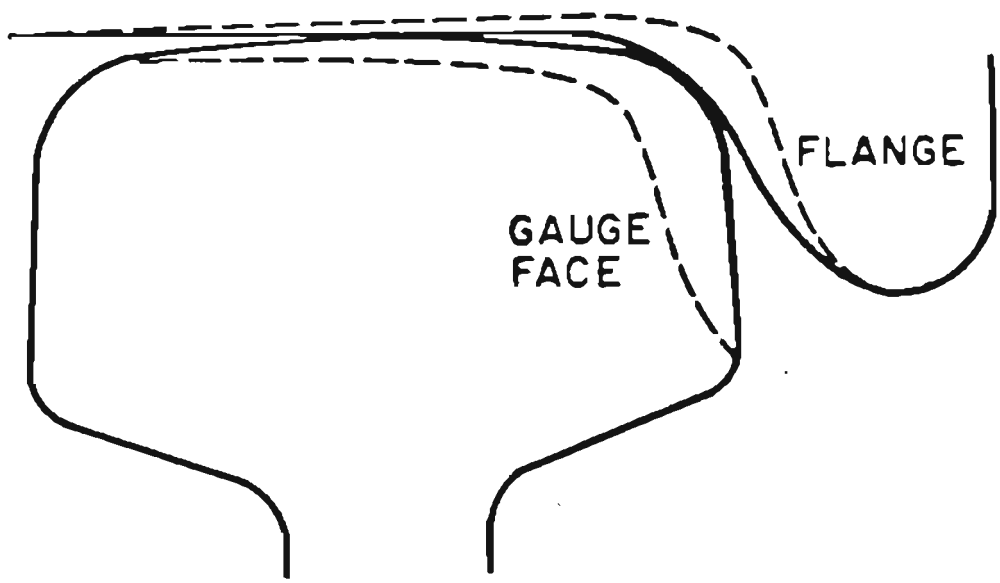

Figure 1. Schematic diagram of the wheel flange/rail gauge face contact zone. Broken lines indicate possible worn profiles.

In the past, several approaches have been used to improve rail performance. One was the upgrading of material, as in 1776 when the first all iron rail was made in Sheffield, England. [1] Then came a period of improved rail geometry with little change in materials. With the advent of steel, cast and wrought iron rails were outdated and replaced. Steel rails too have been subjected to numerous geometric re-configurations. [2] Recently improvements have taken the form of alloy additions and heat treatments. [3-4] With each improvement engineers have been convinced that the then present system had been perfected.

All rail improvements have been restricted by the economics of the times. Steel was available but not employed until after 1863 when the Bessemer steel making process reduced the cost to a level that was competitive with wrought iron rails. [5] Improved chemistries were not employed until alloy content could be economically justified.

Included in the economic considerations was the need to test new rails. Full scale, multi-year in-service trials are not only expensive, but are also subject to a host of variables and are potentially dangerous because of unpredictable failures. To avoid the in-service trial problems research is transferred to the laboratory, where several projects have been used to search for an accurate rail ranking procedure. As early as 1922, the famous Amsler twin disk wear and lubrication tester was first developed to replicate the wheel/rail interaction. [6] In Canada a one-eighth scale test machine has been developed that uses specimens taken from actual rail and wheel and subjects them to a situation similar to that found in the rail/wheel interaction. [7]

Recent work at British Rail has used a pin-on-ring machine to develop a carbon equivalent equation that has been successfully used to predict rail life. [8] In Japan, a full-size test rig has been constructed and is undergoing evaluation. This machine spins two full sized horizontally oriented wheels against a circle of rail. [9]

A laboratory procedure, however, is useless until there is substantive data from a service environment that validates the laboratory data. This need has been addressed with a full scale test facility built by the Department of Transportation (DOT) in Pueblo, Colorado. The Facility for Accelerated Service Testing (FAST) initially consisted of a 8 km (5 mile) loop on which a 9100 Million Gross Ton (MGT) train completes approximately 100 laps per day. [10] But due to the costs of such a project, an accurate rail steel ranking laboratory test is still important.

Laboratory projects have met with a variety of success with each exhibiting strengths and weaknesses. An example of a test strong point would be specimens that are machined from actual rails and wheels. In this manner material differences are one variable removed from the comparison. Disadvantages usually incorporate elements that are common to the real world situations like size, complexity and ultimately, cost. The laboratory procedure developed in this project was a relatively simple one that provides a link to the closely documented conditions at FAST. Two different machines were considered possible candidates for the laboratory duplication of gauge face/wheel flange contact. Both a pin-on-disk machine and an Amsler machine were investigated, again with varying success, from poor with results

wrought with more questions than answers, to exceptionally good with extremely close correlation to the closely documented, full-scale field results. A unique aspect of the pin/disk testing was the range of loads involved. For example, Welsh was restricted to loads below 3 kg (6 lb) [11] and Clayton tested between 70 and 200 kg (155 - 440 lb). [8] The present pin/disk machine is capable of a complete range of loads from 3 to 271 kg (6 - 600 lb).

Another aspect of this rail investigation project was concerned with microstructural influences on rail performance. As mentioned previously, improvements have been made with both alloy additions and heat treatments. What has not been clearly defined are some of the individual influences of the two factors. For example, although it is possible to obtain like pearlite lamellae spacing with both methods, the bias of each has not been separated, if indeed it is possible to isolate them. Do the alloy additions only provide a second means of obtaining the final pearlite spacings and therefore mechanical properties, or do they provide a significant secondary benefit? References discussing relative benefits are available from those industries that use pearlitic steels, most notably the rail industry [4] and the wire drawing community. [12] These references, however, found limitations of either heat treatments and resorted to alloying or vice versa, again thinking that the systems had been fully investigated. Pearlitic steel, of which most rail is made today, is still very attractive because of its many advantages and the extensive amount of work done with it. It was hoped that the wear properties could be further enhanced through an improved understanding of wear mechanisms and

relations to physical characteristics.

Today, commercially produced rail chemistries include a standard carbon steel rail, a class of Improved Strength (IS) standard carbon rails, and several "premium" rails with combinations of higher chromium, molybdenum and silicon. Because of the additional costs of the premium rails, they are usually reserved for more severe wear locations like high tonnage lines and curves.

Heat treated rails, either hardened throughout or head hardened, exist in the range up to 38 Rc (352 BHN) hardness. The rail (and wheel) heat treating has generally consisted of a relatively modest quench of air or liquid to produce harder yet fully pearlitic structures from the austenitic hot working microstructures. [2] The wear resistance of these rails appears to be many times superior to non-heat treated rail. The formation of bainite is usually avoided due to lack of experience with this microstructure in heavy haul service and the fear that impact toughness might suffer.

BACKGROUND

The metallurgy of rail wear requires homework in two primary areas. The first concerns the specific steel that makes up the vast majority of rail and wheel in existence today, pearlitic eutectoid steel. Though rails include many variations of pearlite derived from heat treatment and chemical composition modifications, the predominant microstructure remains pearlitic. The second issue is that body of information that deals with the wear of metals and, in particular, rail steel.

Pearlite

Pearlite, or "pearly" constituent, is the name originally given by Sorby in 1864 to the lamellar structure of the iron-iron carbon eutectoid because of its mother-of-pearl appearance under an optical microscope. [13] The term can be used to describe an alloy of any system whose microstructure takes the form of alternating plates or rods of different compositions, but for this report pearlite will be restricted to that lamellar eutectoid structure of iron and iron carbide found in the iron rich steel alloy system. Pearlite actually consists of alternating plates of a saturated solution of less than .025 weight % carbon in alpha iron and an intermetallic compound, iron carbide, with 6.67 wt. % carbon, designated Fe_3C. The overall structure, if truly eutectoid, is .83 wt. % carbon remainder iron, with the width of the cementite plate averaging one-seventh that of the alpha iron due

to the relative amounts and densities of iron and carbon.

Pearlite is formed in a eutectoid reaction from a high temperature solution of carbon in gamma iron, called austenite, that exists between the temperatures of 723 °C (1333 °F) and 1491 °C (2715 °F) at carbon weight percents up to 1.7%. The eutectoid reaction is a nucleation and growth process, and in this system, generally agreed to be nucleation saturated, meaning that growth is rate controlling in the process, not nucleation. [14-15] Nucleation sites are normally on prior austenite grain boundaries but sometimes at imperfections or impurities inside the austenite grain itself. There are multiple nucleation sites per austenite grain, so one former austenite grain is transformed into several pearlite nodules with various lamellae orientations. There are two theories regarding the actual eutectoid transformation that describe the diffusion of the elements during the austenite-pearlite reaction. One is termed volume diffusion and contends that carbon diffusion takes place prior to the transformation front and that this diffusion rate (carbon in gamma iron) is the growth rate controlling mechanism for a given set of conditions. [16] The other theory of transformation, boundary diffusion, maintains that carbon diffusion and segregation occurs right at the gamma-to-alpha iron transformation interface. [17] And, though most scholars agree with the volume diffusion theory, there are still some experimental variations that need to be explained if it is indeed correct.

It has been shown by several researchers that the rate of pearlite growth is directly related to the interlamellar spacing of the final structure. [18-20] Since important mechanical properties are controlled

by plate spacing, those factors that influence the rate of transformation are of practical importance. The longer the transformation event, the farther the carbon diffuses resulting in more and more segregation or wider plates. There are two major determinants in the kinetics of the transformation: temperature and chemical composition. It is not possible to completely separate these two because, for example, chemical composition changes alter the transformation temperature. (In this discussion the phrase "transformation temperature" will be used to describe the temperature a material of given composition should transform under equilibrium conditions while "temperature of transformation" will be used to designate the temperature of the material bulk at the time of transformation. These two temperatures are usually not equal.) For a set chemical composition, the time to transform will decrease for increasing difference between the transformation temperature and the actual temperature of transformation. Restated, lower temperatures will result in greater temperature difference and driving forces, and therefore faster transformations and finer pearlite spacings.

Elements other than iron and carbon have two effects on the system. The first, as previously mentioned, is that they change the equilibrium transformation or critical temperature of the alloy. This means that for a given temperature of transformation and different alloying elements, greater driving forces can exist, modifying the rate of transformation and final structure. The second is that they change (usually decrease) the diffusion rates of other elements, especially carbon, in the iron matrix. Secondary effects of alloying elements, such as precipitation hardening also affect final mechanical properties,

but for the present discussion they will be separated from the pearlite spacing effects.

Strong carbide forming elements like chromium (Cr), manganese (Mn) and molybdenum (Mo) tend to partition to the carbide lamellae while ferrite stabilizers, cobalt (Co), silicon (Si) and nickel (Ni) will migrate to the alpha plates. This partitioning effect, called solute drag, will also modify to a lesser degree the transformation rates. It is possible, however, to complete the transformation below the "partitioning temperature" and freeze most substitutional alloying elements in metastable positions.

WEAR FUNDAMENTALS

Certain concepts exist in the study of wear that are relevant to the present discussion. The concepts include a wide range of ideas that help or attempt to explain phenomena researchers have observed. Everything from experimental techniques to conceptual models and predictive equations can be included in this list. Following is a directed catalog of those most pertinent to this work.

Machines and Methods

Although the field of tribology can be positively identified as far back as 1900 B.C., (Fig. 2) [21], advances in experimental methods have not proliferated until the last three or so decades. Wear testing machines cover a wide range of sizes, types and configurations. But research and technology have progressed hand in hand; advances developed in research and perfected in manufacturing are fed back into the research loop and result in better precision.

A common method of classifying wear machines is by specimen configuration. Pin on disk, pin on ring and pin on drum are examples of a type of machine that runs a pin, usually less than 2.5 cm (1 inch) diameter against a rotating plate, ring or cylinder. An advantage of this type of machine is the wide array of wear environments that can be simulated. The two major components, the pin and mating disk, ring or cylinder, can be made of any number of similar or dissimilar materials. The cylinder can be covered with an abrasive paper if the interest is

in abrasive rather than metal against metal wear. This type of machine can be almost any size, from table top models with coin sized specimens to large stand alone rigs that are capable of 3000 Newtons (675 pounds) or more load. Other wear machine configurations include crossed cylinder, disk on disk, ring on ring like the Amsler machine, and scratch testers that reduce the wear incident to one event. Finally, a wide array of specifically designed machines exist that attempt to reproduce one particular wear system and are dedicated to that one task.

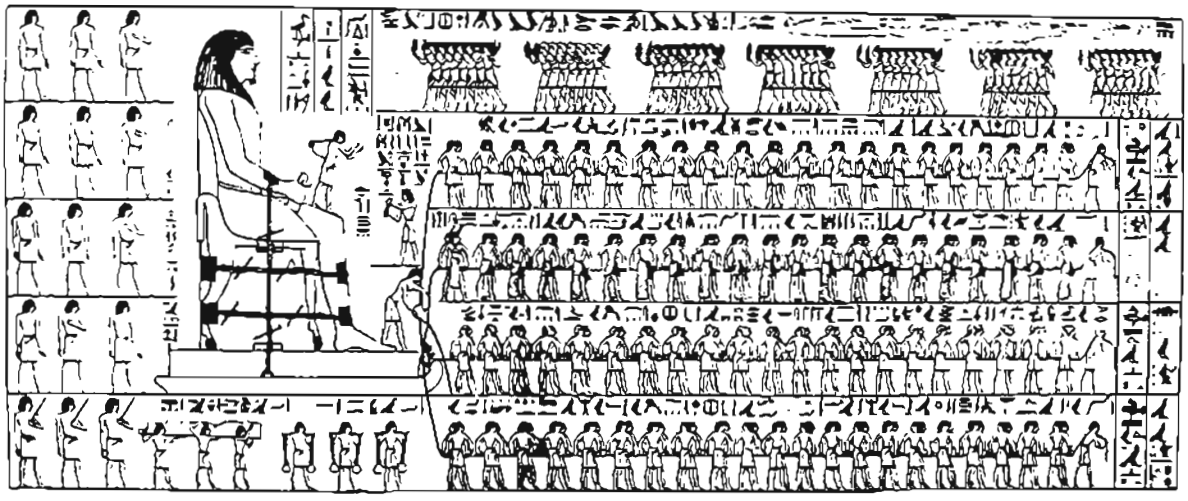

Figure 2. An early record of a tribologist on the job. Note the lubrication engineer riding on the front of the statue sled applying lubricant to the sliding path.

Other tools commonly used in wear research are those machines and techniques that provide characterization of the materials encountered. All types of microscopy, optical (OM), scanning electron (SEM) and transmission electron (TEM) are employed to examine and identify original materials and conditions, final surface states and nature of fractured particles. Suh [22] used the TEM to develop the delamination theory of wear by observing dislocation densities and crack behavior in various layers of material both at and near the surface. Precision sectioning, used in this project and described later, examination of wear debris, and reconstruction of events via material response, i.e. transformation products as indicators of elevated temperatures, can all be utilized.

Because wear of materials is for the most part a surface circumstance, there are many techniques used to quantify surface encounters. Radioactive isotope tracing and electrical resistance provide measurements of true contact areas, dynamic contact conditions and material transfer to and from the parent mass. Force measurements furnish information for friction calculations which are essential in determining types and degrees of bonding and interlocking between surfaces and asperities on the surfaces.

Wear Types

The philosophy "Ad Nomen Est Nostra" or "To Name is to Know," has evoked a collection of terms for the types of surface interactions observed. Numerous authors have through the years offered their views on the most efficient ways to categorize different wear mechanisms and

the list now includes adhesion, abrasion, corrosion, surface fatigue, erosion, cavitation, oxidative, delamination, non-adhesive, and adhesive/non-adhesive. Though this list is not all inclusive, one quickly concludes that consensus is not universal.

General agreement does exist, however, regarding a few of what can be called major wear types. Archard and Hirst [23] offered two primary types, adhesion and abrasion, with adhesion resulting in higher weight loss rates than the abrasion. This model is based on the adhesion making up the "run in" wear rate, and the abrasion the "steady state." Another article by the same authors [24] divided wear further into a mild regime and a severe regime. The adhesion or run in portion are the initial stages and consist of metal to metal contact and "self machining" of both parts. Once the parts have self machined to a custom fit, the debris trapped in the contact zone cause the abrasion segment of the process. In both publications the authors state the need to come to grips with the role of debris in all wear modes.

Kerridge and Lancaster [25] attempted to do just that and agreed debris formation is a two step process. The first involves material being transferred from the parent component to the mating one, and then the transferred layer is broken free by subsequent passes of the two bodies.

Sheasby [26] took the idea one step farther by attempting to eliminate any generated debris from the wear environment and concluded that if indeed the debris can be excluded, the overall wear rates will decrease between one and four orders of magnitude.

Richardson [27-28] conducted a comprehensive study of debris

characteristics and their influence on the wear process. Debris and adjacent material hardnesses were the primary variables in the investigation that developed relative wear resistances for many combinations of hard and soft materials and abrasives.

Debris is important not only in the wear process itself, but also as a tool in the characterization of that process. It is one of the most useful pieces of evidence produced. Many researches have analyzed the particles of actual failures or simulated situations to deduce after the fact what mechanisms are predominating.

Deformation and Fracture

Although any wear process can be reduced to its simplest elements, deformation of material and eventual fracture, in each individual case the degree of deformation and the degree of fracture to cause failure present vastly different absolute values of material loss. In some cases plastic material flow alone is sufficient grounds for failure of a component. And, because deformation is so prevalent in wear, it has received much attention. There are many aspects of deformation that are relevant. First and foremost is the amount of deformation that is possible. While those values of strain that are cited for example, in tensile testing, are in the range of .25 or .5, strains exceeding 7 have been measured [29] on highly worn surfaces. At strains of that magnitude the question may be asked, "Can the material be considered the same as the original?" Certainly the chemical composition would be the same because no material is necessarily added or lost to any significant depth, but with strains > 7 is it possible that the atomic

order is disturbed to a degree that the original structure is completely lost? This is often the type of structure that the tribologist has to deal with.

Some materials tend predictably to change structure when subjected to these higher strains. Metastable austenite is a common example that can be induced to transform to martensite under suitable strain. This transformation is exploited in many austenitic materials that transform while the part is in service. This strategy not only provides a continuously regenerating hard surface, but also a tough impact resistant sub-surface.

Even materials that cannot transform to harder phases can resist deformation by work hardening mechanisms. Along with deformation comes a reduction in ductility and an increase in hardness and tensile strength. In some situations this strength increase is a significant factor in reducing wear rates and this effect can be used as an engineering tool as a wear resistance enhancer.

Classical dislocation theory was the basis for Suh's [22] delamination wear mechanism. It states that surface stresses generate dislocation motion and pile ups until a crack is formed some finite distance below the surface. Under continued stress the crack grows and results in flaking or delamination of small debris particles. Several authors [30-32] have found that there is a pattern of dislocation layers at or near the surface. At the immediate surface there is usually a dislocation free zone, attributed to the ability of the dislocations to escape the free surface. Directly below is a layer with high dislocation densities due to the stress levels which are always higher some finite distance

below the surface and the fact that the dislocations are pinned and cannot escape to the surface.

One of the more difficult aspects of wear to deal with both predictively and post-failure is the presence of wear transitions. A wear transition can be defined as a non-continuous change in wear rate with a small change in some pertinent parameter such as load. Stress or strain of the surface layers often results in material response that causes such a discontinuous change in wear behavior. Examples of transitions exist for many combinations of materials and wear types. Welsh [11, 33-34] found transitions that increased wear rates by four fold. An explanation of this behavior states that the surface condition can be such that certain loads can be supported to a critical level, after which the surface layers are quickly damaged and removed. For example, if the surface work hardens, it would be better able to support loads higher than non-worked material. Welsh also submits that when an oxide layer is present in combination with a strong substrate, that the combination will provide protection for the component. Clayton [8] also observed a transition in pin/ring testing of a steel system between the loads of 70 kg (155 lbs) and 200 kg (450 lbs). Friction induced high flash temperatures have also been credited with transformation products located on surfaces that also provide protection with hardnesses higher than the base material.

Predictive Relationships

The natural progression of research tends to be away from stone engravings toward predictive mathematical models. Although tribology has not advanced to the point where all wear influences can be entered into an equation, there have been attempts to produce predictive relationships of wear rates as a function of load, friction, material. Of the more famous is Archard's wear equation [35]

$$W = KP/3H$$

where

W = wear rate

K = probability of removing a particle

P = load

H = hardness

And, although this relationship between wear and applied load does sometimes produce substantive results, its applications are limited due to the wide assortment of wear environmental parameters. A primary goal of this project was the development of a method to predict relative wear resistances of various rail alloys from laboratory testing.

Pearlite Deformation and Fracture

Research directed toward wear of pearlitic materials takes many forms. Much of the most applicable work addresses the deformation and fracture modes of the material without specific reference to a wear mechanism. Several authors treat pearlite as a very effective composite and discuss deformation in terms of dislocation motion in the two phases. Rosenfield [36] concluded that Fe_3C plates are effective dislocation barriers, and any stress buildup must be enough to cleave the cementite. Gensamer et al. [37] suggested that mechanical properties are related to the mean free path of a dislocation in the continuous phase, in this case ferrite, which is related to an average length and width of the plates. This agrees well with the idea that narrower spacing, and therefore shorter mean free dislocation paths, produce high yield strengths and better wear resistance.

Pickering [38] elaborated on the idea by showing that the distances dislocations move in the ferrite plates are short. Consequently, strain can only be accommodated by an increased number of dislocations, quickly exhausting soft sources, activating hard ones, and resulting in rapidly increasing work hardening.

Concentrating more on the actual deformation, Puttick [39] determined that favorably oriented colonies yield by slip parallel to the lamellae. In colonies where orientation does not permit this, fine slip begins in the ferrite and general yield occurs by accumulation of fine slip at structure imperfections. This produces large shear strains which may be accommodated by deformation of ferrite, cementite

and the ferrite-cementite interface. Cracks are initiated, one of which grows to a critical size, followed by fracture. This work also showed that the initiation of fracture of pearlitic steel, at least at room temperatures, is not associated with the two phases in any simple way, such as parting at the cementite/ferrite interface, but usually takes place at several types of locations.

Alexander and Bernstein [40] described a combination of ductile microvoid coalescence and brittle fracture. Microvoid coalescence occurs in both ferrite and cementite lamellae, followed by brittle fracture across the entire prior austenite grain once a void has reached a critical size. Finer pearlite spacing in this case would delay the arrival of the critical crack, while a smaller prior austenitic grain size would reduce the brittle crack length. This explanation agrees with the widely held idea that spacing controls yield strength while grain size controls impact properties.

Pickering [41] performed microscopy on strained pearlite and determined that cementite plates are not as brittle as originally thought. In addition, thinner cementite plates can deform more than thicker plates, absorbing significant amounts of deformation before cracking actually starts. In all, Pickering listed three types of cementite deformation: 1) plastic deformation as evidenced by blurring of diffraction patterns, 2) slip and shear of the plate as evidenced by discontinuous steps on plate edges, and 3) brittle cracking. He then concluded that all three of these lead to dislocations in ferrite and bulk deformation.

Puttick [39] agreed with Pickering that cementite in fact appears

to be able to accommodate shear displacements of up to a micron or more without fracture. A limited amount of interfacial slip can occur between the ferrite and cementite phases and such relative movement might nucleate slip in the ferrite at the sharp step projections of the slipped cementite.

A study on pearlite interlamellar spacing was performed by Shen [42] who employed crossed cylinder wear testing of 1078, 1070, 1060, 1045, 1018, and 1008 steels under a load of 10 N and a speed of 4.2 cm/sec, all in an argon atmosphere. The various chemistries and heat treatments provided a variety of pearlite volume fractions and lamellae spacings. The primary conclusion was that smaller interlamellar spacing and increased pearlite volume fraction decreased wear. Lamellae direction, however, had the greatest affect on wear rates, reducing them by a factor of ten when oriented perpendicular to the sliding direction.

Beagley conducted tests [43] of rail steel on an Amsler wear testing machine. From the data he made three dimensional graphs of wear rate and slide/roll ratio and contact stress. He noted two distinct wear regimes, mild and severe, with the mild producing shiny surfaces and debris that was 80% oxide, and 20% metal. The severe regime generated matted gray surfaces and all metal debris. Beagley theorized that the severe wear was a fatigue failure, caused by repeated deformation of the surfaces.

Bhattacharyya [44] also recognized interlamellar spacing/wear rate relationships with pin/ring testing of 1018, 1040, 1095 steels and loads between 1.11 and 267 N (0 to 60 lbs). He found that below a

certain pearlite interlamellar spacing (less than 300 nm), the load that caused a mild to severe wear transition increased dramatically. Or, if the lamellae spacing was small enough, there was a significant improvement in wear resistance. His explanation: if the cementite plates are spaced closely they carry the applied load and the wear will be reduced. Spherodized steels did not display this effect.

From Clayton's [8] pin/disk tests, performed with 14 different heats of steel under 75 to 200 kg load, relationships were developed between wear and the mean ferrite path (average distance a dislocation can travel without encountering an obstacle), tensile strength, and a chemical composition term. Of notable significance is the ability to predict wear rates from the laboratory generated data.

Salesky's microscopy study [32] of pearlite, bainite and martensite specimens subjected to sliding wear supported previous findings. He found thin surface layers, sometimes recovered, adjacent to zones with high dislocation densities, and a distinct boundary between the two. A more practical observation, related to pearlite lamellae spacing, was the absence of large undeformable particles which appeared to be a key to improved wear resistance, reinforcing the theory that finely distributed hard phases can effectively carry the load and improve wear resistance.

How does all this pearlite information relate to rails? Can any of this information be applied to rail? The rail suffers a spectrum of damage from rolling mill new to unrecognizably altered, so at some point the laboratory conditions are encountered. In the past, many of

these basic ideas have lead to the use of finely spaced pearlite to produce much improved wear properties. What remains is to refine the test methods and better define the wear/property relationships.

Experimental

WORN RAIL EXAMINATION

A detailed rail gauge face examination was performed to determine the exact nature of the gauge face wear process. The four rails examined were obtained from the Facility for Accelerated Testing (FAST) in Pueblo, Colorado. The rail had been in service for 76.5 MGT of unlubricated wear in the high rail of section 07 (Fig. 3). Most of the information extracted from this examination came from the chromium-molybdenum rail #310618-42-WWR (X31) though the gauge face of the other three FAST rails appeared similar.

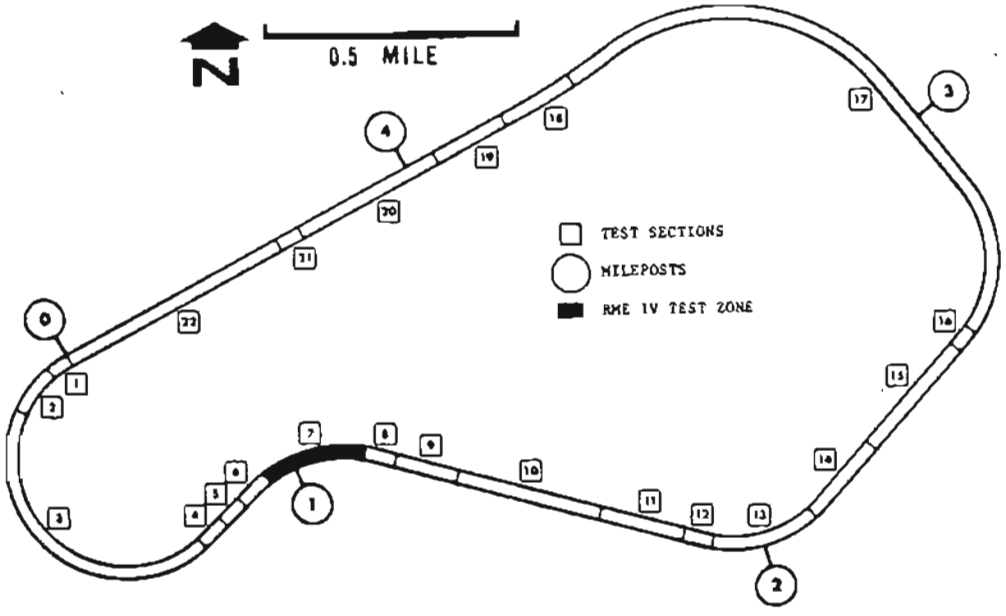

Figure 3. Map of the Facility for Accelerated Service Testing (FAST) in Pueblo, Colorado.

Cleaning

The FAST rail was cleaned with soapy water and a soft bristle brush, followed by a methanol rinse. More drastic cleaning measures tended to remove critical details.

Worn Surface Examination

Three stages of photography were used to provide positive surface feature documentation. The first was a 35 mm macro-photograph of the wear surfaces after cleaning and prior to sectioning. This recorded the overall appearance of the surfaces and provided a map of features for later use. Care was taken to record the exact location of each frame.

After sectioning, the surface features were photographed at higher magnifications. This was done in a scanning electron microscope (SEM) at an approximate magnification of 10X. The 35 mm pictures were used to provided location information of the SEM photograph areas. These higher magnification photographs permitted detailed surface feature comparison.

The third photographic record was an optical microscopy (OM) cross sectional view of individual surface features. Since cross sections were taken through precisely located surface features, sub-surface characteristics could be related directly to the surface.

The critical aspect of the metallography was the ability to grind into a specimen that was nickel plated and mounted for good edge retention to a specific surface feature. This was accomplished with a custom designed and built metallography specimen grinding fixture that

permitted grinding a precise distance into a metallographic specimen. The fixture consisted of a donut shaped body that held a 1 1/4" (32 mm) specimen mount and an inner threaded cylinder that progressed into the body exactly .125" (3.175 mm) with each complete turn of the cylinder. The mounted specimen was pushed out of the bottom of the fixture body by the inner cylinder. Since the distance from the specimen edge to the feature of interest had been measured, it was possible to set the specimen protuberance that distance beyond the fixture base and grind until the base contacted the grinding surface, which also coincided with the feature's center. This exposed cross sections of areas that had been documented precisely from the surface.

The cross sections were polished and etched with 2% Nital, and photographed in the standard manner on an optical microscope.

A complete listing of all materials and their chemical compositions and hardnesses can be found in Table I, page 47.

PIN/DISK TESTING

Pin/Disk Machine

The pin on disk wear machine consists of a base, a central column, and a pivoting beam which supports a specimen chuck, loading weights, and a counterweight (Fig. 4). A variable speed motor is housed in the base directly below the rotating disk.

The machine's overall dimensions, including the beam, are 81 cm (32 inches) wide, 193 cm (76 inches) long, and 178 cm (70 inches) high. The base of the machine is 81 cm (32 inches) wide, 168 cm (66 inches) long, and 122 cm (44 inches) high. The central column is located mid-width in the base, 46 cm (18 inches) from one end. It supports the beam 53 cm (21 inches) above the base's top surface.

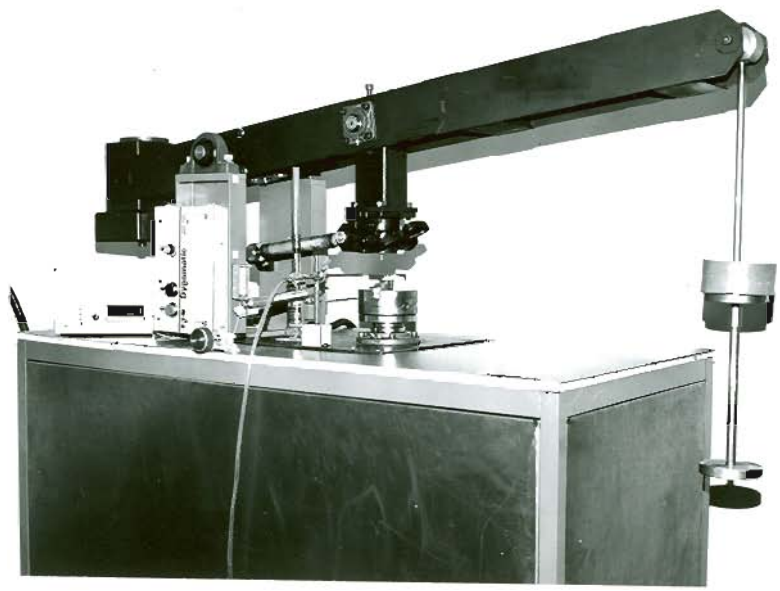

Figure 4. Pin-on-disk machine.

The beam, 16.5 cm (6.5 inches) wide, 13 cm (5 inches) high, and 193 cm (76 inches) long, supports three components. On one end, 46 cm (18 inches) from the central column, is a 77 kg (170 pound) counterweight. This counterweight balances the beam. Mounted 46 cm (18 inches) on the other side of the column is the specimen holder. It is a quick release chuck with a maximum capacity of 2.5 cm (1 inch). The weights used to load the specimen are hung from a pan located at the end of the beam on the same side of the column as the specimen holder, 91 cm (36 inches) from the specimen holder and 137 cm (54 inches) from the central column.

The disk chuck, either three or four jawed, is located directly below the specimen holder and driven through two bearings by a 7.5 HP, 3 phase, 60 cycle, 1750 RPM Eaton Dynamatic Ajusto Spede motor. The motor is mounted vertically inside the base and has an integral 45 volt DC clutch, capable of producing disk speeds from approximately 70 to 1700 RPM.

Other machine capacities are: maximum specimen diameter, 2.5 cm (1 inch); maximum specimen length, 23 cm (9 inches); maximum applied load, 91 kg (200 pounds) in the weight pan (equivalent to 273 kg (600 pounds) on the specimen), and maximum wear track diameter, 21 cm (8.25 inches).

Instrumentation

Two test parameters are instrumented. The first is the amount of wear (length) a specimen suffers. This is measured with a Linear Voltage Displacement Transformer (LVDT) attached to the bottom of the counterweight on the end of the beam. Since the counterweight is the same distance from the central column (but opposite side) as the

specimen holder, the specimen length is read directly by the LVDT.

The second test parameter recorded is the number of rotations of the disk. This is done with an optical sensor located next to the motor shaft and a reflective plate mounted on the shaft that passes in close proximity to the sensor. Each disk rotation is detected and then recorded by the computer.

The heart of the data system is an Apple IIe computer. It has been equipped with a data I/O board through which the various test parameters are passed to the computer. The compatible software collects the data, stores it on a floppy diskette, draws a wear vs. travel distance curve during the test (real time), computes such values as wear rate in mm^3/cm sliding after the test, and recalls and re-plots the test data as required.

Pin/Disk Machine Modification

The original pin/disk machine design had one thrust bearing located below the disk chuck and above the motor. Under some more arduous testing conditions (high loads and low speeds) there was a problem with excessive disk vibration. In analyzing the source of the machine vibrations it was determined that the thrust bearing supporting the disk chuck was acting as a fulcrum between the motor/shaft flexible coupling and the specimen chuck. The pin sliding on the disk produces lateral forces on the chuck, and because there was only one bearing in the shaft connecting the motor flexible coupling and the disk chuck (Fig. 5), there was little lateral restraint on the disk. The final result was lateral motion of the disk and a slip/stick

interaction between the pin and disk which was manifested as pin vibration.

To correct the problem the motor was moved approximately 30 cm (12 inches) lower and a second bearing was installed between the motor and the original bearing. The second bearing provided a second restraint point on the shaft and minimized the lateral play at the disk chuck. In addition, the pin chuck's horizontal restraining arm was improved by increasing its size and making the mechanical joints more rigid.

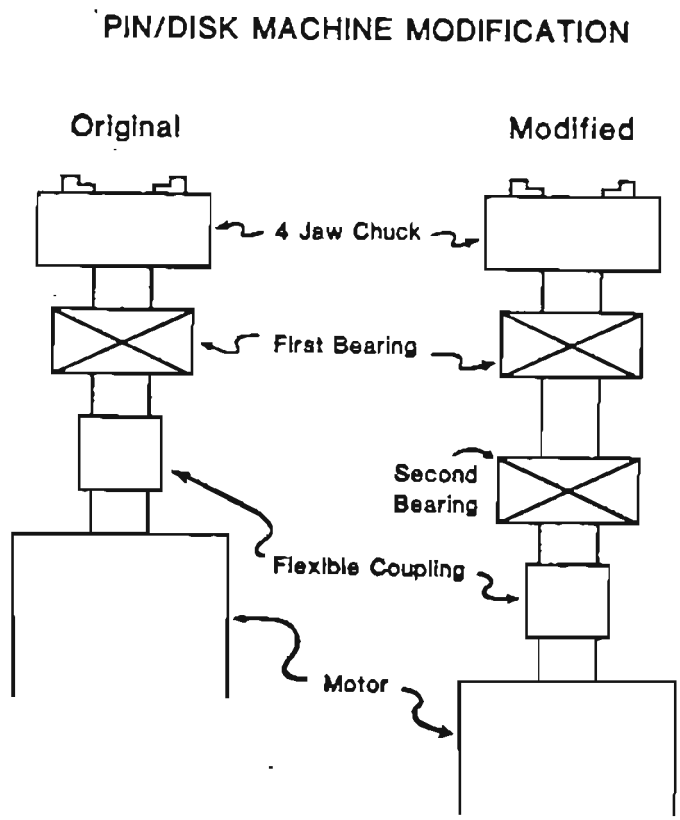

Figure 5. Pin/disk machine drive shaft modification. A second bearing was added in the drive line to prevent lateral disk movement.

Standard Carbon Test Series

Six mm (1/4 inch) diameter pins were machined from the head of standard carbon rail steel with the pin length parallel to the rail running direction. Wheel steel, 12 mm (1/2") thick was used for the disks. The rail and wheel chemistries are listed in Table II.

Table II

Pin/disk Standard Carbon Series Materials
Hardness and Chemical Composition

	Hardness Rc (BHN)	Chemical Composition (Wt. %) C	Cr	Mo	Mn	Si	S	P	Cu	Ni	V
Std. C Pin-Disk Pins (Rail X21)	22 (236)	.75	.02	.02	.98	.25	.03	.04	.07	.09	.004
Disks (Wheel W3)	22 (236)	.66	.04	.01	.68	.53	.02	.002	.09	.03	.009

Prior to testing, the pins and disks were washed with soapy water and rinsed with acetone. Tests were run with 3 to 271 kg applied pin load using a 45 mm diameter wear path. Disk speed was 70 RPM, resulting in a relative sliding velocity of 16.5 cm/sec. Exactly 12.7 cm (1/2 inch) of the pin was allowed to protrude from the specimen chuck at the start of all the tests. Dry compressed air was directed onto the contact zone to minimize bulk temperature effects. Because this series was performed prior to the completion of the computer data collection system, pin wear was measured by periodic weighing. From the weight loss and travel distance a volume loss per sliding distance (mm^3/cm) was calculated and plotted as a function of applied load.

The first standard carbon rail test series produced wear data that

raised the question of the influence of the vibration or rigidity of the test rig. A second series, utilizing the same procedures as the first series, was run to analyze vibration effects on the machine.

Vibration Test

The results of the first standard carbon test series suggested that the pin/disk machine compliance might be affecting wear rates. The possibility was considered that vibration might influence the test conditions such that wear rates were altered independent of other test conditions. An experiment was conducted to confirm or deny the relationship between vibration and applied load.

The vibration was checked with a piezoelectric accelerometer. The accelerometer generates a voltage when accelerated in a particular direction, and since the specimen vibration was in question, the accelerometer was mounted on the specimen chuck. The accelerometer signal was routed through an appropriate amplifier into a Sony-Tek digital storage oscilloscope. Wear tests were run with loads from 9 kg to 180 kg, with peak and mean acceleration signals recorded along with the wear data.

Modified Machine Series

After the first vibration series had been run and analyzed, modifications outlined in the Machine Modification section were deemed appropriate and made. To test the improved design, another series of wear tests, identical to the first series, was performed. 6 mm (1/4") diameter pins were machined from the same standard carbon rail stock

with the pin axis parallel to the rails rolling direction as before. They were installed in the pin chuck with 12.7 mm (1/2 inch) stick out. The pins were run against the same standard carbon disks used in the first series after the disks had been resurfaced. Resurfacing consisted of removing the previous wear path with a six bit shell mill and then surface grinding the disk with an 80 grit wheel on an automatic surface grinding machine. As before, the wear path was 45 mm diameter and the disk speed averaged 70 rpm resulting in a sliding speed of 16.5 cm/sec. The pins were cooled with a jet of dried compressed air.

The test data was collected and recorded by the computer system and included pin length and volume loss, disk revolutions, sliding distance and test time. Pins were weighed before and after the test as a check of the computer data.

To check the vibration characteristics of the machine the piezo-electric accelerometer, amplifier, and oscilloscope used in the first vibration tests were re-used. The accelerometer was attached to the specimen chuck in the same location as before and the peak-to-peak vibration voltages were recorded approximately mid-way through each test. For two of the tests vibration records were taken every 1 second for the duration of the entire test. This was done to check for any trends in the vibration characteristics over the course of a single test.

AMSLER TWIN ROLLER TESTING

Amsler Twin Disk Rolling/Sliding Machine

Twin disk testing was carried out with an Amsler rolling/sliding contact rig (Fig. 6). The Amsler machine has two horizontal and

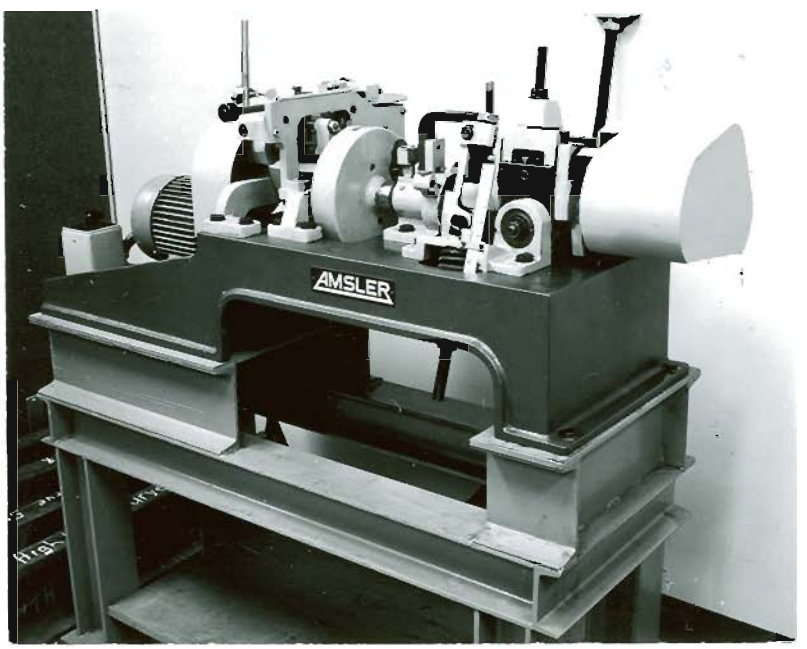

Figure 6. Amsler twin roller wear and lubrication test machine.

parallel shafts, with the lower turning 1.104 times faster than the upper. The slide/roll ratio, δ, or amount of slip between the rollers, can be calculated from

$$\delta = \frac{2(1.104d_2 - d_1)}{d_1 + 1.104d_2}$$

where d_1 and d_2 are the diameters of the upper and lower rollers respectively. The load is controlled by a coil spring, and the contact

pressure can be calculated using the Hertzian contact formula

$$P_o = 0.418(LE/R)^{1/2}$$

where P_o is the maximum contact pressure, E is Young's modulus, $1/R = 1/R_1 + 1/R_2$, where R_1 and R_2 are the roller radii, and L is the load per unit contact width. All tests were run with a contact width of 5mm.

Standard Carbon Series

Upper Amsler rollers were machined from the same standard carbon rail used for the pin/disk experiments with all the roller axes parallel to the rail length. The rail steel rollers were always 35 mm (1.4 inches) in diameter with an overall width of 10 mm (.4 inches) and a contact width of 5 mm (.2 inches).

The lower rollers were machined from a class U wheel with the rollers' central axes parallel to a tangent on the wheel circumference. Chemistries and hardnesses of both wheel and rail specimens are listed in Table III.

Table III.
Amsler Standard Carbon Series Material Hardness
Chemical Composition

	Hardness	Chemical Composition (Wt. %)									
	Rc (BHN)	C	Cr	Mo	Mn	Si	S	P	Cu	Ni	V
Std. C Amsler Series Upper Rollers (Rail X21)	22 (236)	.75	.02	.02	.98	.25	.03	.04	.07	.09	.004
Lower Rollers (Wheel W1)	22 (236)	.77	.08	.04	.66	.33	.04	.03	.08	.08	.005

The test matrix consisted of 1% to 35% slide/roll ratios and 500 to 1280 N/mm^2 contact pressure, Table IV. The tests were run without lubrication but with dried air directed onto the rollers to minimize heating effects. The rollers were cleaned with soap and water and rinsed with methanol at the test start. Roller wear rates were measured by periodically removing the rollers from the machine and weighing them.

Table IV
Amsler Standard Carbon Series Test Matrix

	Slide/Roll Ratio						
	1	3	5	7	10	25	35
Contact Pressure (N/mm^2)	1280 1140 1080	1280 1140 900 700	1280 1080 900 700	1280 1140 1080 900 800 700 600	1280 1140 1080 1040 900 800 700 600	1080 900 700 500	1080 900 700 500

FAST Rail Series

After the first Amsler series, it was determined that best revenue track simulation was obtained at the highest slide/roll ratios and all the remaining wear tests were performed at 35% and with contact pressures of 500, 700, 900, 1080, and 1220 N/mm^2. Specimens were machined from the four FAST rails which included a standard carbon, two chromium/molybdenum, and a manganese/silicon/chromium/vanadium.

The rail rollers were run against 45.15 mm diameter Class U wheel

rollers. The chemical composition of all four rails and the wheel are listed in Table V. In all cases the rollers were 10 mm wide with a contact width of 5 mm.

Table V
Amsler FAST Series Materials Hardness
and Chemical Composition

	Hardness Rc (BHN)	Chemical Composition (Wt. %) C	Cr	Mo	Mn	Si	S	P	Cu	Ni	V
Upper Rollers Rail X29 (Std. C)	27 (265)	.72	.02	.01	.97	.21	.02	.005	.14	.06	.002
Rail X30 (MnSiCrV)	33 (311)	.67	.82	.02	.93	.61	.02	.005	.04	.06	.14
Rail X31 (CrMo)	36 (336)	.73	.70	.24	.67	.27	.02	.005	.02	.02	.002
Rail X32 (CrMo)	34 (320)	.71	.55	.21	.61	.29	.02	.005	.25	.10	.002
Lower Rollers (Wheel W1)	22 (236)	.77	.08	.04	.66	.33	.04	.03	.08	.08	.005

The rollers were washed, rinsed with methanol and weighed. They were then installed on the Amsler shafts, the wheel on the bottom shaft, the rail on the upper. After the Amsler was run at slow speed (200 RPM) for a set number of revolutions, the rollers were removed and reweighed. They were always handled with cotton gloves to prevent contaminating the wearing surfaces.

Data recorded were the weight loss and revolutions, and, when possible, the work in Newton-meters as recorded by the work integrator on the Amsler. At contact pressures of 1220 and 1080 N/mm^2, however,

the frictional force between the rollers produced torque that was greater than the integrator could record. Wear rates were calculated by linear regression analysis of the weight loss/revolutions data.

Heat Treated Rail Series

Heat Treating

Two rail chemistries, one standard carbon ("A" series) and the other a CrMo ("B" series), Table VI, were heat treated to obtain a variety of pearlite spacings. The materials were first rough machined from the head of an appropriate rail in approximately 30 cm (12 inch) long segments. They were then austenitized at 816 ^{o}C (1500 ^{o}F) for one hour. Both the temperature and time were selected to insure consistent austenite and avoid significant grain growth.

Table VI
Amsler Heat Treated Series Material Hardness and Chemical Composition

	Hardness Rc (BHN)	Chemical Composition (Wt. %) C	Cr	Mo	Mn	Si	S	P	Cu	Ni	V
Upper Rollers Rail X34 (CrMo)	33 (311)	.71	.57	.21	.88	.41	.02	.005	.26	.10	.002
Rail X35 (IS. C)	26 (258)	.63	.14	.05	.88	.17	.01	.005	.29	.13	.002
Lower Rollers Wheel W2	32 (297)	.70	.02	.001	.72	.53	.02	.03	.05	.03	.005

The bars were removed from the austenitizing furnace and immediately immersed in a salt bath maintained at temperatures between 682 °C (1260 °F) and 516 °C (905 °F) depending on the desired spacing. The salt

bath temperature was determined with a chrome alumel thermocouple and digital thermometer. An exact schedule of the heat treatments is contained in Table VII.

Table VII
Heat Treatment Schedule

Sample Designation	Isothermal Quench Temperature °C	(°F)	Soak Time (Hours)
Standard Carbon			
A3	604	(1120)	.5
A4	626	(1158)	1
A5	669	(1237)	21
A6	655	(1211)	1
A7	196	(385)	3.5
Chromium-Molybdenum			
B1	485	(905)	.75
B3	597	(1106)	3.6
B4	659	(1218)	1.5
B5	715	(1319)	46
B6	705	(1300)	24
B7	650	(1202)	2

[Note: all bars austenitized for 1 hour at 816 °C (1500 °F).]

Isothermal transformation times varied from 30 minutes to 46 hours [45]. The bars were taken from the salt bath and final machined into Amsler rollers and tensile bars. The sectioning plan is shown in Fig. 7. The bars were labelled and care was taken to insure that the

specimens were removed from the end of the bar opposite the end that had been grasped with tongs for transfer to and from the furnace and salt pot. This minimized variation in pearlite spacing from roller to roller from the same heat treatment. Prior to final machining hardness surveys were performed along the length of the heat treated bars to prove consistency. In addition, hardness tests were taken on the sides of the individual rollers after final machining and before wear testing to again confirm the consistency of the heat treatments along the length of the entire bar. The final check, of course, was the actual pearlite spacing counts performed after the wear tests were concluded.

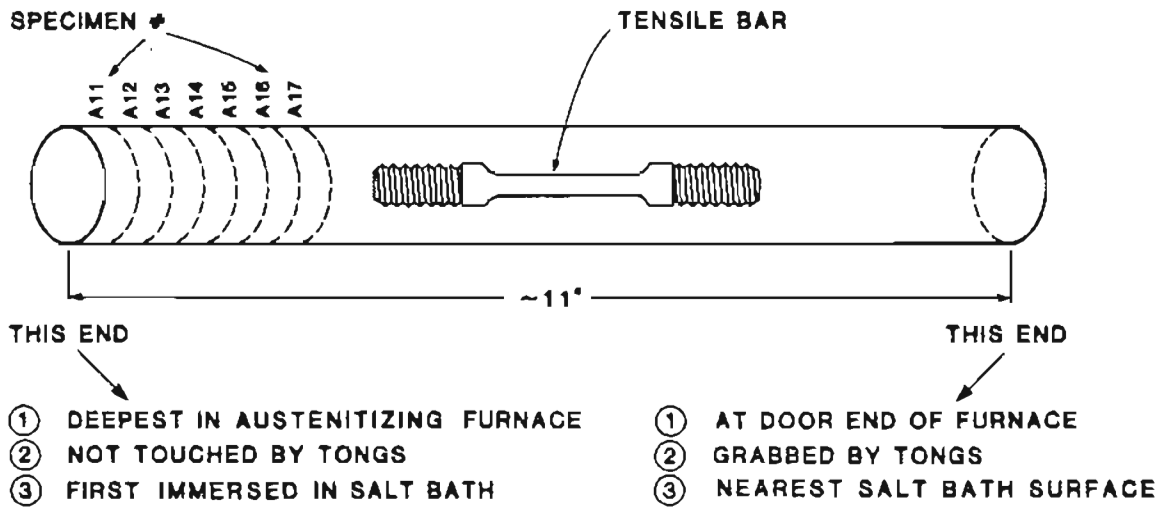

Figure 7. Heat treated bars sectioning plan, bar A1.

To check the consistency of the final interlamellar spacing, measurements were taken on five rollers of heat treatments B1 and A3. In addition, spacing measurements were taken in four quadrants of roller A5 to verify spacing consistency in a single roller. Hardness

tests were performed on all rollers for each heat treatment whether the spacings were measured or not.

Wear tests were conducted in the manner described in the FAST Rail Series, page 37, at 35% slide/roll ratio, no lubrication, air cooling and 500, 700, 900, 1080, and 1220 N/mm^2 contact pressures.

Repeatability Testing

To examine the ability of the Amsler wear tests to repeat nominally identical tests, two sets of wear tests were run, one at 900 N/mm^2 (6 individual tests), and the other at 1220 N/mm^2 (seven tests). Upper Amsler rollers were machined from the old standard carbon rail (X21), and the lower rollers were taken from Class C wheel (W2) stock.

Initial Surface Damage

Two experiments directed toward the initial damage experienced by a roller surface under the rolling/sliding contact were performed. The first examined the weight loss in the initial stages of surface break down and consisted of removing the rollers and weighing them every 10 revolutions for the first 100 revolutions of a 500 revolutions test (specimen A7, 1080 N/mm^2 contact pressure). The second was involved in determining the first incidence of abrasion on the roller surfaces. This test was performed by running the rollers against each other for very short intervals, less than 10 revolutions, and removing and examining them for any groove formation or abrasive particle damage until one such region was found and documented.

Deformation Testing

Material limitations allowed only the heat treated rollers to be subjected to deformation tests which were conducted on the Amsler rig. These tests used 35.0 mm diameter rollers of the same material on both the upper and lower shafts. They were loaded to 1330 N/mm^2 and run at 400 revolutions per minute (RPM) under fully lubricated conditions. To obtain full lubrication, 5 drops of lubricant were deposited on the rollers. The rollers were periodically stopped, de-greased and measured. Roller diameter and contact width were determined by averaging three measurements of each from around the circumference.

During the deformation tests the Amsler machine was set up to provide lateral oscillation of the specimens such that the upper roller moved 3 mm to the left and right of the lower roller centerline once in approximately three seconds.

PEARLITE LAMELLAE SPACING MEASUREMENTS

Pearlite measurements were conducted in accordance with the method outlined by VanderVoort and Roosz [46]. Because the resolution of an optical microscope is not great enough for most of the pearlite spacings, an SEM was used for the line-intercept counts. This necessitated exact SEM magnification calibrations. These were determined with the aid of two microhardness indentations made on the surface of the polished and etched specimen. The distance between the two indentations was accurately determined by calibrating a projected scale in an optical microscope with respect to a grid standard. Then the specimens were transferred to the SEM where the distance between the microhardness indentations were measured on the SEM screen. From two measurements an accurate magnification factor was calculated.

For the line intercept counts a 10 cm diameter circle was placed onto the SEM screen and intercepts of carbide lamellae and the circle for a minimum of ten different pearlite fields were counted. Care was taken to move the specimen in a set pattern between the fields to remove as much bias from the field selection as possible. The SEM magnification was selected to provide as many intersections per field as possible while keeping the 10 cm circle inside the majority of the pearlite nodes. Once the optimum magnification had been determined for a particular specimen it was not changed. The average number of intercepts of the ten fields was used to calculate the mean true

spacing, S, by

$$S = (\pi d/M/n)(.5)$$

where d is the circle diameter, M is the magnification, and n is the average number of intercepts of the lamellae and circle.

The spacing confidence interval values were calculated by performing a student t test on the standard deviation of the average of n, the number of intercepts, and then transferring that confidence interval to the spacing width measurement values.

HARDNESS TESTING

All hardness tests were performed with an appropriate Rockwell hardness scale and converted to other types for comparison. Although it is recognized that Rockwell C Scale (Rc) hardness values less than 20 are inexact, they are included for quick reference along with other, more accurate scales.

Table I

Summary of Materials Hardness and Chemical Composition

	Hardness Rc (BHN)	Chemical Composition (Wt. %) C	Cr	Mo	Mn	Si	S	P	Cu	Ni	V
Std. C Pin-Disk and Amsler Series Pins and Upper Rollers (Rail X21)	22 (236)	.75	.02	.02	.98	.25	.03	.04	.07	.09	.004
Disks (W3)	22 (236)	.66	.04	.01	.68	.53	.02	.002	.09	.03	.009
Lower Amsler Rollers (Wheel W1)	22 (236)	.77	.08	.04	.66	.33	.04	.03	.08	.08	.005
FAST Rail Amsler Series Upper Rollers Rail X29 (Std. C)	27 (265)	.72	.02	.01	.97	.21	.02	.005	.14	.06	.002
Rail X30 (MnSiCrV)	33 (311)	.67	.82	.02	.93	.61	.02	.005	.04	.06	.14
Rail X31 (CrMo)	36 (336)	.73	.70	.24	.67	.27	.02	.005	.02	.02	.002
Rail X32 (CrMo)	34 (320)	.71	.55	.21	.61	.29	.02	.005	.25	.10	.002
Lower Rollers Wheel (W1)	22 (236)	.77	.08	.04	.66	.33	.04	.03	.08	.08	.005
Heat Treated Amsler Series Upper Rollers Rail X34	33 (311)	.71	.57	.21	.88	.41	.02	.005	.26	.10	.002
Rail X35 (IS. C)	26 (258)	.63	.14	.05	.88	.17	.01	.005	.29	.13	.002
Lower Rollers Wheel (W1)	22 (236)	.77	.08	.04	.66	.33	.04	.03	.08	.08	.005
Wheel (W2)	32 (297)	.70	.02	.001	.72	.53	.02	.03	.05	.03	.005

Results

WORN RAIL EXAMINATIONS

Though some surface detail had been lost through corrosion which occurred after removal from track, the damage caused by interaction with wheels on the rail gauge face was very distinctive. The damage could be characterized in terms of grooves and high areas (Fig. 8). The grooves followed the arc of motion of the wheel flange on the gauge face, sometimes attaining 5 mm length and 65 μm depth. The material of the high spots in many cases appeared to have come from the groove directly adjacent to the high spot.

Figure 8. Rail gauge face damage, 2X.

A higher magnification SEM photograph of a portion of the gauge face is shown in Figure 9. Figure 10 is a cross section of Fig. 9 at the groove termination and beginning of the prow. The ability to section through an exact location enables the association of the various surface features to the type of resulting cross section. In the case of Figure 10, the areas of greatest material flow are the prows directly adjacent to groove.

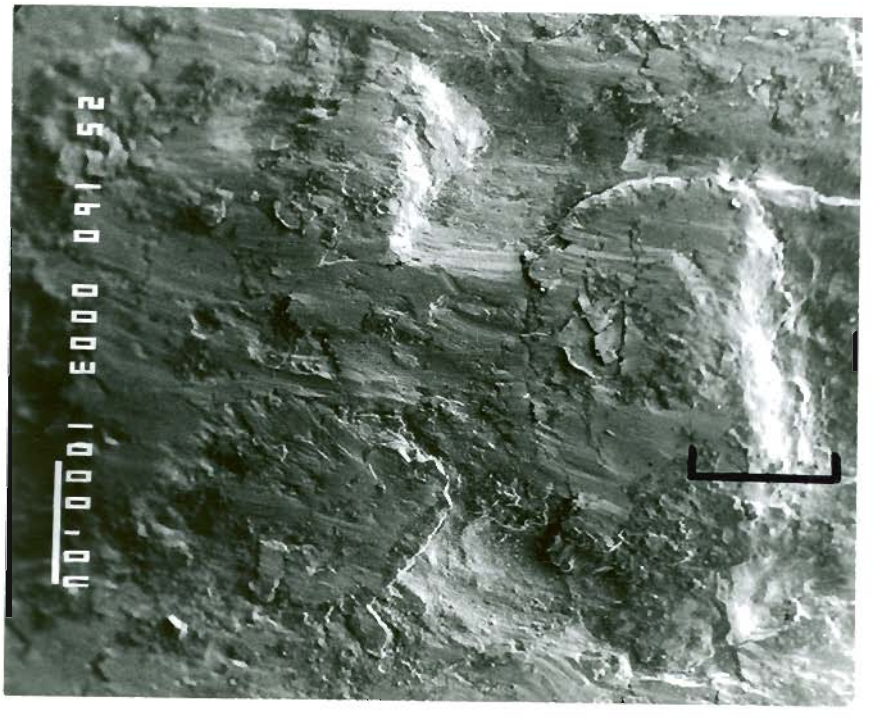

Figure 9. SEM photograph of rail gauge face surface damage.

Figure 10. Rail gauge face cross section at prow shown in Figure 9.

Rail gauge face cross sections revealed a wide range of degree of damage. There were sections with little to no flowed metal, cracks, or uneven surface levels, and there were areas that were extremely disfigured. (Fig. 10 - 11) The upstream side of a groove often had no deformed material, while the directly adjacent mound consisted entirely of flowed, parallel pearlite lamellae. Figure 11 is taken from the same cross section as Figure 10 approximately 12 mm (.5 inches) away from Figure 10. The depth of the deformed material was usually just slightly greater than the groove next to it, often reaching 65 - 75 μm.

Crack-like separations were present and were usually associated with highly flowed metal, though they appeared to be more like cold laps rather than sharp, growing cracks. They were parallel to the flow lines and usually located on the downstream side of a material pile-up. The cracks extended through approximately 3/4 of the depth of the deformed material layer.

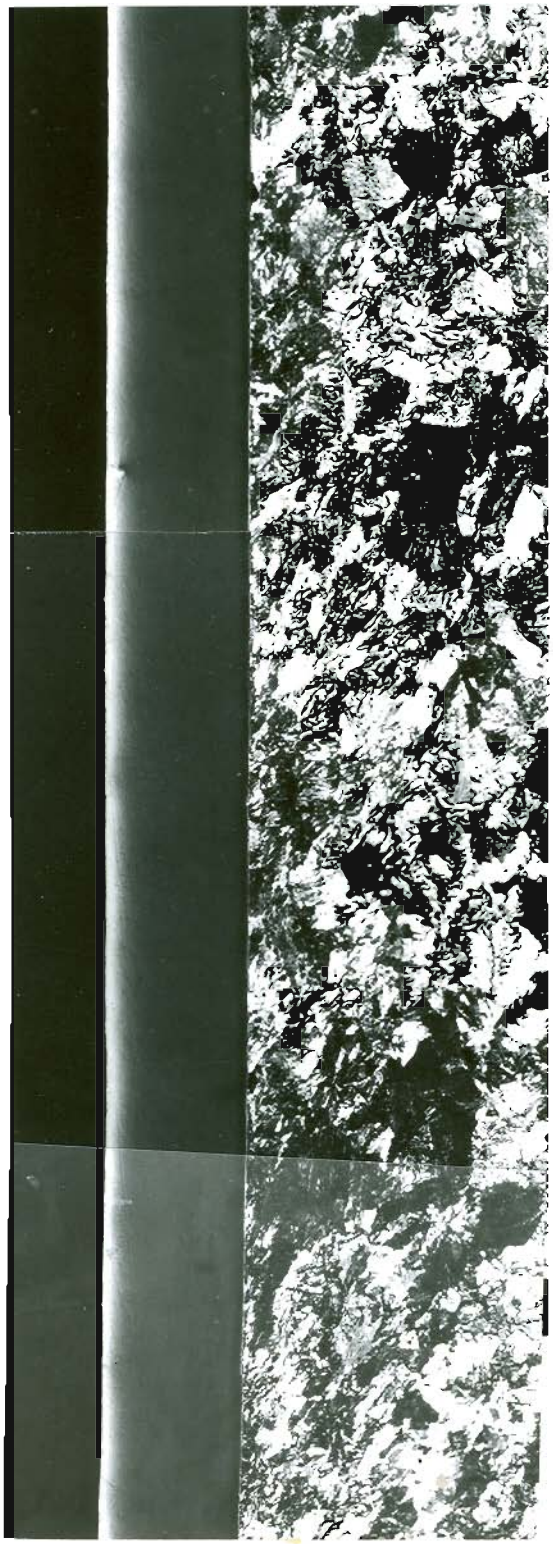

Figure 11. Cross section of rail in Figure 9 approximately 12 mm (.5 in) from location in Figure 10.

FAST RAIL WEAR PROGRAM

The four rails obtained from FAST were from Section 07, taken out after 76.5 Million Gross Tons (MGT) of accumulated unlubricated traffic. The rails were judged by wear rate and a relative wear resistance calculated for each rail. Rail wear was measured with a rail "snap gauge" which positions dial indicators and measures the change in rail profile at two locations at 9.5 mm (3/8 inch) and 15.75 mm (5/8 inch) below the rail center high spot. The relative wear resistance was calculated by comparing all the rails against that rail which suffered the highest wear rate. For example, a relative wear resistance of 2 indicates that a rail wore half as much as the base rail with a relative wear resistance of 1.

The FAST experiments rated the rails in increasing wear resistance as follows: standard carbon, 1.0; MnSiCrV, 1.3; CrMo #1, 2.0; and CrMo #2, 1.7. [47] It is important to remember that this method of ranking rails is based on profile loss, both on the gauge face and running surface, and not a volume or weight loss.

PIN/DISK WEAR TESTS

Standard Carbon Rail Wear Series

The wear data is plotted in Fig. 12 as wear rate against load. It appears that this curve has three wear regimes with wear rates varying between 0 and approximately .27 mm^3 lost per cm of sliding. In the first, between 0 and 54 kg load, wear rate increased linearly with load up to .06 mm^3/cm. At 54 kg the wear rate dropped, and between 54 and 156 kg rose with load, but with decreased slope. Above 156 kg load the wear rate rose sharply up to .27 mm^3/cm at 246 kg.

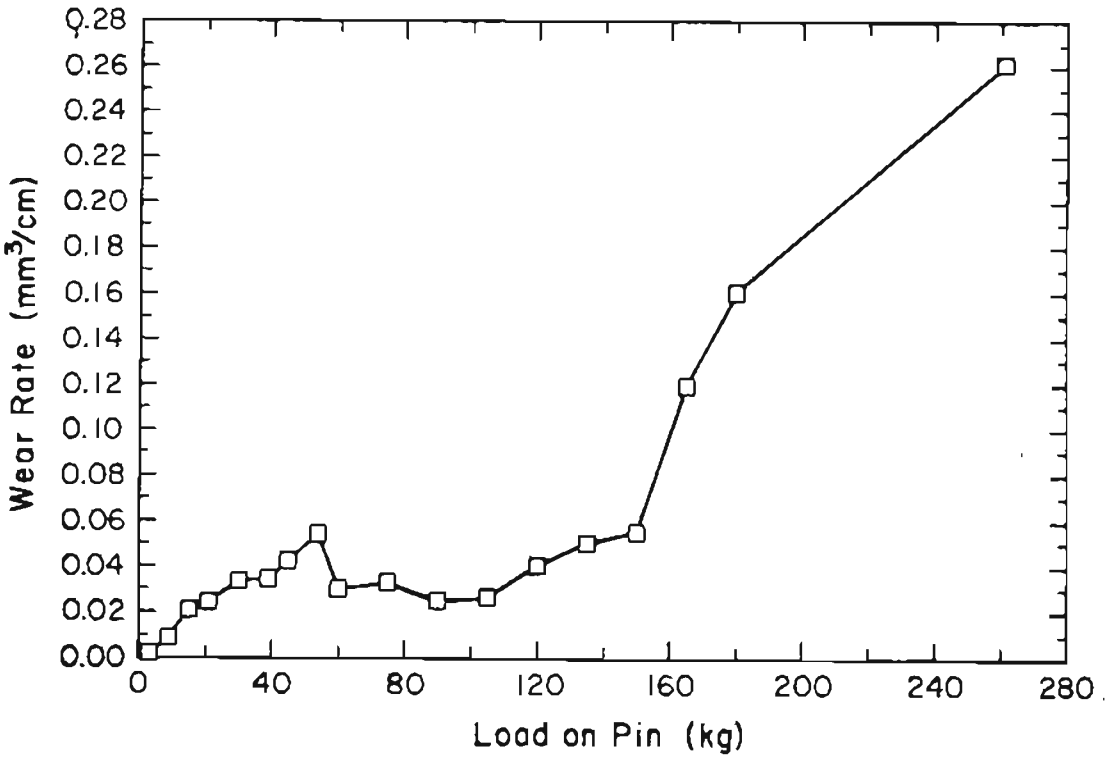

Figure 12. Standard carbon rail steel pin/disk wear rates with increasing load.

An alternative interpretation of the data in Fig. 12 is that the overall trend is linear with the decrease between 54 to 165 kg load region caused by some machine characteristic within that particular load range. The most obvious machine characteristic, vibration, could increase wear rates by increasing the true pin load due to a repeated, impacting type of loading. On the other hand, severe vibration could reduce the true sliding distance by reducing the time the pin and disk are in contact.

A third possible interpretation of the wear rate and applied load relationship is that wear rate is a power function of load with no transitions of any sort and the variation at the lower loads are the result of statistical experimental variance.

SEM/OM examination of the worn pins failed to reveal any major changes in the wear surfaces that might indicate a change in wear mechanism. The features observed at 162 kg (Fig. 13a) were just an exaggerated example of those observed at 6 kg (Fig. 13b). Lower load pins had grooves that commonly traversed the entire pin face, while the high load pins had broader, shorter, and less distinct grooves. In many cases a groove terminated at a mound of material that was the same width and height as the groove itself, similar to a third body abrasive particle (Fig. 14).

There was usually extruded material attached to the pin sides and trailing edges, with the higher loads producing more displaced material than the lower ones.

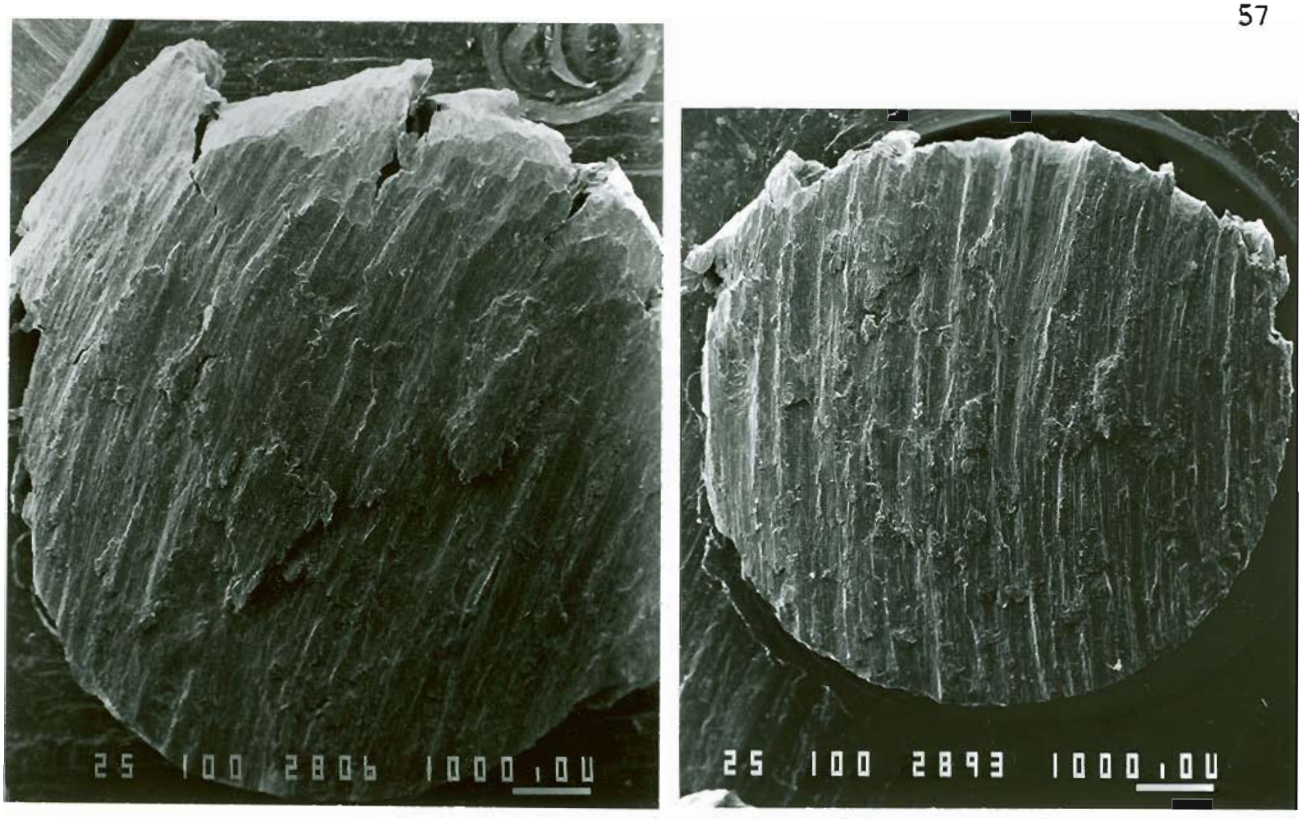

(a) (b)

Figure 13. Wear surfaces, 6 mm (.25 in.) diameter standard carbon rail steel pins, (a) 165 kgs applied load and (b) 6 kgs applied load, 20X.

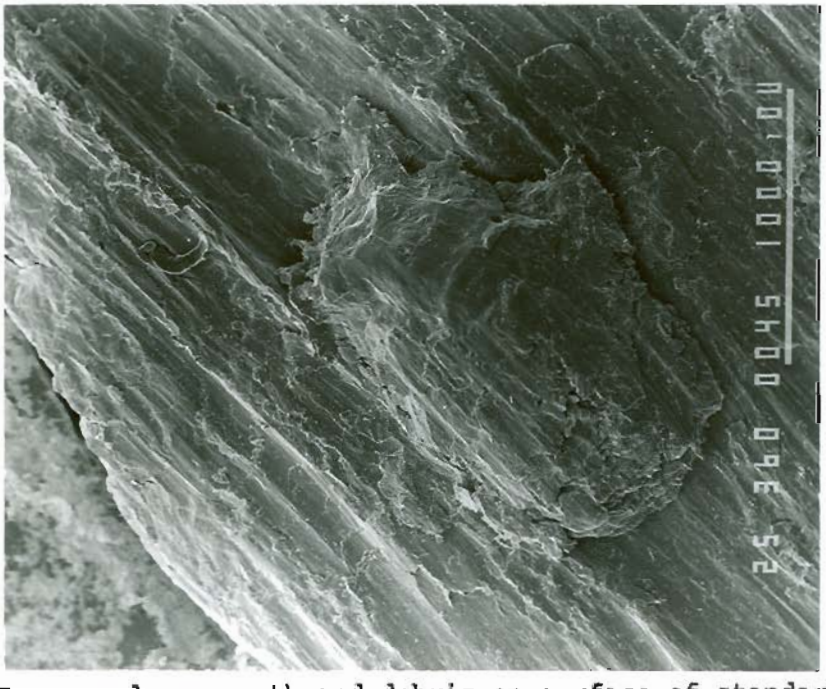

Figure 14. Impressed wear path and debris on surface of standard carbon rail steel pin, applied load 174 kgs.

Pin/Disk Machine Vibration Testing

The accelerometer mounted on the specimen chuck produced vibration records that could be utilized in several ways. For the conditions tested the peak-to-peak acceleration values were monitored and recorded approximately mid-way through each test. These peak-to-peak accelerations were the best indications of vertical impacting of the pin on the disk. The vibration values were then compared to the wear rate curve obtained in the standard carbon series at each applied load (Fig. 15). The middle region of lowest wear corresponded to the highest vibration and where the wear rate increased significantly the vibration decreased. Based on this it was concluded that the dip in the standard carbon wear curve could be explained in terms of machine vibration effects.

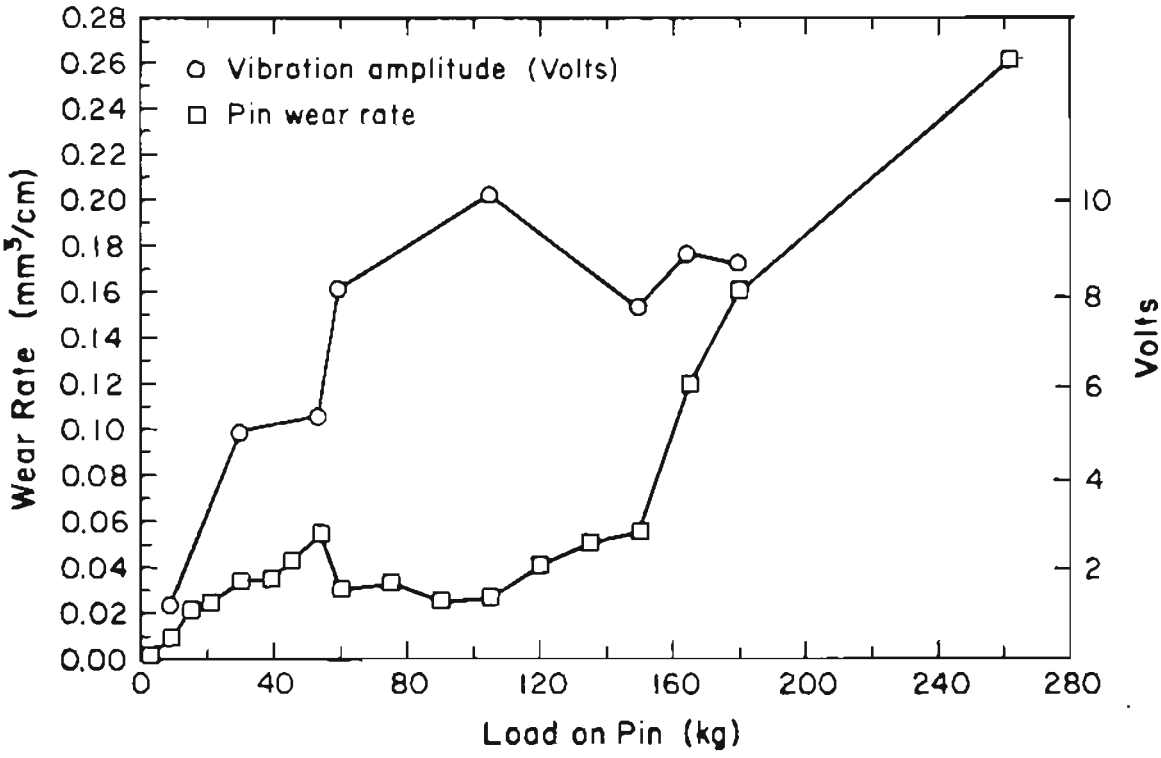

Figure 15. Standard carbon rail steel wear rates and peak-to-peak vibration values with increasing applied load.

During the course of the testing, however, the machine vibration did not remain constant throughout each individual test and raised a question as to the validity of recording only one vibration value and using it to characterize an entire wear test. Other wear tests were performed, this time recording the accelerometer output every second until a steady state condition with little to no change in peak-to-peak values was obtained, approximately 80 seconds or one-fifth the duration of a 400 second test. From this, it was seen (Fig. 16) that there is some initially high vibration level that asymptotically approaches the lower steady state value.

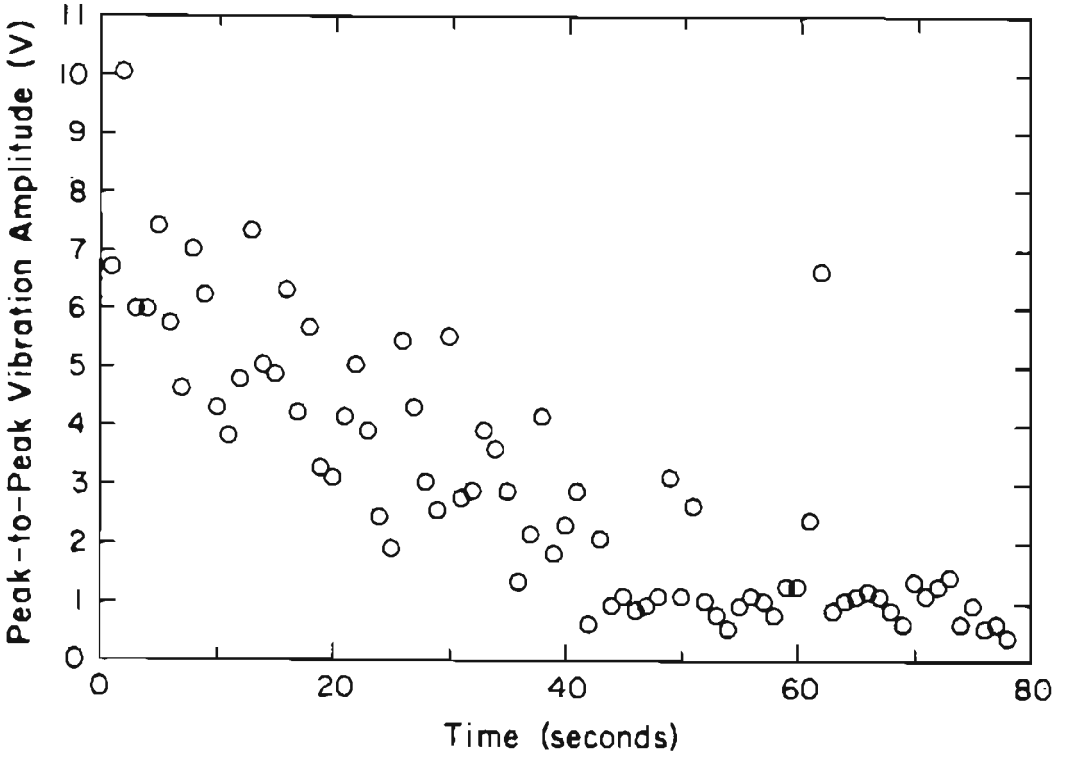

Figure 16. Peak-to-peak vibration of a pin/disk test for the first 80 seconds of a 400 second test.

With a complete picture of the vibration signature, the pin/disk machine was re-evaluated to identify possible vibration sources and any appropriate changes that might improve the machine. Two components were modified. The first was the disk drive line and the second was the pin chuck retaining arm. Alterations were made as outlined in the preceding Experimental chapter.

Pin/Disk Post Modification Wear Test

The post-modification wear and vibration results are shown in Fig. 17. It can be seen that the wear rates followed the same general pattern as the original tests. That is, wear rates initially increased linearly with load, then decreased in a mid-range section, and finally entered a region of rapid wear rate increase with load increases. It should be noted, however, that the second test series generated lower wear rates for equal loads over the entire curve with wear rates as little as one-tenth the original rate. The range of loads that produced the first series mid-range drop (50 to 120 kg) moved to between 70 to 180 kg. The highest wear rate, originally .27 mm^3/cm slid at the highest load, dropped to .24 mm^3/cm.

Pin vibration values decreased to less than half those produced with the original machine configuration. As before, there was an increase in vibration in the mid-range where the wear rates decreased. In general it was observed that both pin and disk lateral motion were significantly reduced, in fact almost eliminated.

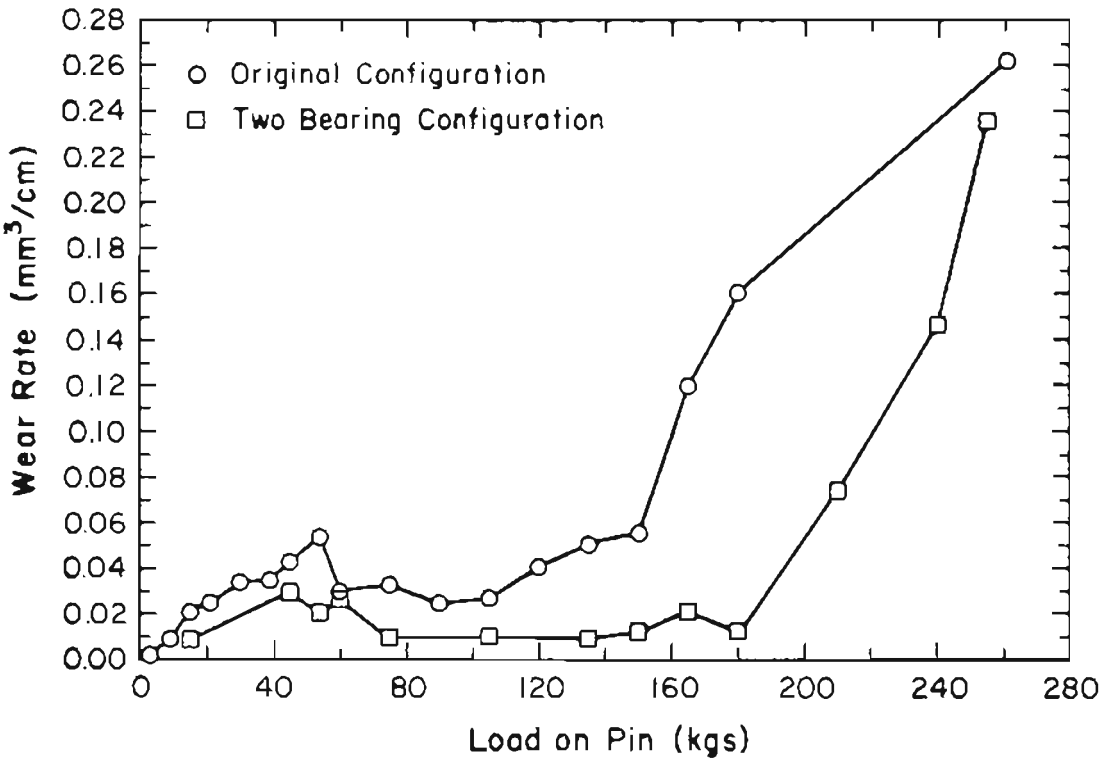

Figure 17. Standard carbon rail steel wear rates before and after pin/disk machine stiffening modifications.

HEAT TREATMENTS

Of the fourteen heat treatments performed on the seven standard carbon rail bars and seven CrMo rail bars, five of the former resulted in significantly different hardnesses, and of the CrMo, six different hardnesses were obtained. Although the isothermal quench temperatures were closely controlled and systematically changed, there were several transformation temperatures that caused a duplication of hardnesses around 27 Rc (267 BHN) (Fig. 18). [48]

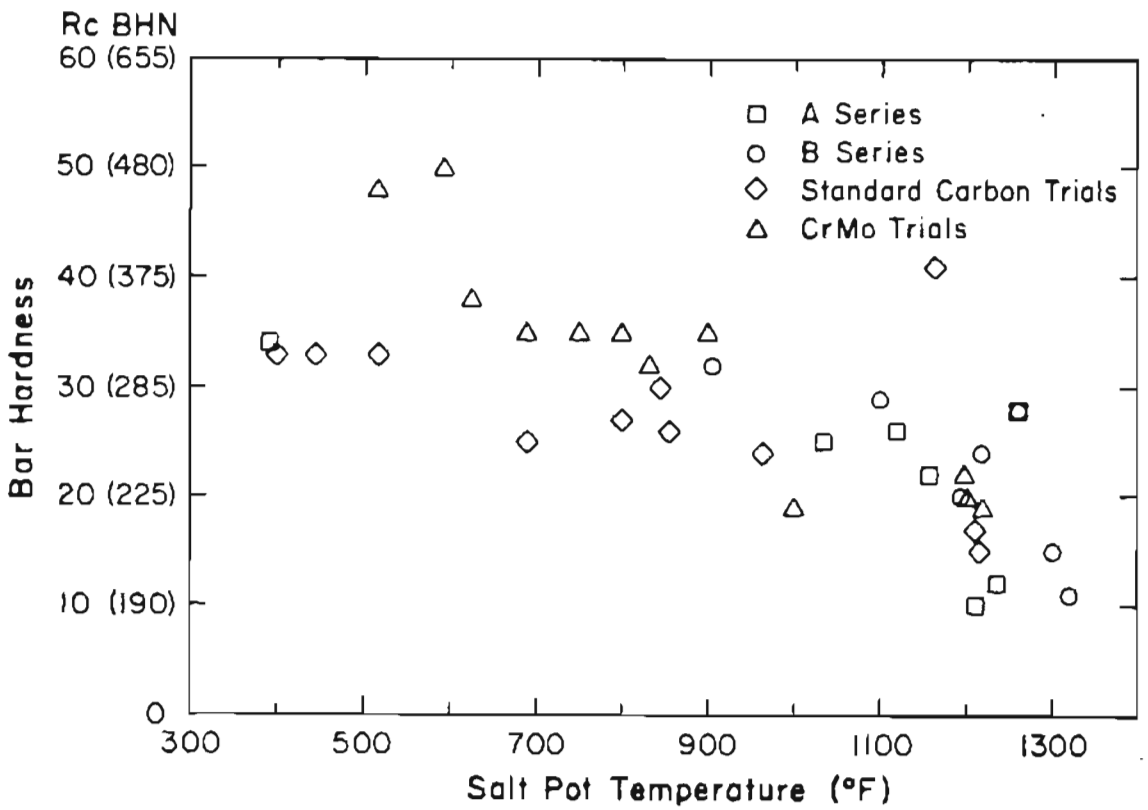

Figure 18. Isothermal transformation temperatures (salt bath quench temperature) and resulting average hardness.

Table VIII lists each heat treatment isothermal quench temperature, average hardness, and pearlite interlamellar spacing.

Bars A1, A2, and B2 were not tested because of the heat treatment hardness duplication. The highest hardness was 35 Rc (322 BHN) obtained with both chemistries, and the lowest, 91 Rb (190 BHN or 10 Rc) also produced in both the standard carbon (X35) and CrMo (X34).

The final microstructures of the heat treated steels included coarse to fine pearlites, and a structure that resembles a spheroidized pearlite. None of the microstructures contained any free ferrite, bainite, or martensite. The microstructure of Class U wheel steel is shown in Fig. 19. Photomicrographs of all the as-received and heat treated microstructures are included in Appendix I.

Table VIII

Heat Treating Schedule

Sample Designation	Isothermal Quench Temperature °C (°F)	Time Hours	Hardness Rc	Hardness BHN	Pearlite Inter-Lamellar Spacing, 2(Std.Dev.) (nm)
Old Std C (X21)	(As received)		22	236	252, 26
FAST Rails					
Old Std C (X29)	(As received)		27	265	225, 17
MnSiCrV (X30)	(As received)		33	311	151, 10
CrMoI (X31)	(As Received)		36	336	143, 12
CrMoII(X32)	(As Received)		34	322	156, 22
Heat Treated Rails					
A0 (X35)	(As Received)		26	258	188, 17
A31	604 (1120)	.5	26	258	183, 12
A32			25	252	199, 26
A33			27	265	201, 26
A34			26	258	229, 20
A35			25	252	266, 34
A4	626 (1158)	1	22	236	220, 28
A55	669 (1237)	21	(10)	190	469, 35
A55					458, 63
A55					437, 52
A55					438, 66
A6	655 (1211)	1	(10)	190	352, 40
A7	196 (385)	3.5	34	322	118, 22
B0 (X34)	(As Received)		33	311	166, 12
B11	485 (905)	.75	33	311	141, 36
B12			34	322	150, 22
B13			35	328	122, 18
B14			35	328	122, 12
B15			32	305	140, 14
B3	597 (1106)	3.6	28	270	170, 16
B4	659 (1218)	1.5	24	247	231, 27
B5	715 (1319)	46	(11)	195	391, 47
B6	704 (1300)	24	(15)	205	472, 27
B7	650 (1202)	2	20	228	315, 24
W1	(As Received)		22	236	214, 29
W2	(As Received)		32	301	162, 11

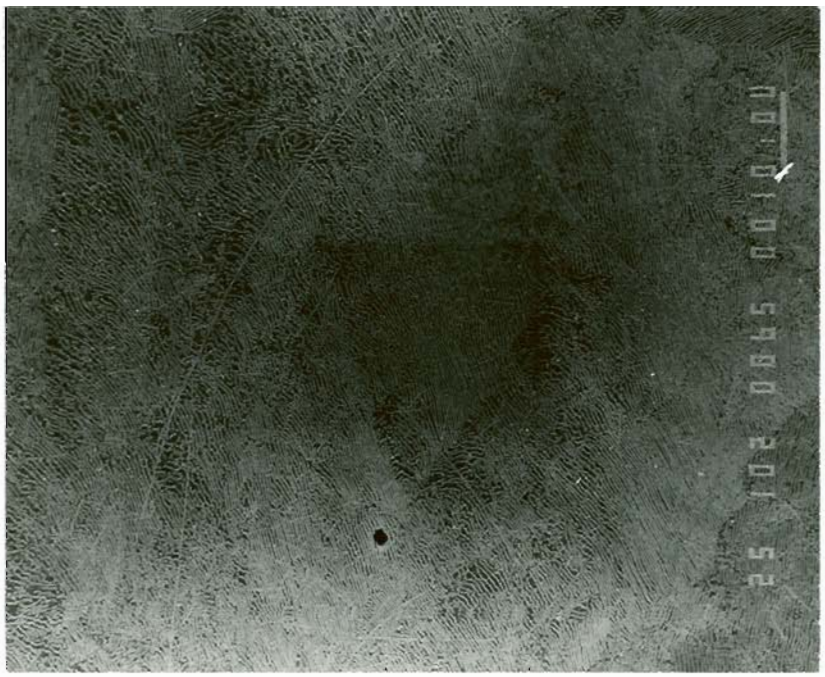

1000X

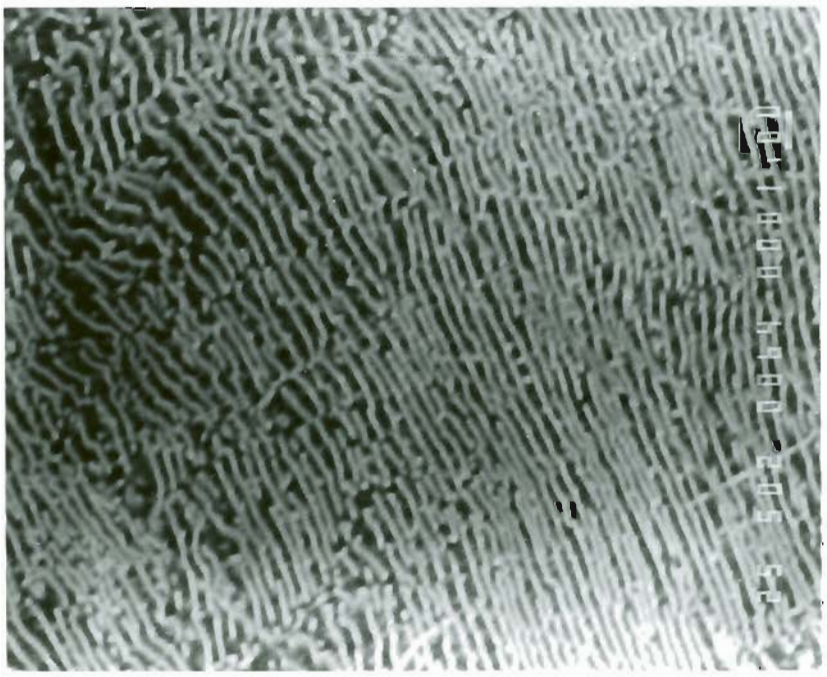

5000X

Figure 19. Class U Wheel (W1) microstructure, pearlite interlamellar spacing 214 nm.

PEARLITE INTERLAMELLAR SPACING MEASUREMENTS

The spacing measured for each heat treated bar is listed in Table VIII (page 64) together with the isothermal quench temperature and average hardness. The greatest spacing, 475 nm, resulted from the highest quench temperature in the standard carbon, and conversely, the finest spacing, 118 nm, occurred at the lowest transformation temperature with the standard carbon rail. The two chemistries performed similarly with the controlling parameter being temperature, not chemistry (Fig. 20).

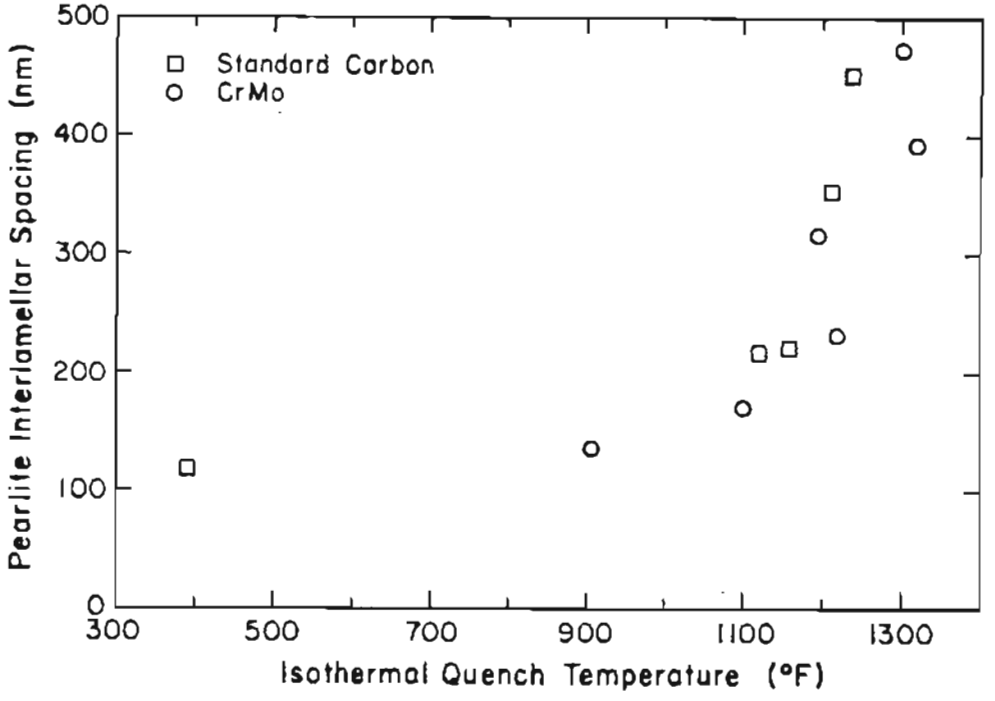

Figure 20. Isothermal transformation temperatures (salt bath quench temperature) and pearlite interlamellar spacing (nm).

Lamellar spacings were closely related to final material hardness with higher hardnesses corresponding to finer spacings (Fig. 21). For comparison, commercially available Class U standard carbon rail has an interlamellar spacing of 215 nm, while a head hardened rail is 120 nm.

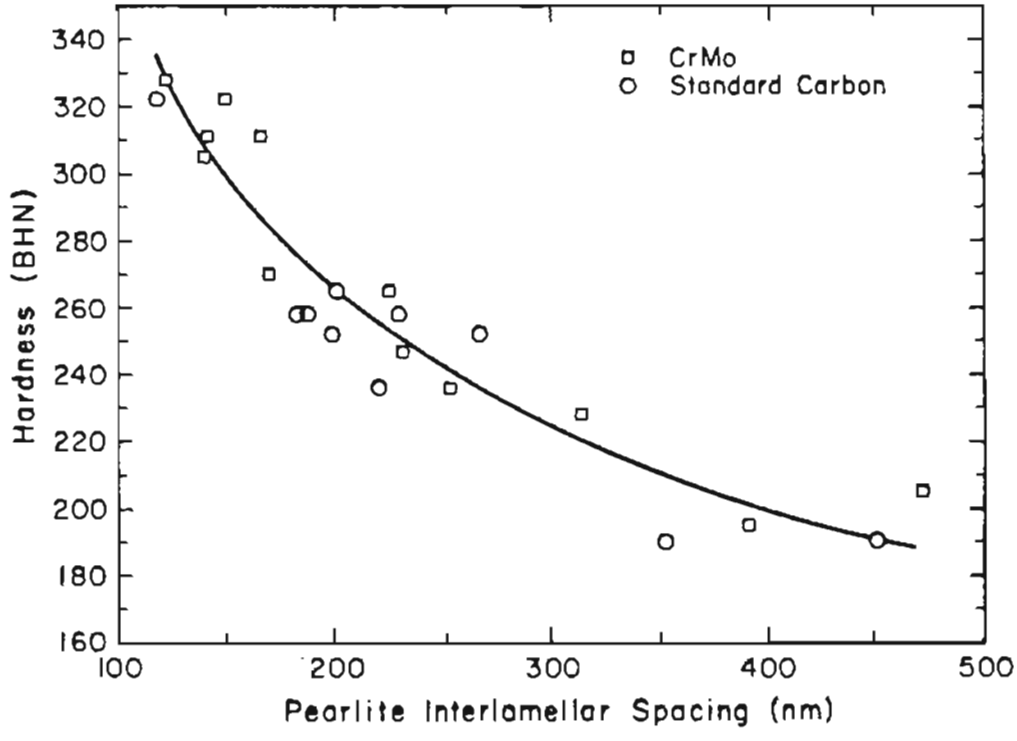

Figure 21. Heat treated rail hardness and pearlite interlamellar spacing.

The consistency of the heat treatments was checked in two ways. Interlamellar plate spacings were measured in four quadrants of a single roller machined from the standard carbon bar A5. The values varied from a high of 469 nm to a low of 438 nm with the average and standard deviation being 452 nm and 14 nm respectively. This is a 7% variation which is within 1% of the accuracy of the lamella measuring method, indicating that spacing of one roller did not change within the

accuracy of the spacing measurement technique.

The second method of checking the consistency of the heat treatments involved measuring the variation of spacings along the length of two bars. The ideal situation would be identical pearlite spacings from the end of the bar at the first Amsler roller, to the opposite tensile bar end. The spacing from all five rollers of one CrMo bar was measured and showed no systematic change from end to end with less than a 19% total change between the highest and lowest. One of the standard carbon bars, however, had a range of spacings that started at 183 nm at the end first immersed in the salt bath, and progressed gradually to 266 nm at the tensile bar. Due to this variation, the interlamellar spacings were taken for all rollers from this heat treated bar. This was the A3 bar and since all other heat treatments had longer transformation times, this was taken to be the worst case because heat removal rate was not as critical for the remaining temperatures. Systematic variation was shown not to have occurred in the other bars by hardness testing all rollers.

The accuracy of the spacing measurement technique was verified in several ways. The first was a systematic error analysis on the various sources of error in the lamellae measuring process. These sources included the magnification calibration, the actual intercept counting, and the precision of the intercept circle superimposed on the SEM viewing screen. The analysis found that the most critical factor is the actual counting of the lamellae/circle intercepts. In most cases, this number was two to three orders of magnitude more sensitive than the next most sensitive parameter, which was the calculation of the

true SEM magnification. Further, the actual SEM magnification cannot be greater than 4% different from the calculated magnification. The analysis also showed that the total accumulated error in the spacing measurements should not exceed 6% of the final value.

A second gauge of the spacing measuring procedure can be found in the standard deviation of the spacing measurements. The spacing standard deviations did not diverge more than 9% from the associated average, with most standard deviations approximately 5% of the average.

The third check investigated what influence the number of counted fields had on the measurement accuracy. In one specimen fifty fields were counted and compared to the results of ten, twenty, thirty and forty fields. Using a statistical significance test it was determined that there was no discernable difference between the spacing established with ten or fifty fields.

AMSLER TESTING

Amsler Standard Carbon Rail Wear Series

From observations of the wearing rollers it was noted that the three wear regimes recorded by Bolton and Clayton were all represented in these tests. [49] Type I wear involves the flaking of both oxide and metal wear debris normally accompanied by very low wear rates (Fig. 22). In the present tests Type I wear occurred for all the tests at 1%, 3%, and 5% slide/roll ratios, and some tests at 7% and 10% (Tables IX and X). Type I wear rates ranged from 5 to 200 μg/meter rolled and increased with both contact pressure and slide/roll ratio level. In this range wheel wear rates were higher than those of the rail.

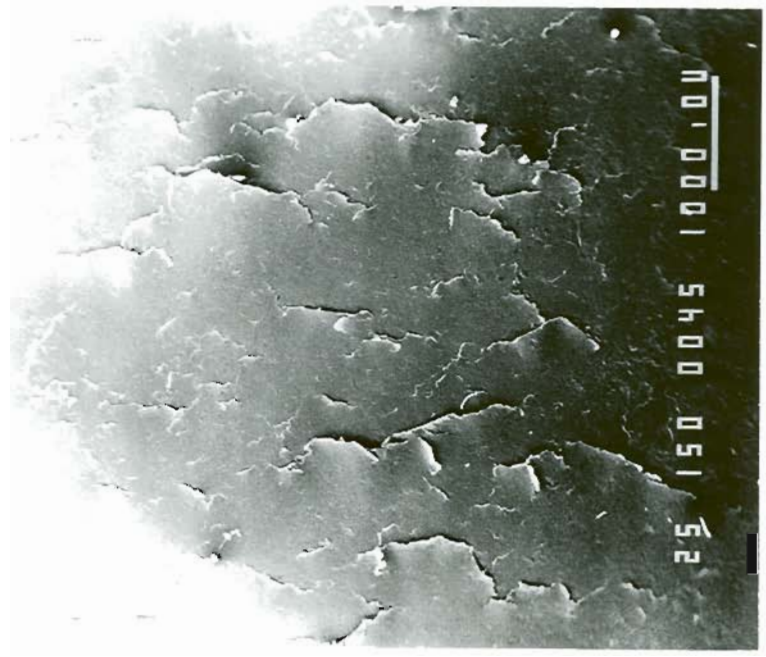

Figure 22. Amsler roller wearing surface with Type I wear mode.

Table IX
Standard Carbon Rail Amsler Wear Rates ($\mu g/m$) and Types

Slide/roll Ratio	CONTACT PRESSURE (P_o) (N/mm^2) 500	600	700	800	900	1040	1080	1140	1280
35	10200		26700		51100		68400		
	III		III		III		III		
25	3500		10900		17800		35600		
	III		III		24200		III		
					III				
10		190	200	270	150		210	170	55
		II	II	II	190		I-II	I	I
					II				
7		70	160	160	190	130	220	120	120
					130	80		150	70
		II	II	II	I-II	I-II	I	I	I
5			50		80		100		150
			I		100		60		I
					I		I		
3			10		30			60	70
			I		I			I	I
1							20	10	20
							I	I	I

Table X
Class U Wheel Steel Amsler Wear Rates ($\mu g/m$) and Types

Slide/roll Ratio	CONTACT PRESSURE (P_o) (N/mm^2) 500	600	700	800	900	1040	1080	1140	1280
35	2100		5300		11400		17600		
	III		III		III		III		
25	1300		3100		6000		10600		
	III		III		7500		III		
					III				
10		170	210	230	160		180	160	100
		II	II	II	210		I-II	I	I
					I-II				
7		110	160	220	150	230	210	180	200
		II	II	II	110	210	I	230	220
					I-II	I-II		I	I
5			60		110		140		200
			I		140		120		I
					I		I		
3			10		30			100	100
			I		I			I	I
1							10	10	20
							I	I	I

Type II wear involves wholly metallic wear debris and generates a rougher surface topography often associated with ripples (Fig. 23). The anticipated jump in wear rates expected between Types I and II was not apparent (Figs. 24 - 27), nor was there the anticipated increase in wear rate with increasing contact pressure. Indeed the data of Figs. 25 and 26 indicate a fall in wear rate with increasing contact pressure. It should also be noted that this decreasing wear rate was accompanied by a reversion from Type II wear to Type I (Table IX and X) as the load was increased. At the lower end of the tested range for 7% and 10% slide/roll ratios, the wear rate did increase as the load increased as long as the wear mode remained in the Type II regime. In Type II wear the wheel wear rates were again somewhat higher than those of the rail specimens.

Figure 23. Amsler roller wearing surface, Type II mode.

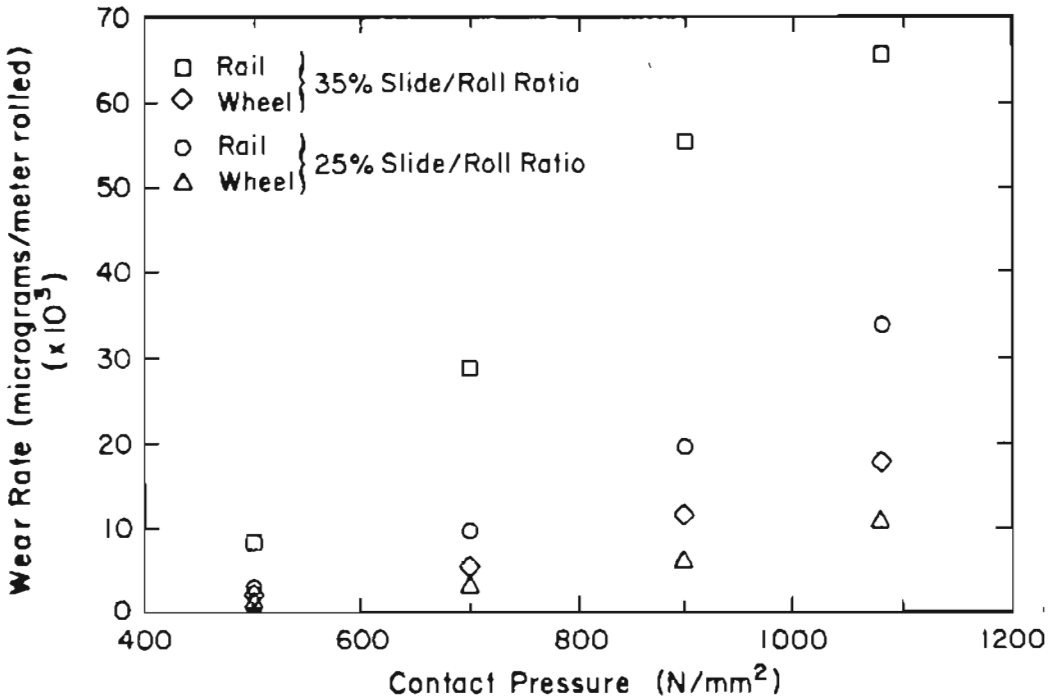

Figure 24. Standard carbon rail (X21) and Class U wheel (W1) Amsler wear rates, 1%, 3% and 5% slide/roll ratio.

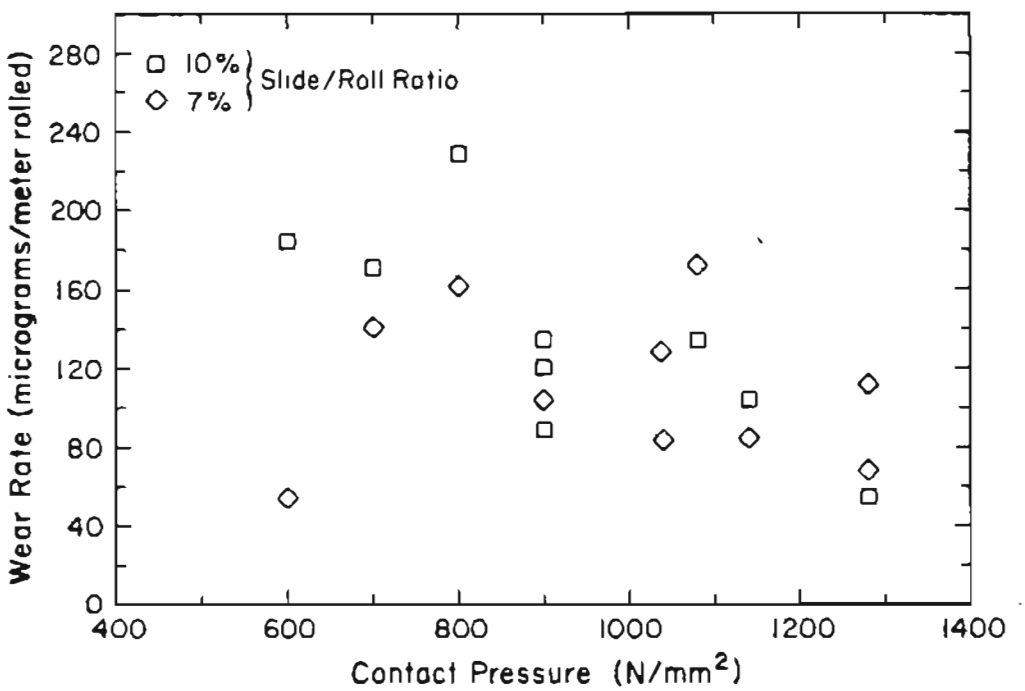

Figure 25. Standard carbon rail (X21) Amsler wear rates, 7% and 10% slide/roll ratio.

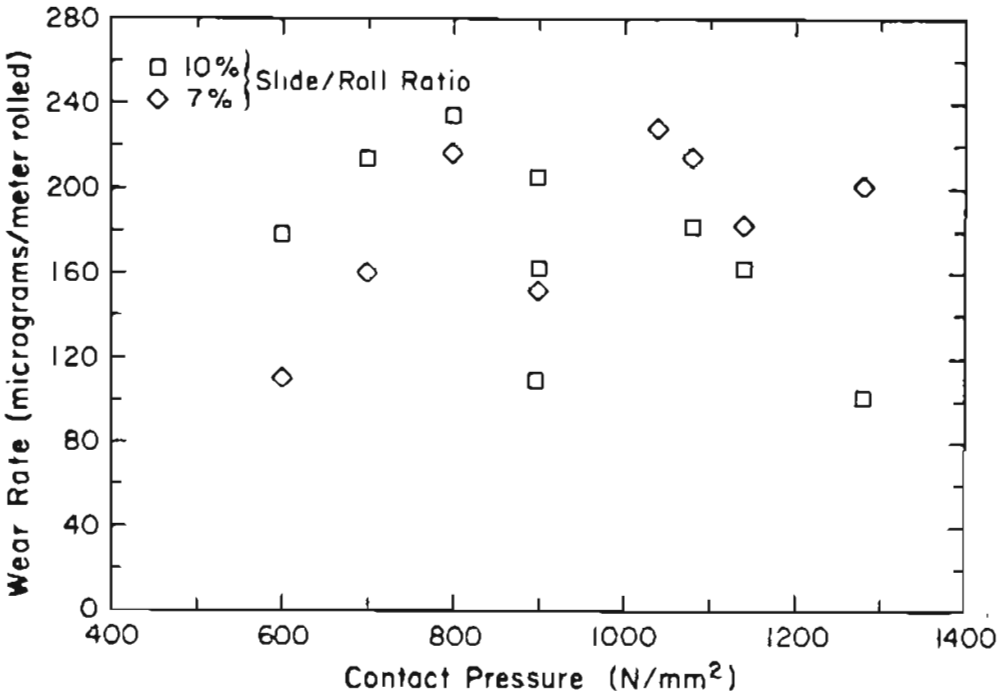

Figure 26. Class U wheel (W1) Amsler wear rates, 7% and 10% slide/roll ratio.

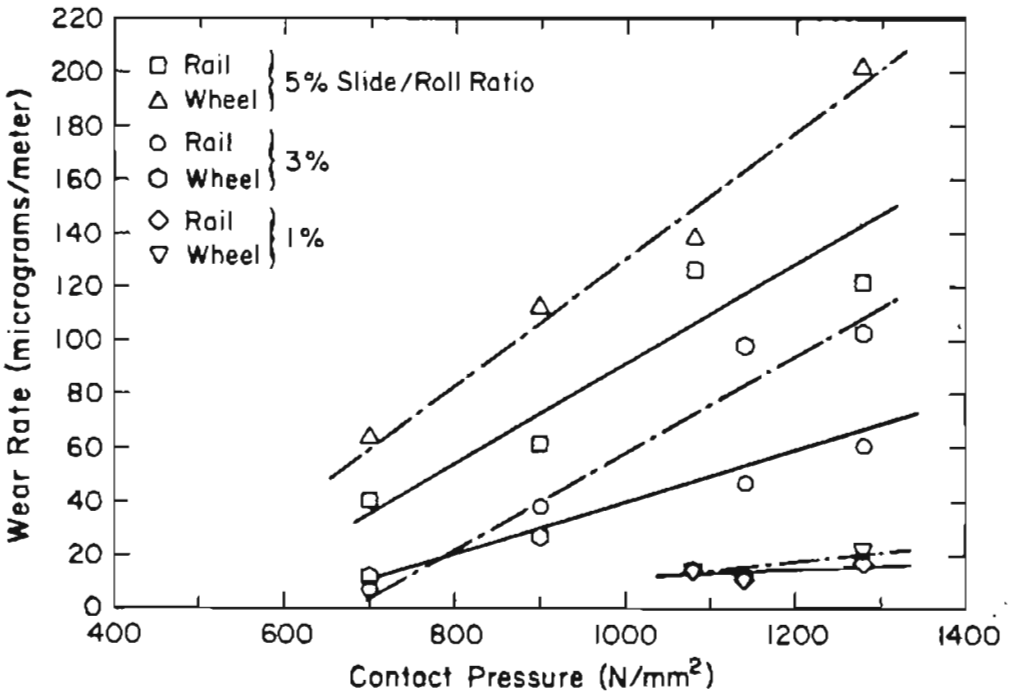

Figure 27. Standard carbon rail (X21) and Class U wheel (W1) Amsler wear rates, 25% and 35% slide/roll ratio.

There was a very clear distinction between Types I and II and Type III in terms of wear rate, with Type III being 1 or 2 orders of magnitude greater depending on contact pressure. Type III wear was observed for all tests at 25% and 35% slide/roll ratio and is associated with very rough surfaces which are heavily gouged (Fig. 28). From the visual appearance of the rollers, Type III wear more closely simulates the type of damage seen in the FAST rail and therefore the investigation of worn Amsler rollers was focused on Type III wear.

Gouge marks up to 4 mm long preceded large mounds or high spots of material. The mounds' leading edges had steep, cliff-like slopes, while the trailing edges tapered more gradually to the original surface height. The tops of the high spots appeared to have been flattened by the successive rolling contacts.

Figure 28. Amsler roller wearing surface, Type III wear mode.

Cross sections of the Amsler specimens showed no uniformly damaged layer (Fig. 29). There were areas which were heavily damaged, and there were other areas which had almost no disturbed layer at all. Cross sections of the high spots revealed flow lines roughly parallel to the surface. Pearlite lamellae could be seen gradually bending over from the original random orientations to become parallel to the surface. Most of the high spots appeared to have at one time been part of the structure directly below it. There were a few smaller areas that seemed to have been re-deposited from other locations.

There were a limited number of what appeared to be cracks that were situated parallel to flow lines, usually associated with the mounds. They were shallow and never penetrated deeper than the deformed layer.

Figure 29. Amsler roller cross section, 1220 N/mm^2 contact pressure, 35% slide/roll ratio, 100X.

Sections taken perpendicular to the rolling direction indicated that there was little plastic flow away from the radial centerline toward the roller edges. A limited amount of mushrooming could be seen at the edges, but never more than approximately .25 mm (.01 in.). Cracks were rarely seen in a transverse section.

A critical factor in determining the wear type and rate is the level of friction sustained during the test. In all cases the coefficient of friction (μ) was between 0.60 and 0.67, the limiting friction for dry steel on steel.

Amsler FAST Rail Wear Series

By the time testing had progressed to this point it had been decided that the 35% slide/roll ratio conditions best simulated the gauge face wear conditions and all subsequent Amsler wear tests were conducted at that slide/roll ratio.

The wear rates (μg/m) of the rail and wheel are shown in Figs. 30 and 31 and listed in Tables XI and XII. The rates varied from a low of approximately 5000 μg/m at 500 N/mm^2 to over 110,000 μg/m at 1220 N/mm^2 for the standard carbon rail. As expected, the standard carbon rail had higher wear rates than did either of the CrMo steels, approximately twice as high. The two CrMo rails and the MnSiCrV rail had approximately the same wear rates which increased with load from 5000 μg/m at 500 N/mm^2 to approximately 50,000 μg/m at 1220 N/mm^2. In all cases the wear could be classified as Type III wear as per the terminology of Bolton and Clayton. [49] This type of wear is characterized by deep gouging and large size debris material removal.

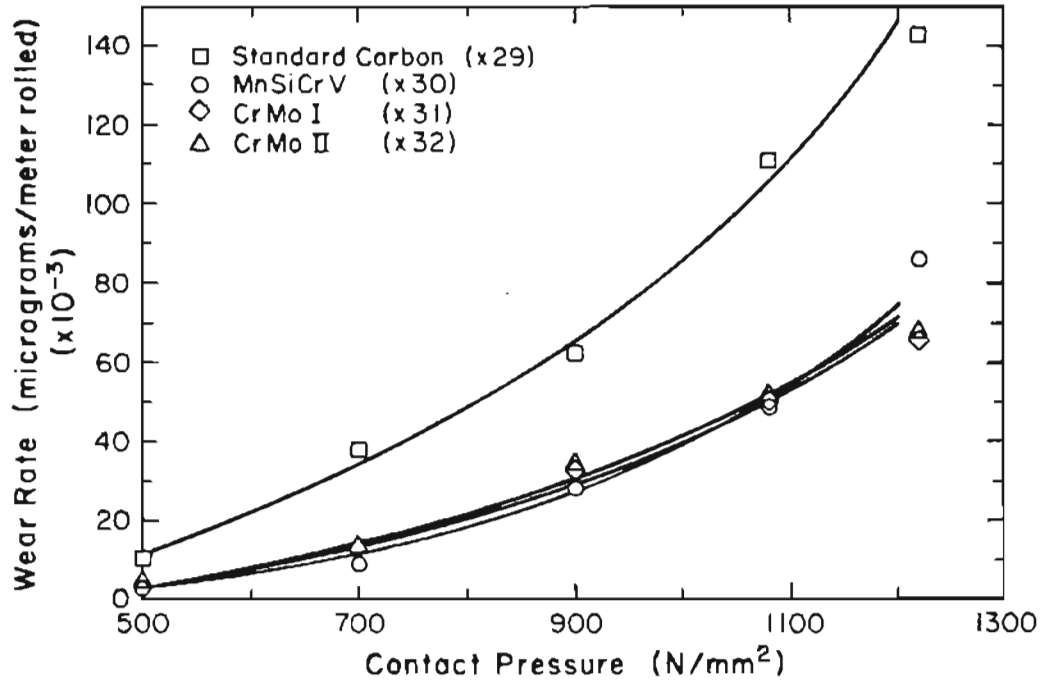

Figure 30. FAST rail Amsler wear rates, 35% slide/roll ratio.

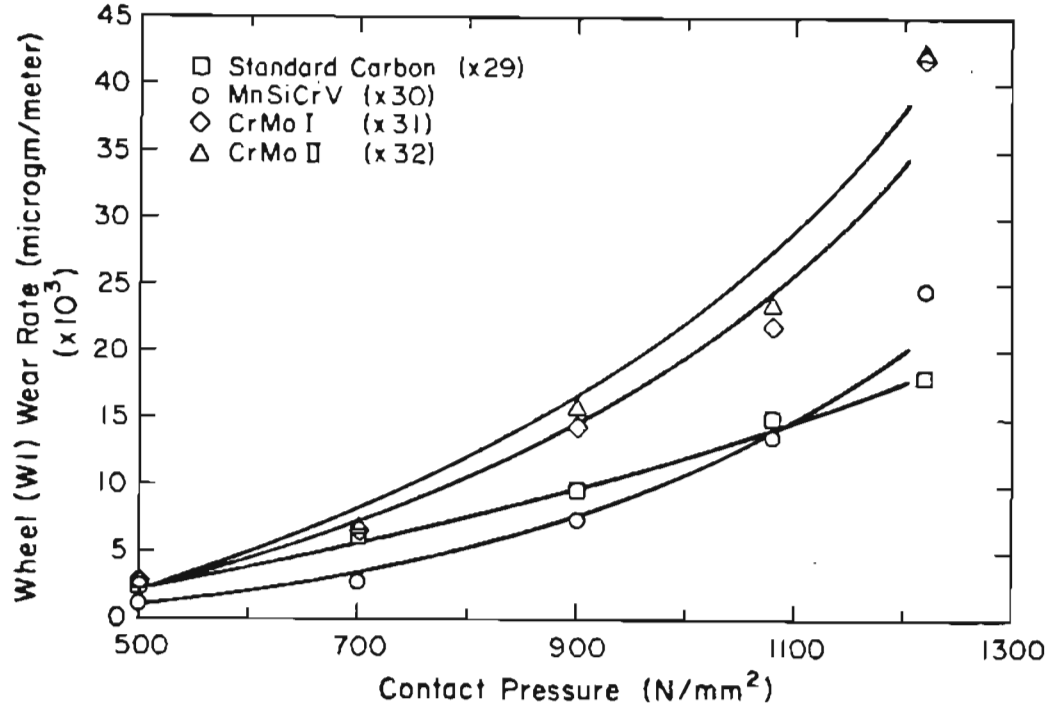

Figure 31. Class U wheel (W1) Amsler wear rates against FAST rails.

Table XI

FAST Rail Amsler Wear Rates on Class U Wheel

Rail and Number	Contact Pressure (N/mm^2)				
	500	700	900	1080	1220
Old Standard Carbon (X29)	10400	37800	62200	110700	143000
MnSiCrV (X30)	3700	9100	28400	49000	86500
CrMo I (X31)	4300	12900	33000	51000	65900
CrMo II (X32)	4600	13600	34600	52300	68200

Table XII

Class U Wheel Amsler Wear Rates on FAST Rails

		Contact Pressure (N/mm^2)				
		500	700	900	1080	1220
Class U Wheel on:	X29	2400	6000	9500	14900	18000
	X30	1100	2700	7400	13500	24600
	X31	2600	6500	14300	21900	41900
	X32	2600	6800	15700	23500	42400

The wear rates of the wheel steel at these higher slide/roll ratios was always less than that of the rail. The rates ranged from a low of 2000 $\mu g/m$ to a high of almost 24,000 $\mu g/m$, about one-fifth of the highest rail wear rate. The wheels suffered greatest wear rates when run against the two CrMo rails, the lowest wear rate for the MnSiCrV and intermediate against the standard carbon rail.

A regression analysis of the wear data indicated that a power relationship provides a better correlation coefficient than does a linear type. The best fit relationships for the rail and wheel wear rates are shown in Table XIII.

Table XIII

Regressed Wear Rate/Contact Pressure
for FAST Rail Amsler Series

[Wear Rate (μgm/meter) = $a(Po)^b$]

	Rail			Wheel		
	a	b	r	a	b	r
X29	1.85E-4	2.890	.993	2.0E-3	2.253	.996
X30	8.07E-7	3.562	.995	4.10E-7	3.474	.995
X31	1.65E-5	3.127	.996	1.80E-5	3.012	.995
X32	2.30E-5	3.084	.996	1.50E-5	3.053	.997

The Amsler laboratory wear experiments, using the average relative wear resistance for the five contact pressures tested, rated the FAST rails as: standard carbon, 1; MnSiCrV, 2.59; CrMo I, 2.31; and CrMo II, 2.22.

Another measure of Amsler roller wear is the reduction of diameter as material is removed during the course of the test. Wear rates in mm lost/meter rolled and relative wear resistances can be calculated from the loss of diameter. These wear rates for the FAST rails on the Amsler tests ranged from .0054 to .0032 (Table XIV). The corresponding relative wear resistances were standard carbon 1.0; MnSiCrV, 1.3; CrMo I, 2.0; and CrMo II, 1.7. These values are closer to the actual rankings realized at FAST than the Amsler weight loss rankings.

Table XIV

FAST Rail Amsler Diameter Loss (mm/m) and
Relative Wear Resistance

	FAST		Laboratory Tests at 1220 N/mm^2			
Rail Steel	Average Wear Rate, mm/MGT	Relative Wear Resistance	Wear Rate$_2$ x 10^{-2} $\mu g/m$ rolled	Relative Wear Resistance	Average Wear Rate$_5$ x 10^5 mm/m	Relative Wear Resistance
X29	.226	1.00	1354	1.00	538	1.00
X30	.173	1.31	729	1.86	413	1.30
X31	.112	2.02	634	2.14	319	1.69
X32	.127	1.78	654	2.07	323	1.67

Amsler Heat Treated Rail Wear Series

Heat treated roller wear rates, both standard carbon and CrMo, increased with decreasing hardnesses and increasing interlamellar spacings and with increasing contact pressures (Figs. 32 – 35). They varied from a low of 13 $\mu g/m$ at the lowest contact pressure and highest hardness to 175500 $\mu g/m$ at 1220 N/mm^2 and the lowest hardness. The wear rates of each of the heat treated steels are listed in Tables XV and XVI.

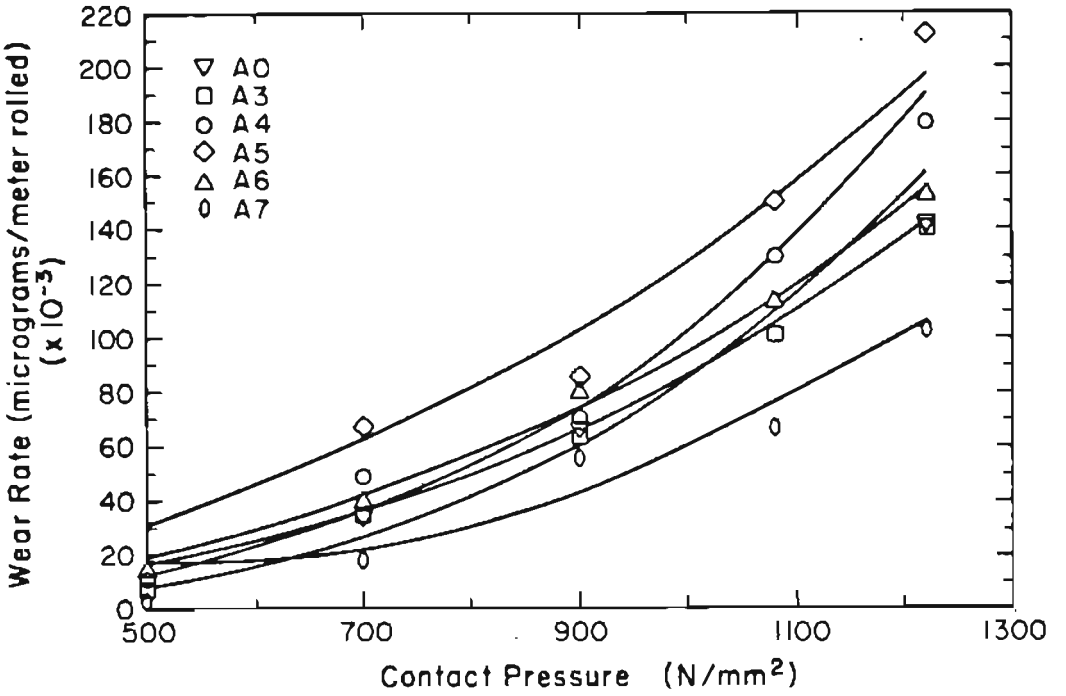

Figure 32. A Series (X35) heat treated rail Amsler roller wear rates.

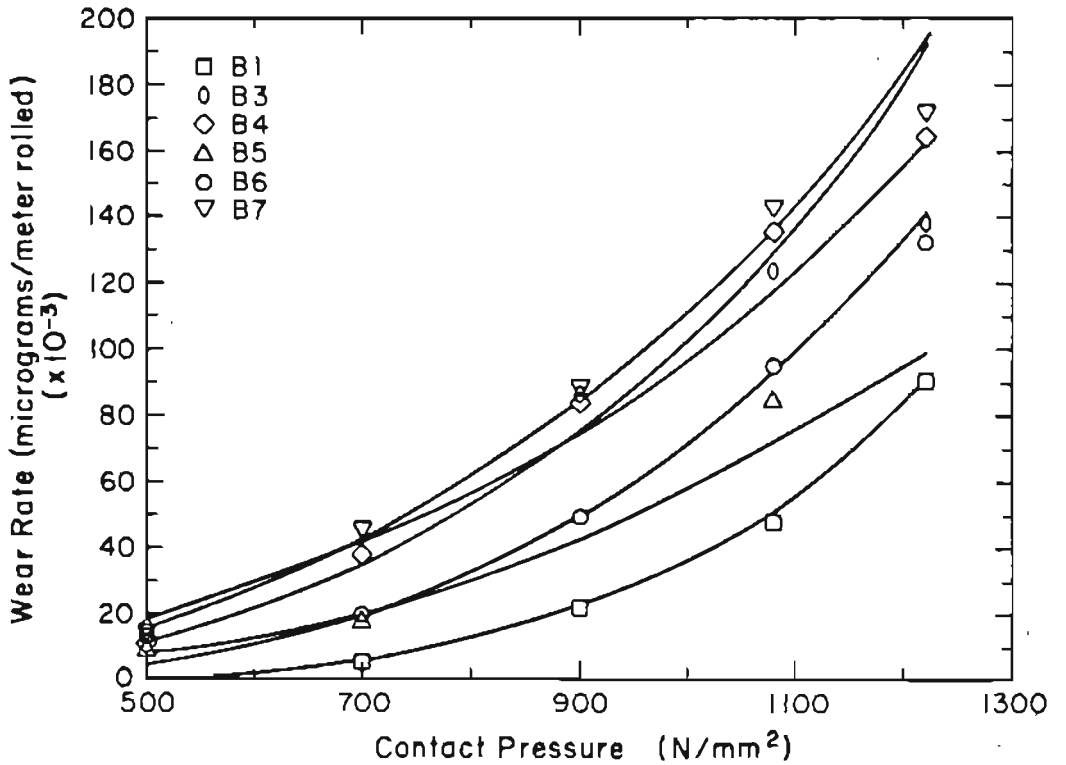

Figure 33. B Series (X34) heat treated rail Amsler roller wear rates.

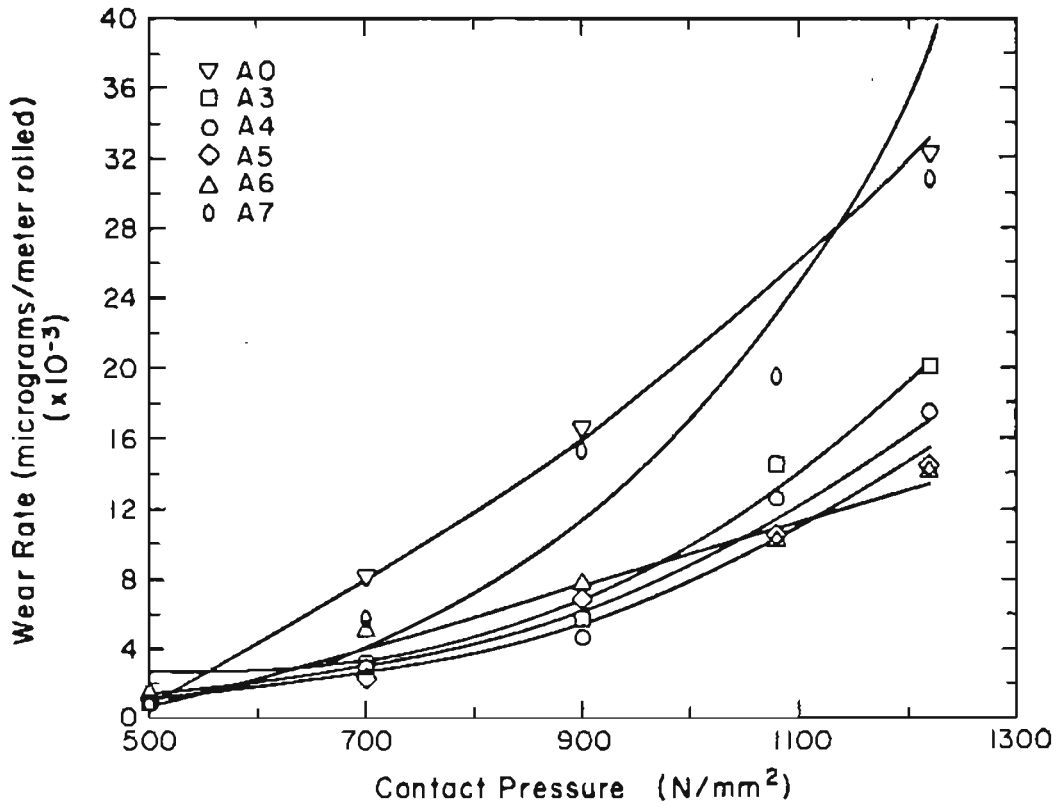

Figure 34. Class C wheel (W2) Amsler roller wear rates on A Series heat treated rail.

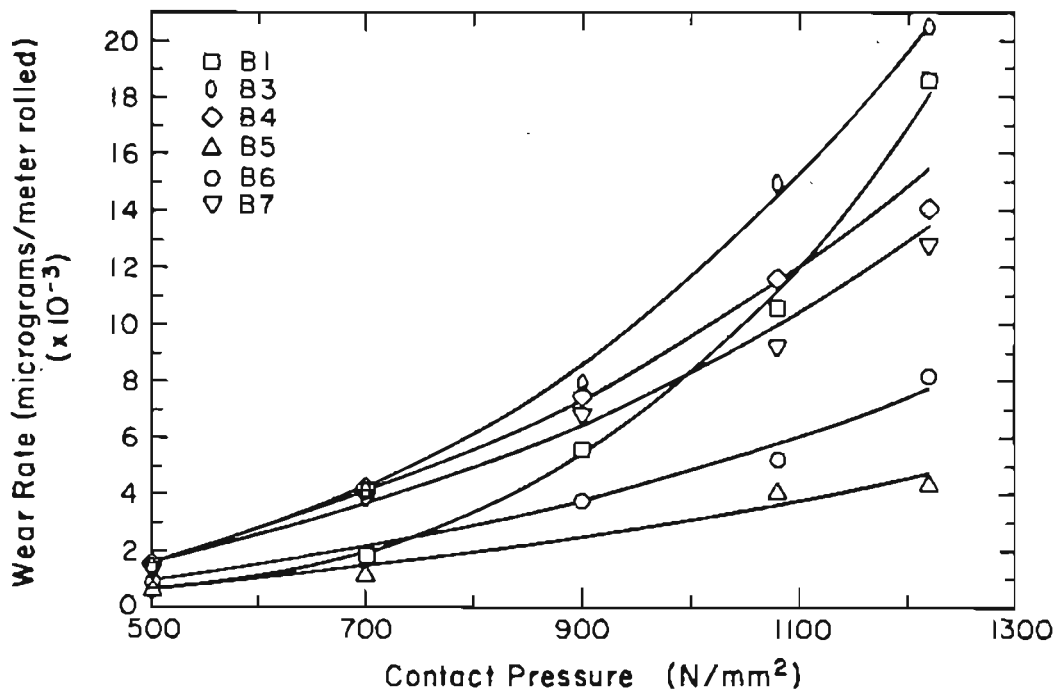

Figure 35. Class C wheel (W2) Amsler roller wear rates against B Series heat treated rail.

Table XV
Heat Treated Rail Amsler Wear Rates

Po (N/mm^2)	500	700	900	1080	1220
A Series Rail (micrograms/meter rolled)					
A0	33400	66200		141800	
A3	6900	34900	63500	101200	140500
A4	10500	49200	70700	130100	179400
A5		67200	85900	149800	212100
A6	14700	39800	80400	113900	152800
A7	(Type I)	18100	55800	66800	102700
B Series Rail					
B0	3200	7000	17000	43100	63500
B1	(Type I)	5400	21700	47700	90200
B3	(Type I)	20100	49300	94800	132100
B4	11000	38100	84200	135100	164600
B5	9200	18000		84600	91300
B6	15600		84900	123500	137800
B7	14100	45500	88300	142300	171700

Table XVI

Class C Wheel Steel Wear Rates Against Heat Treated Rail

Po (N/mm^2)	500	700	900	1080	1220
W2 Wheel on A Series Rail (micrograms/meter rolled)					
A0		8100	16500		32200
A3	900	3100	5700	14500	20000
A4	900	3000	4600	12600	17400
A5		2300	6900	10400	14300
A6	1500	5100	7800	10200	14100
A7	(Type I)	5700	15300	19400	30800
W2 Wheel on B Series Rail					
B0	800	1500	4600	10900	16100
B1	(Type I)	1800	5600	10500	18500
B3	(Type I)	4200	7900	14900	20500
B4	1500	4100	7500	11600	14000
B5	600	1200		4000	4300
B6	900		3700	5200	8100
B7	1300	3800	6800	9100	12700

The results of a regression analysis performed on the wear rates are included in Table XVII. The equations are all non-linear with an accelerating wear rate as contact pressure is increased. From the regression data for these curves it is seen that the wear rate response to increasing contact pressure is not the same for all materials. Apart from one exception, A6, the exponent is greater than two and since for line contact pressure is proportional to the square root of the load, the relations indicate a slight acceleration in wear rate with increasing load.

Table XVII

Regressed Wear Rate/Contact Pressure
for A and B Series Rails

[Wear Rate ($\mu g/m$) = $a(Po)^b$]

	Rail			Wheel		
	a	b	r	a	b	r
A0	1.36×10^{-3}	2.599	.99	7.24×10^{-4}	2.482	.99
A3	1.22×10^{-5}	3.28	.97	3.18×10^{-7}	3.498	.99
A4	7.43×10^{-5}	3.049	.96	9.84×10^{-7}	3.315	.98
A5	6.7×10^{-2}	2.095	.94	1.18×10^{-6}	3.278	.98
A6	1.35×10^{-3}	2.618	.99	7.48×10^{-4}	2.365	.99
A7	6.93×10^{-5}	2.977	.94	1.74×10^{-8}	3.995	.96
B0	1.26×10^{-6}	3.456	.98	1.39×10^{-7}	3.575	.98
B1	3.02×10^{-11}	5.015	.99	4.3×10^{-9}	4.090	.99
B3	3.45×10^{-6}	3.435	.99	2.13×10^{-5}	2.911	.99
B4	6.2×10^{-5}	3.073	.99	2.32×10^{-4}	2.534	.99
B5	2.92×10^{-4}	2.764	.98	3.70×10^{-4}	2.301	.99
B6	2.34×10^{-3}	2.538	.98	3.68×10^{-4}	2.370	.99
B7	3.75×10^{-4}	2.823	.99	3.08×10^{-4}	2.474	.99

The effect of interlamellar spacing on wear rate at the five different contact pressures is presented in Figs. 36 through 40. A regression analysis was performed on the wear rates of both Series A and B separately and combined. Table XVIII contains the results of the analysis. Heat treatment B5, which was consistently out of line with the other data points, was omitted from the regression analysis.

Table XVIII also shows that the relation between wear rate and interlamellar spacing is not the same at all contact pressures. The relation exponent, which can be taken as an evidence of level of spacing influence, decreases as the contact pressure is increased.

Table XVIII

Pearlite Interlamellar Spacing and Wear Regression Relations

[Wear Rate ($\mu g/m$) = $a(S_t)^b$]			
Po	a	b	r
1220	10431	0.47	0.64
1080	2138	0.70	0.73
900	788	0.80	0.67
700	7.97	1.51	0.79
500	5.51	1.33	0.81

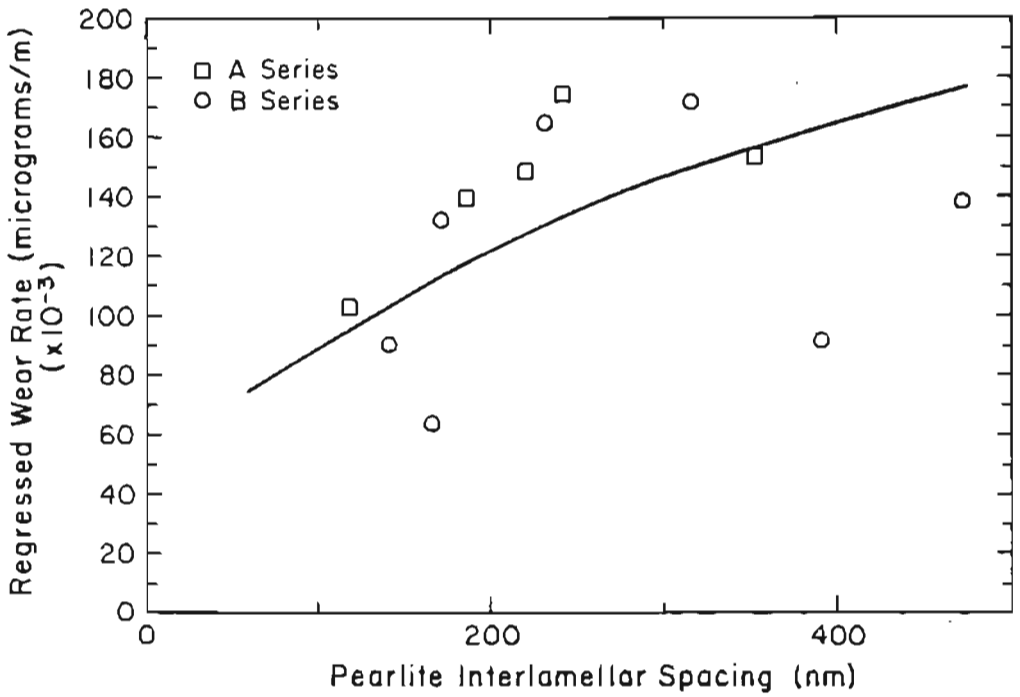

Figure 36. Amsler wear rates versus pearlite interlamellar spacings at 1220 N/mm^2 contact pressure.

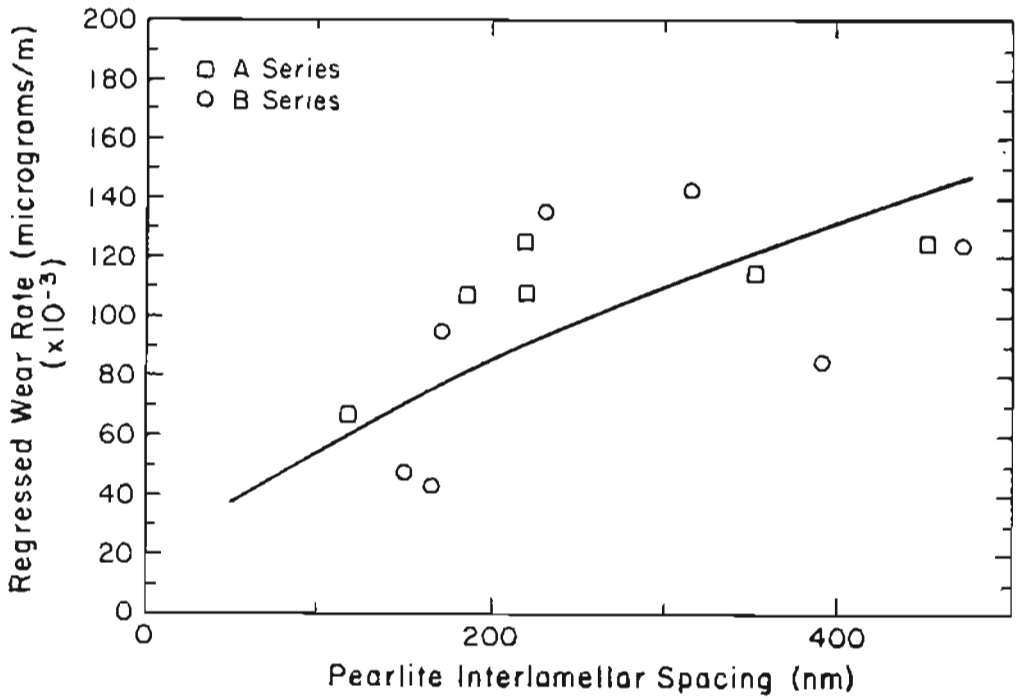

Figure 37. Amsler wear rates versus pearlite interlamellar spacings at 1080 N/mm^2 contact pressure.

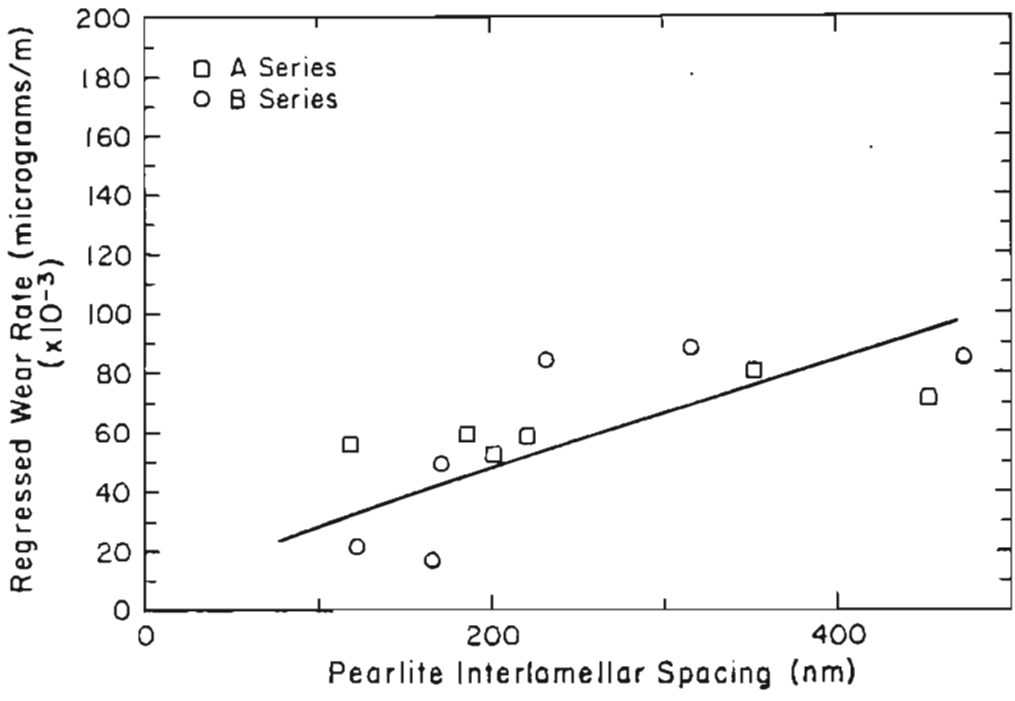

Figure 38. Amsler wear rates versus pearlite interlamellar spacings at 900 N/mm^2 contact pressure.

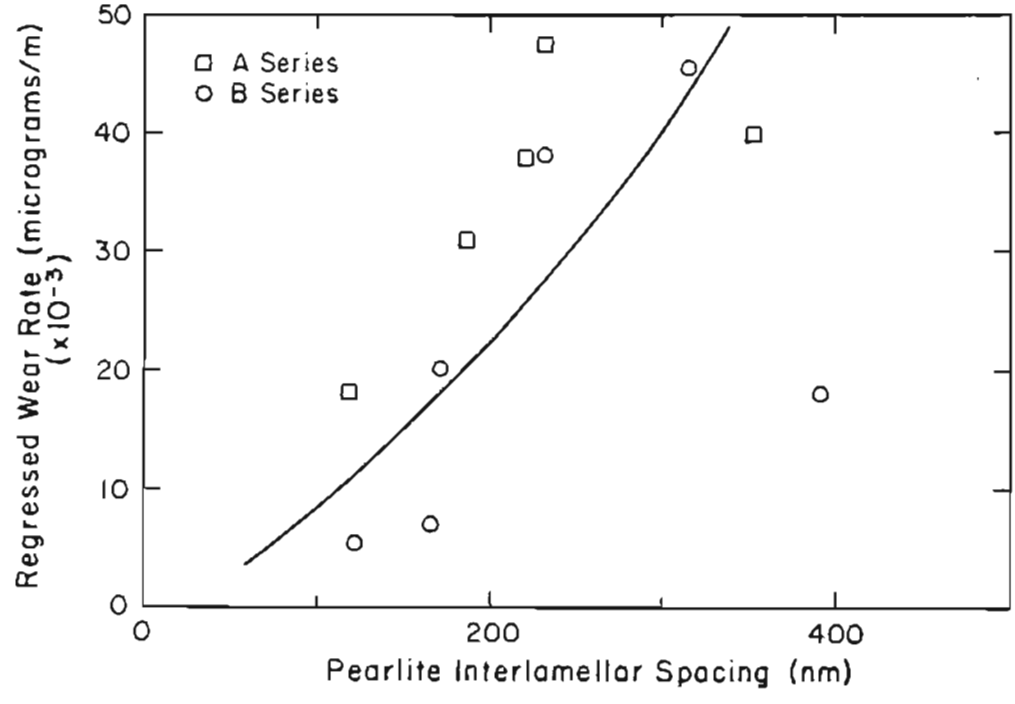

Figure 39. Amsler wear rates versus pearlite interlamellar spacings at 700 N/mm^2 contact pressure.

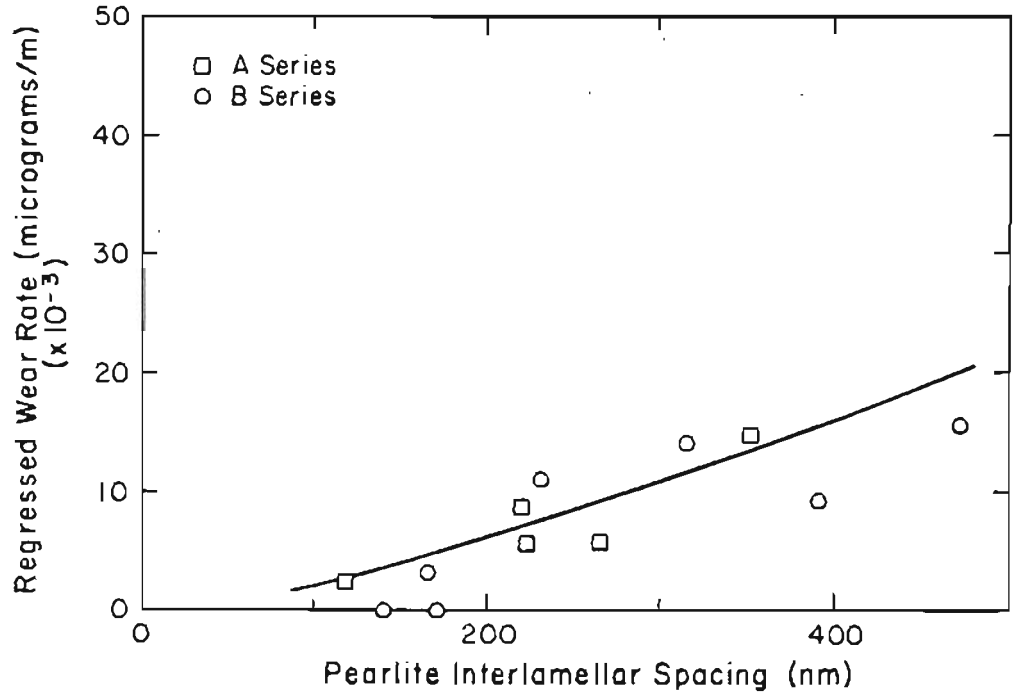

Figure 40. Amsler wear rates versus pearlite interlamellar spacings at 500 N/mm^2 contact pressure.

Amsler wear rates in this project have generally been stated in terms of weight loss per distance rolled, but for comparison with field measurements the μg/m units have been converted to inches/MGT. Most of the Amsler test wear rates were in the range of one half million inches/MGT (one-half inch/ton).

Because roller diameter is reduced during each wear test, the original slide/roll ratio of 35% is not maintained throughout the test. Roller diameters were measured after the completion of several wear tests and the slide/roll ratio re-calculated based on the worn diameters. The slide/roll ratio was found to increase slightly in most cases by a few percent, and in the worst case increased to 40% from the original 35%.

With one notable exception, the wear rates obtained were as

expected: the higher hardness microstructures possessed better wear resistance. The softest heat treated CrMo specimens, the B5 series, although only a hardness of 90 Rb (10 Rc or 187 BHN), had wear rates that were comparable to those of the 34 Rc CrMo. The microstructure was different from that of the other steels, tending toward spheroidized pearlite. Because previous researchers have found no advantages in such a microstructure [44], another heat treatment was performed (B6) in an attempt to duplicate the microstructure and verify the wear rates. Although the B6 microstructure was comparable to that of B5, the wear rates were not. The wear rates of B6 were close to that predicted by the spacing/wear rate relations.

Initial Roller Surface Damage Investigation

The determination of break-in wear rates was conducted on specimen A7 at 1080 N/mm^2 contact pressure and consisted of weight loss measurements every ten revolutions (except at 30) for the first 100 revolutions and at 100 revolution intervals thereafter until a total of 500 had been reached. The amount of material lost increased linearly as the percent of damaged roller surface increased. The first 300 revolutions of the test are shown in Fig. 41. The wear rate between 0 and 100 revolutions was 7100 $\mu gm/m$, compared to the final steady state wear rate of 66,800 $\mu gm/m$.

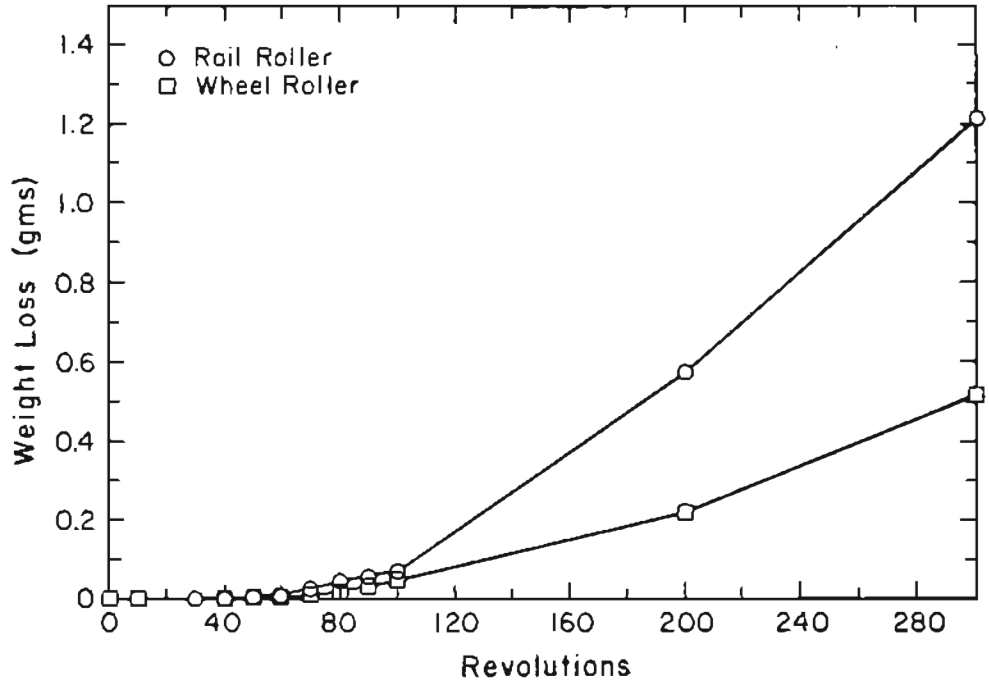

Figure 41. Weight loss vs. revolutions for the first 300 revolutions of the total 500 of test A7 at 1080 N/mm^2.

The second test in investigating the initial stages of surface damage documented the first occurrence of a Type III wear scar produced by a particle caught in the contact zone. Fig. 42 is a composite of SEM photographs of that first groove on the rail roller. The scar measured approximately 3 mm long and .25 mm wide. There were other isolated spots of damage on the roller surface which were not Type III, but Type I in nature. Original machining marks were visible on most of the surface. The damage occurred after approximately 25 revolutions.

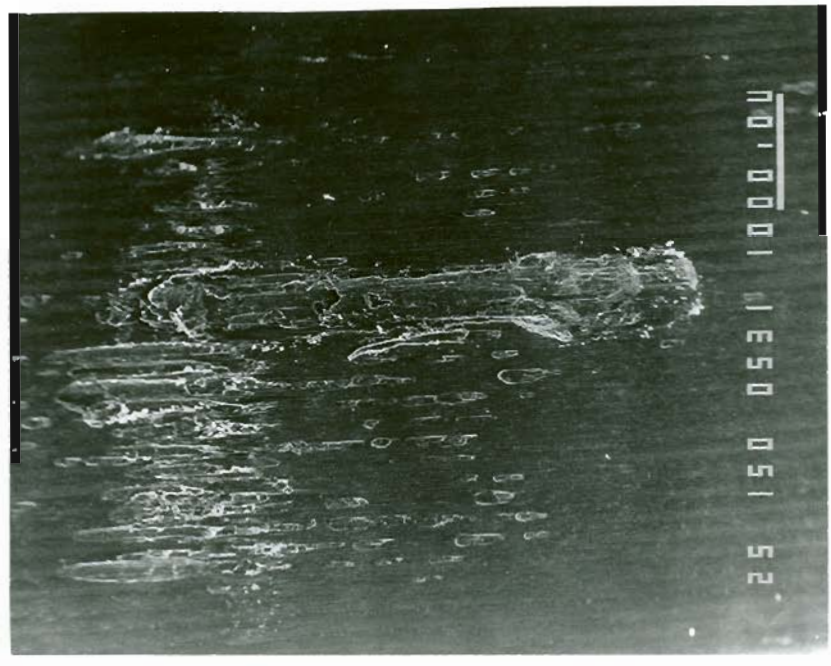

Figure 42. The first Type III wear groove produced on an Amsler roller after approximately 25 revolutions at 1220 N/mm^2 contact pressure.

Amsler Heat Treated Rail Deformation Series

The lubricated deformation tests were performed on the Amsler rig with identical 35.0 mm diameter rollers on both top and bottom shafts. A typical diameter loss and contact width increase vs. revolutions is converted to a semi-logarithmic plot of dimensional change vs. log of revolutions for data analysis (Fig. 43). The rate of dimensional change was calculated by a linear regression analysis of the semi-logarithmic plots of dimensional change vs. revolutions. Deformation rate is defined as the change in dimension (either diameter loss or contact width increase) per base 10 logarithm of the revolutions.

The rate of contact width increase and roller diameter decrease are listed in Table XIX and are plotted in Fig. 44. Softer rollers in all cases experienced higher deformation rates. The actual deformation

rates covered a range of .198 mm/m to .361 mm/m diameter loss, and .634 mm/m contact to 1.073 mm/m width increase from the highest to the lowest hardness. There did not appear to be a distinction between standard carbon and CrMo of similar hardnesses.

The soft CrMo material that unexpectedly performed so well in the wear tests did not display any exemplary deformation characteristics. It had a deformation rate of .361 mm/rev, which was what would be predicted based on its hardness and the hardnesses and deformation performances of the other materials.

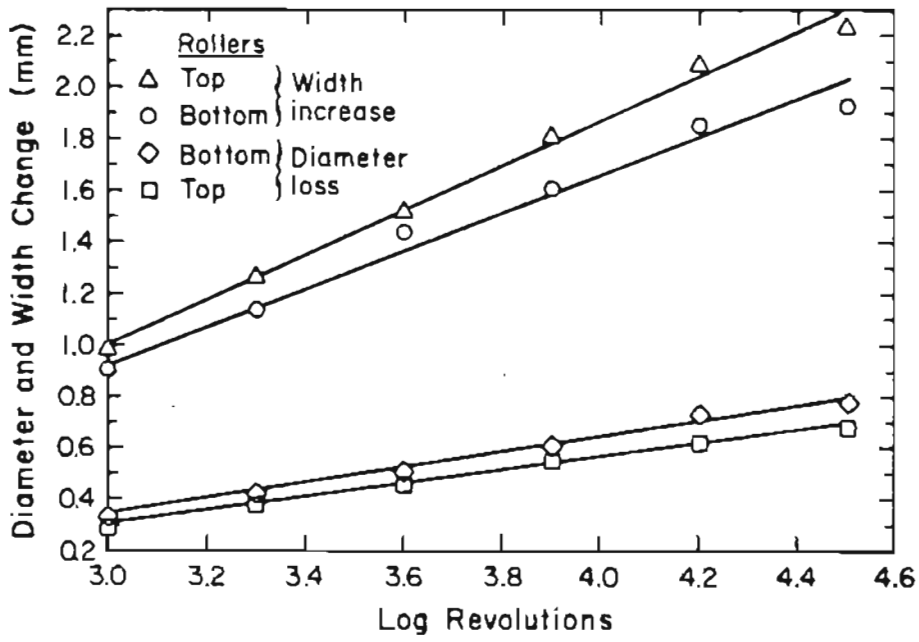

Figure 43. Typical semi-log Amsler roller diameter loss and contact width increase with increasing deformation test revolutions.

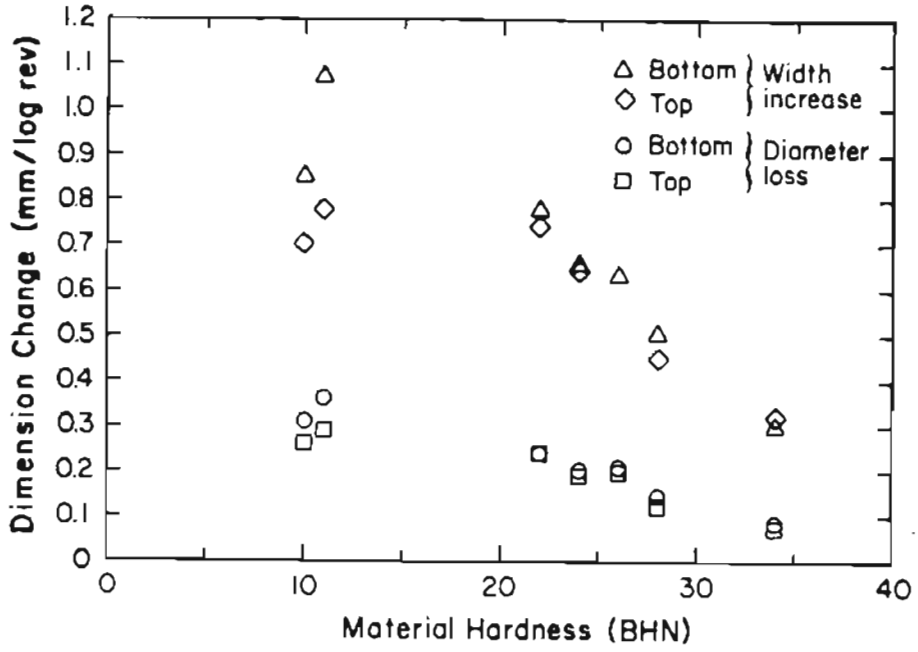

Figure 44. Heat treated Amsler roller deformation rates.

Table XIX

Deformation Rates of
Heat Treated Rails (mm/log m)

	Diameter Loss		Contact Width Gain	
	Top	Bottom	Top	Bottom
Standard Carbon				
A3	.198	.206	.647	.634
A4	.241	.239	.741	.778
A5	.261	.311	.702	.854
CrMo				
B1	.074	.084	.315	.304
B3	.123	.144	.452	.505
B4	.191	.201	.648	.658
B5	.290	.361	.779	1.073

Wear rates of the specimens under the fully lubricated deformation tests were very low, approximately 40 $\mu g/m$, and did not contribute to the diameter changes.

Repeatability Series

The series performed to identify the ability of the Amsler test rig to produce consistent results given nominally identical test parameters resulted in standard deviations that were between 4% and 12% of the average wear value for all those tests. The average wear rates were 135800 and 65400 $\mu g/m$ with standard deviations of 15990 and 2690 $\mu g/m$ for the rail at contact pressures of 1220 and 900 N/mm^2 respectively. Table XX lists each individual test result and these results are summarized graphically in Fig. 45 by comparing them to wear rates of the standard carbon rail at the two contact pressures tested.

Table XX

Amsler Repeat Tests Wear Rates ($\mu g/m$)

	1220 N/mm^2		900 N/mm^2	
Test	Rail	Wheel	Rail	Wheel
1	116100	12200	69600	7100
2	162200	13300	63600	6900
3	140700	13800	61700	6100
4	153900	13100	66000	7100
5	137600	12400	65600	7100
6	141000	12600	66000	6900
7	136400	14000		
Average	141100	13100	65400	6870
Standard Deviation	14540	692	2660	388

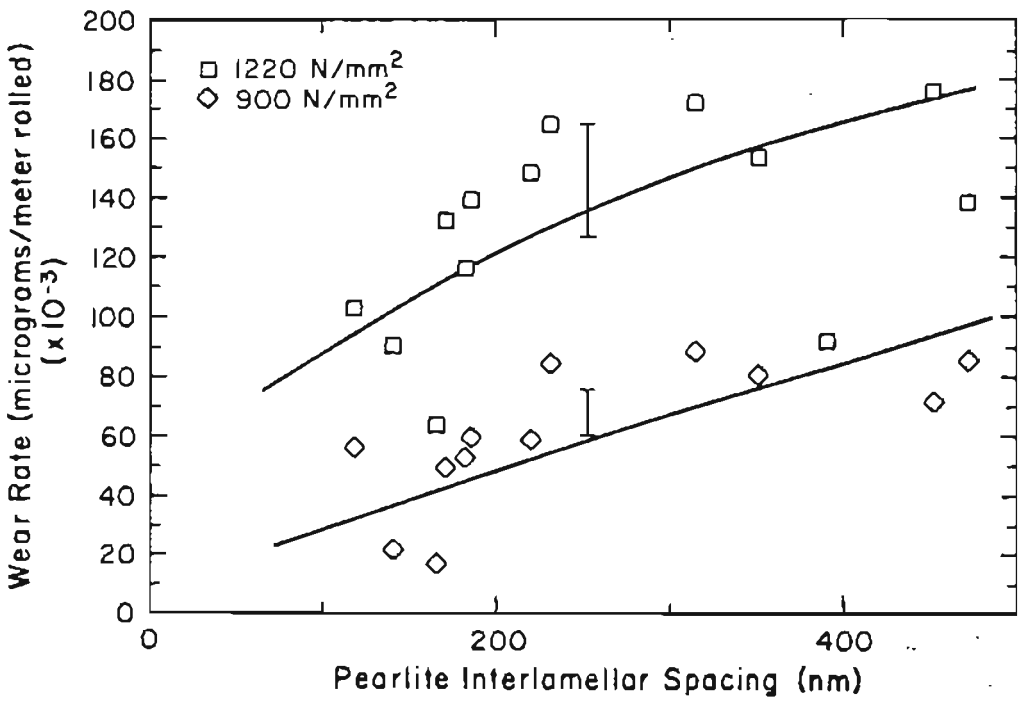

Figure 45. Standard carbon rail Amsler wear rates with Repeatability data superimposed at 900 and 1220 N/mm^2 contact pressures.

Wheel Steel Hardness Effects on Rail Steel Wear Rates

There were three opportunities in the Amsler wear tests to analyze the effect of varying the hardness of one component on the wear rates of the mating component. The first was comparing the wear rates of one rail run against two wheel steels. The second combination was five rail steels against the Class U (W1) wheel. The third chance, the most comprehensive comparison, was the Class C wheel steel (W2) run against fourteen rail steel conditions. Table XXI lists the various combinations that occurred during this program.

Table XXI

Dissimilar Mating Roller Combinations

Wheel	Rails
Class U (W1)	X21, 29, 30, 31, 32
Class C (W2)	X21, A0, A3, A4, A5, A6, A7 B0, B1, B3, B4, B5, B6, B7

The only rail steel that was run against both wheel steels was a standard carbon rail (X21), Table XXI. At three of the five contact pressures the rail had higher wear rates against the softer W1 wheel than against the harder W2 (Fig. 46). In four of the five contact pressures the difference was greater than 20%. Specifically the rail repeatability (X21 on W2) standard deviations were 4% and 12% at 900 and 1220 N/mm^2 respectively, while the rail wear rate against W1 was 25% on W2 at 900 N/mm^2 and 19% different at 1220 N/mm^2.

As expected it was found that the harder wheel possessed greater

wear resistance against X21 than did the softer wheel, Table XXII and Fig. 47. In all cases the softer wheel experienced a higher wear rate. Where the repeatability tests demonstrated no greater than a 10% variation among the wheel wear rates, the two dissimilar wheels displayed 32% and 43% divergence from each other at 900 and 1220 N/mm^2 respectively. The other three contact pressures had even a greater difference. A Student t significance test of the wheel data indicated that there is nearly 99% chance at both contact pressures that the two wheel wear rates belong to different populations.

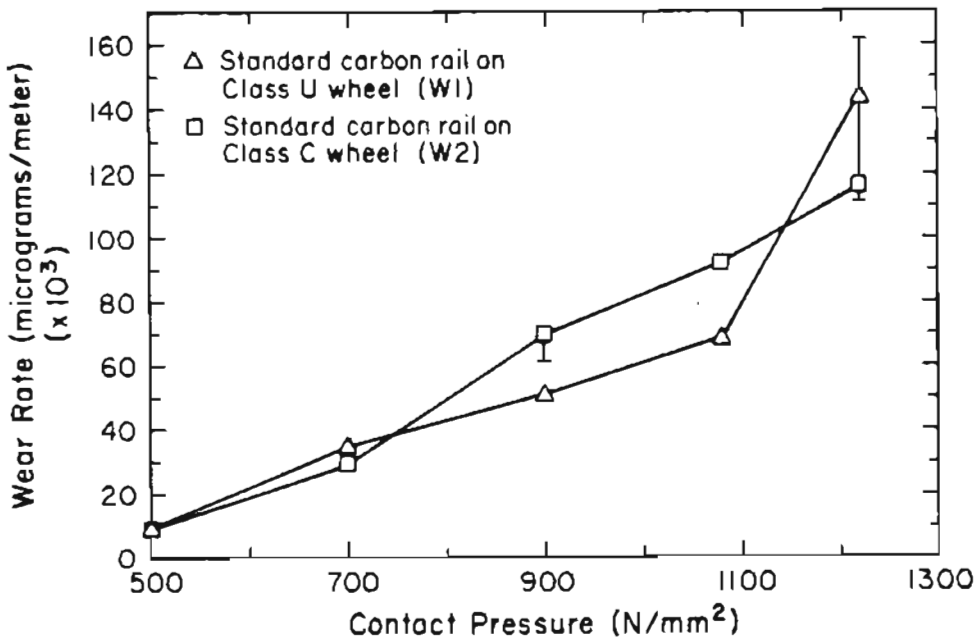

Figure 46. Comparison of standard carbon rail (X21) wear rates against Class U (W1) and Class C (W2) wheels. Error bars are not indications of statistical testing of the data in the figure, but are the range of rail wear rates produced in the repeatability tests.

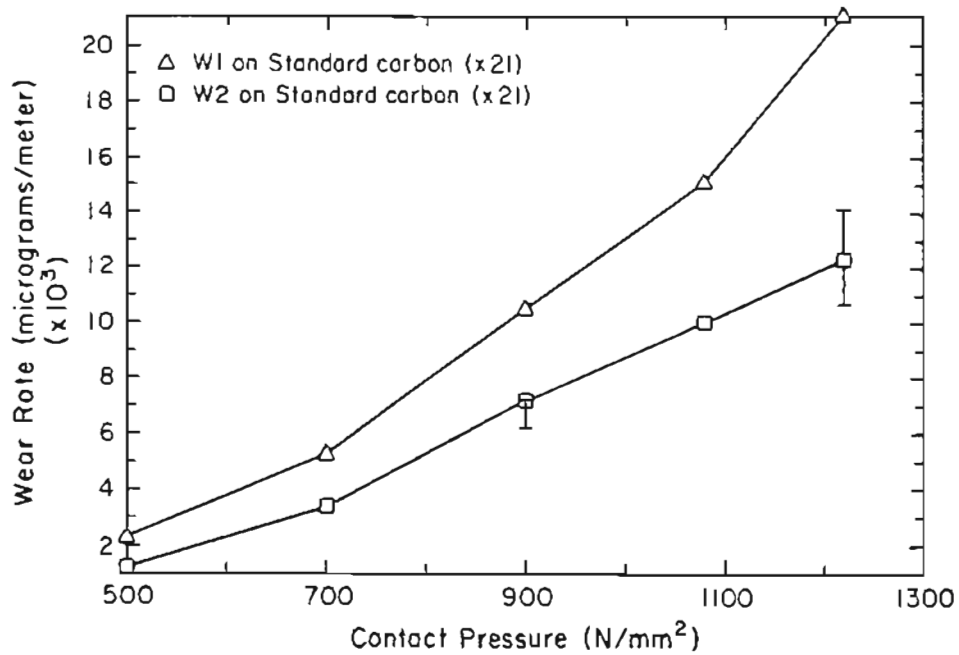

Figure 47. Comparison of wheel steel wear rates against standard carbon rail (X21). Error bars indicate the full range of wheel wear rates experienced in the repeatability tests.

Table XXII

Comparison of Wear Rates ($\mu g/m$) of
Standard Carbon Rail on Class U (W1) and Class C (W2) Wheels

Standard Carbon Rail Wear Rates on Dissimilar Wheels					
	Contact Pressure (N/mm^2)				
Rail	500	700	900	1080	1220
X21 (on W1)	9370	34620	51130	68430	144000
X21 (on W2)	8890	29400	69600	92000	116000
Wheel Wear Rates on Standard Carbon Rail					
	Contact Pressure (N/mm^2)				
Wheel	500	700	900	1080	1220
W1 (on X21)	2300	5230	10430	15020	21000
W2 (on X21)	1230	3380	7120	9940	12200

The second combination of wheels and rails was Class U wheel (W1) against two standard carbons (X21, X29), one MnSiCrV (X30), and two CrMo's (X31, X32). In this comparison, the effect of changing hardness of one component (rail) on the wear rate of the other (wheel) was checked by plotting the wear rate of the wheel against the different hardnesses of the rails for each of the five contact pressures (Fig. 48). At all contact pressures there is no increase in wheel wear rate until a rail hardness of 34 Rc (322 BHN) is reached. The only two rails that caused significantly higher wheel wear rates were the two CrMo's, with hardnesses of 34 Rc (322 BHN) and 36 Rc (336 BHN). The increase in wheel wear rate at the two highest hardnesses became less pronounced as the contact pressure was reduced.

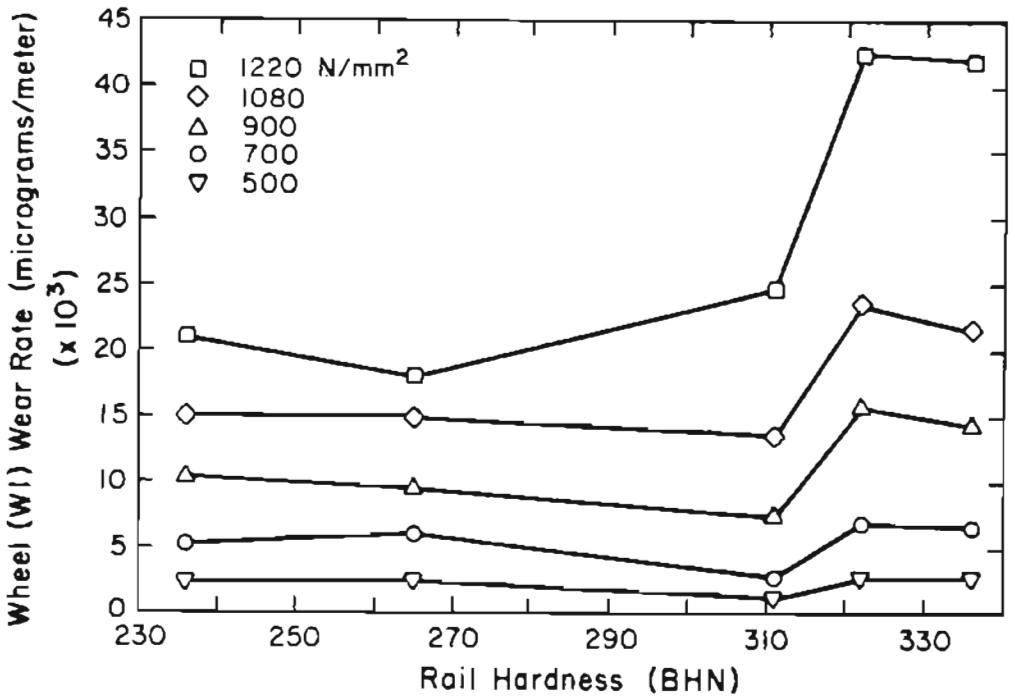

Figure 48. Class U wheel steel (W1) wear rates against five rail steels at five contact pressures.

The third wheel/rail matrix that could be used to judge changing hardness of one component on the wear rate of the other was the fourteen heat treated rail conditions that were run against one wheel steel, Class C (W2) (Figs 49 - 53). In these comparisons, wheel wear rates generally increased with increasing rail hardness. The wheel wear rate increase was again less pronounced as the contact pressure was reduced. Contrary to the rails run against the Class U wheel, at like hardnesses the standard carbon rails caused higher wheel wear than did the CrMo.

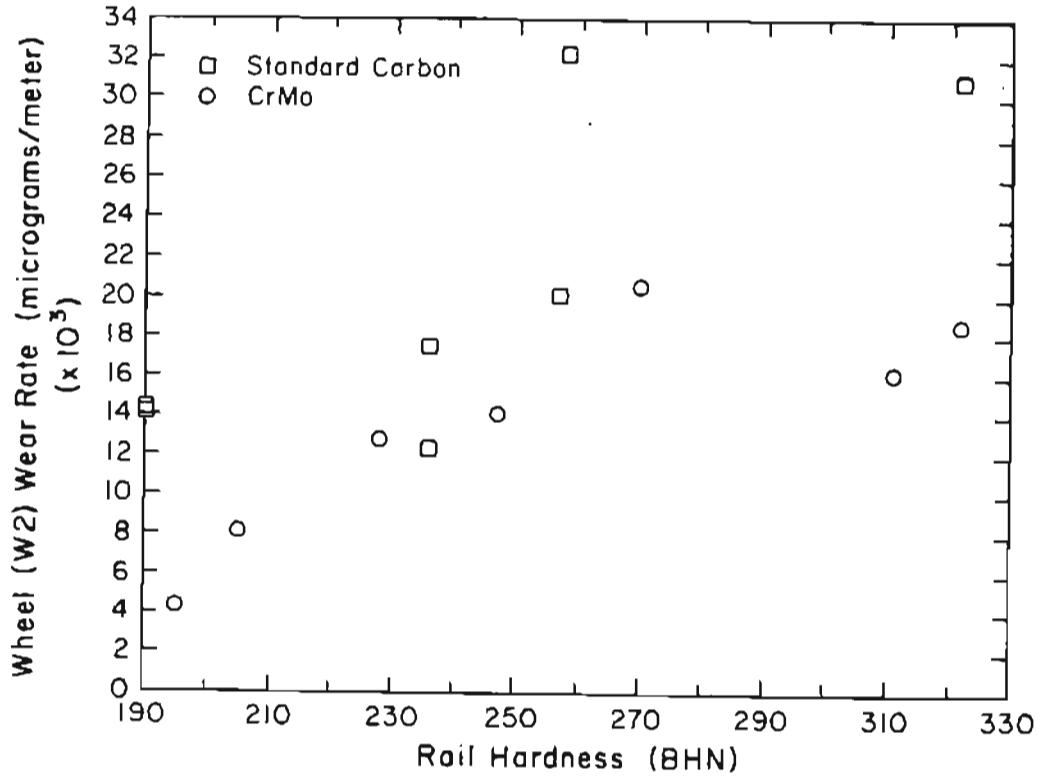

Figure 49. Class C wheel steel $(W2)_2$ wear rates against heat treated rail steels at 1220 N/mm^2 contact pressure.

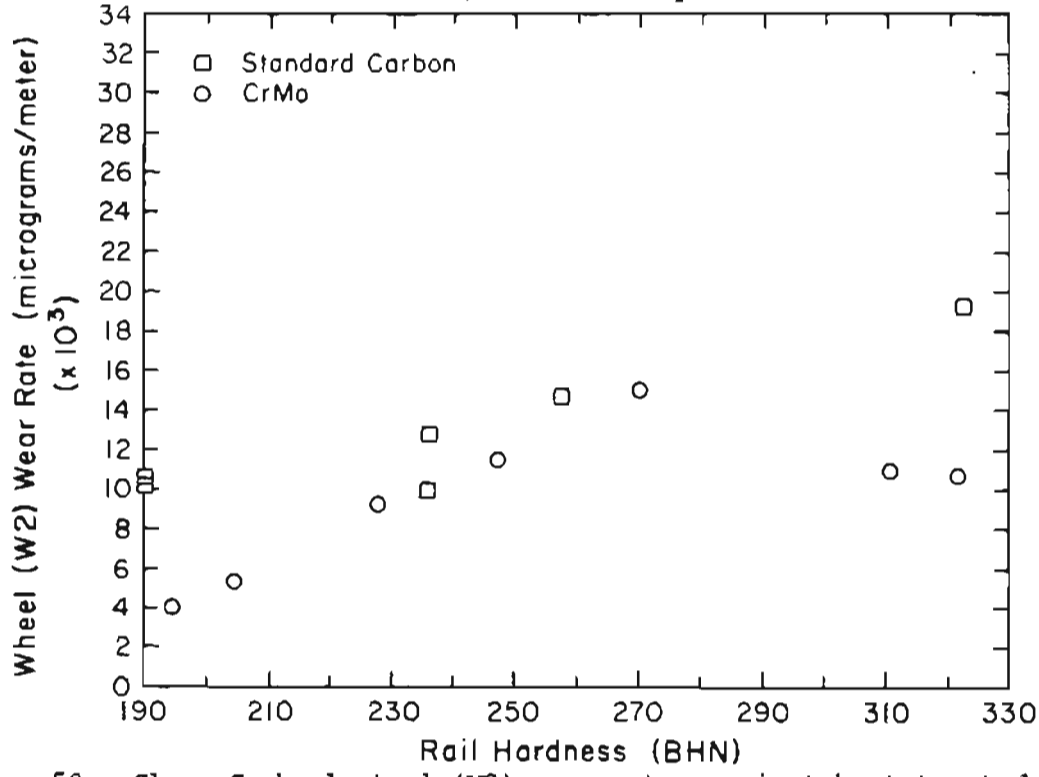

Figure 50. Class C wheel steel $(W2)_2$ wear rates against heat treated rail steels at 1080 N/mm^2 contact pressure.

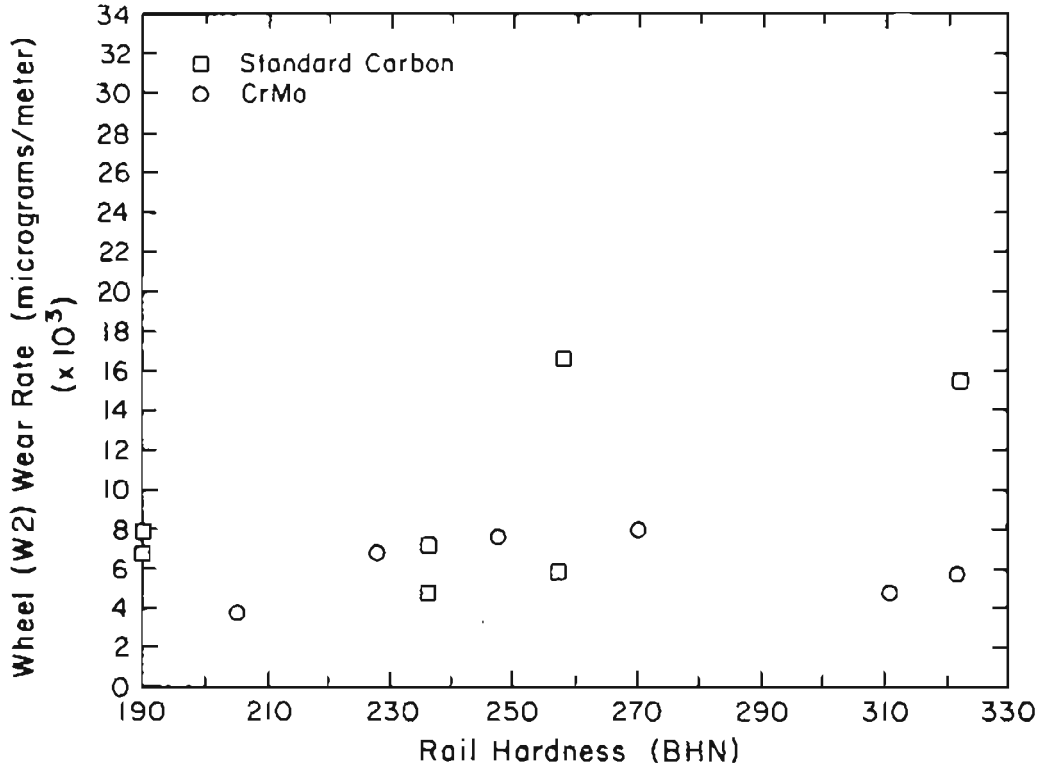

Figure 51. Class C wheel steel (W2) wear rates against heat treated rail steels at 900 N/mm^2 contact pressure.

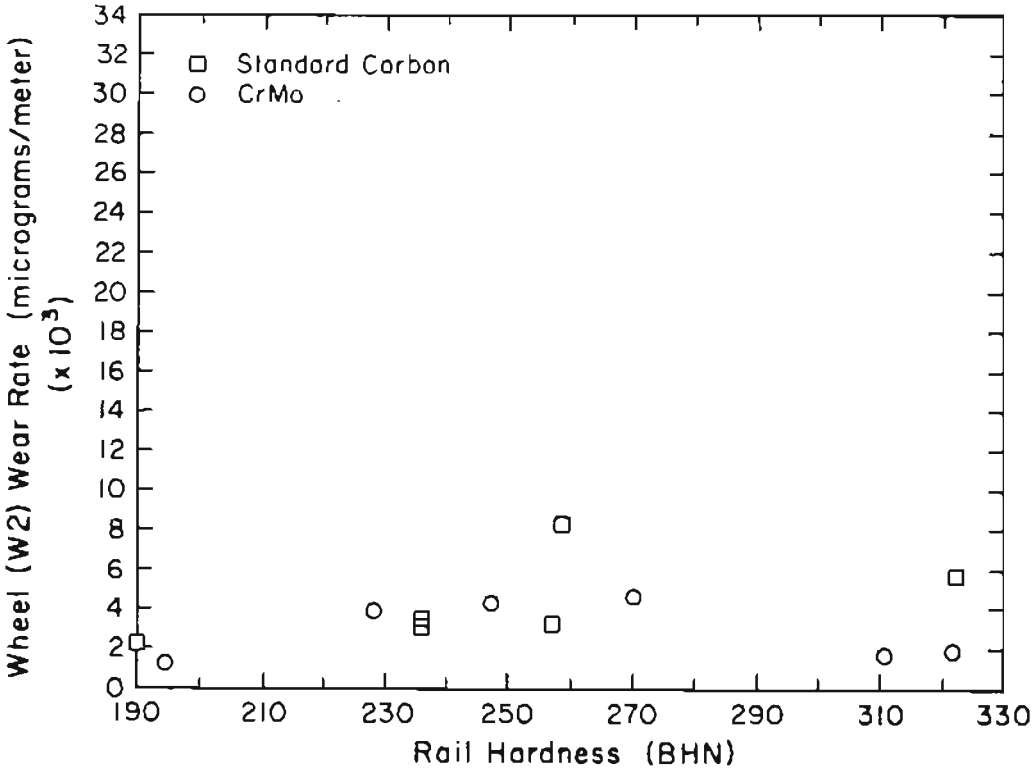

Figure 52. Class C wheel steel (W2) wear rates against heat treated rail steels at 700 N/mm^2 contact pressure.

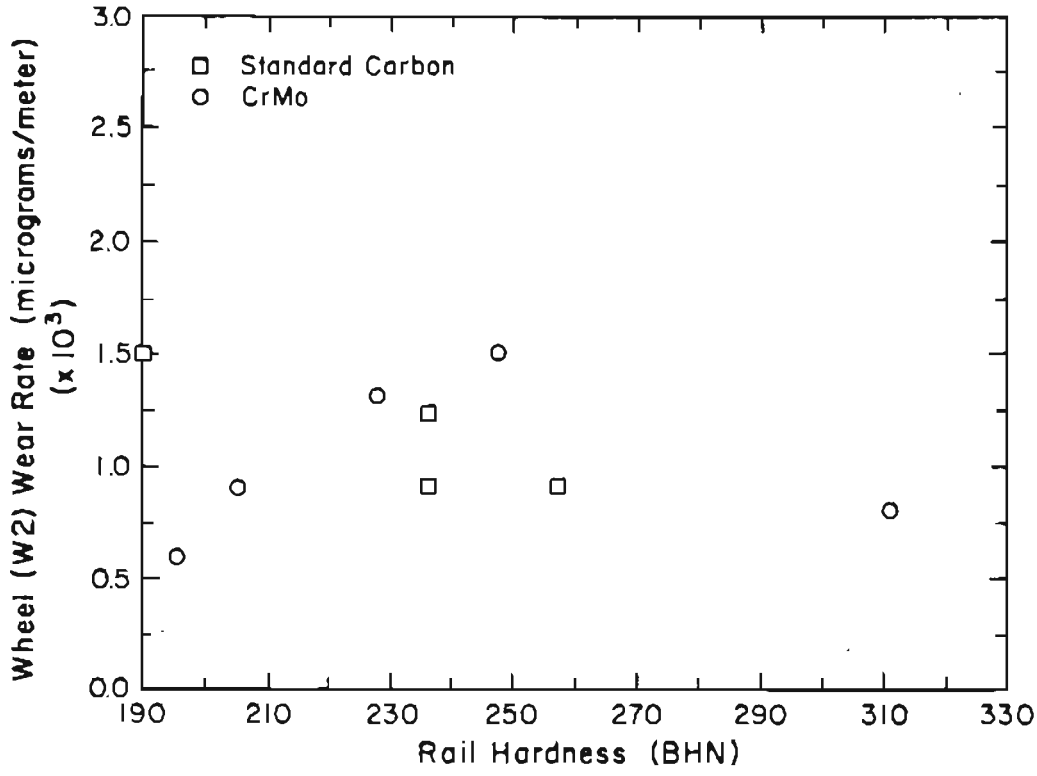

Figure 53. Class C wheel steel (W2) wear rates against heat treated rail steels at 500 N/mm^2 contact pressure.

Old Standard Carbon vs. Improved Standard Carbon Rail

The standard carbon rail used at the beginning of this program (X21) was manufactured in 1977 under the old manufacturing specifications. The standard carbon rail used for later portions of the project (X35) was manufactured in 1984 under the new Improved Standard (IS) specifications which include higher manganese contents and up to 0.3 wt. % chromium. During the course of testing these two rails were subjected to the same tests making it possible to compare the performance of the two standards.

Concerning chemical composition, the old standard rail contained slightly more carbon, phosphorous and sulfur, and significantly less chromium and copper. The older rail was also 4 Rockwell (22 BHN) hardness points softer, and had a pearlite lamellae spacing of 215 nm

compared to the new rail's 186 nm, Table XXIII.

The newer rail, however, experienced higher wear rates at all but one of the five contact pressures, Table XXIV. It is not possible to make a firm statement concerning their relative performances, however, based on the Amsler repeatability data, the differences were still within the 95% confidence interval of two standard deviations.

Table XXIII

Comparison of Old Standard Rail and Improved Standard (IS) Carbon Rail

	Lamella Spacing (nm)	Hardness Rc (BHN)	C	Cr	Mo	Mn	Si	S	P	Cu	Ni	V
Old Standard (X21)	215	22 (236)	.75	.02	.02	.98	.25	.03	.04	.07	.09	.004
Improved Standard (X35)	186	26 (258)	.63	.14	.05	.88	.17	.01	.01	.29	.13	.002

Table XXIV

Comparison of Old Standard Carbon Rail and Improved Standard (IS) Carbon Rail Amsler Wear Rates ($\mu g/m$)

Rail	Contact Pressure (N/mm^2)				
	500	700	900	1080	1220
Old Standard (X21)	8890	29400	69600	92000	116000
Improved Standard (X35)	11206	30916	59330	107054	139070
W2 on Old Standard	1230	3380	7120	9940	12200
W2 on Improved	3120	7830	14400	23900	26200

TENSILE TESTS

The results of the six tensile tests performed are shown in Table XXV and include .2% offset yield strength, true ultimate tensile strength, and a ductility measurement, percent reduction in cross sectional area. Those bars with the highest hardnesses and finest pearlite spacings were the strongest and vice versa. Although the ductility of standard carbon specimens increased with interlamellar spacings, the hardest CrMo tensile bar reduced 39% while the softer two lost only 35% cross sectional area. The pearlite interlamellar spacing for the appropriate heat treatments are included in Table XXV for comparison.

Table XXV

Tensile Test Results

Specimen	Lamella Spacing (nm)	.2% Yield Strength (KSI)	Ultimate Strength (KSI)	% Reduction in Area
Standard Carbon				
A3	216	67.4	165.6	27
A4	220	60.4	158.6	28
A5	452	44.6	154.4	34
CrMo				
B1	135	83.8	240.3	39
B4	231	75.1	220.3	35
B5	391	62.9	182.1	35

Discussion

LABORATORY PROCESS DEVELOPMENT

One of the first and very critical steps of this program was the development of a laboratory test procedure that closely simulated the wheel flange on a rail gauge face. Without an accurate duplication there would be no way to verify or judge the subsequent work with pearlite interlamellar spacings and wear characterization. Two test machines, a pin on disk machine and an Amsler sliding/rolling test rig, were considered based on past work, types of configurations available, and economic factors. After the two candidates had been used to test materials under the complete range of contact pressures, the advantages of the Amsler machine run under high load, high sliding/rolling conditions were apparent. There were many more similarities between the Amsler test conditions and the rail gauge face than between the pin/disk machine and the rail. Those similarities included the nature of the interaction between components in the contact zone, the degree and type of damage both surface and subsurface, and the wear and deformation rates based on relative wear resistance.

The relative motion between a point on the wheel flange and rail gauge face forms an arc with a range of diameters increasing with the distance from the running surface. It is not possible to say, however, that any one point on the flange maintains a constant contact with the rail. In fact, based on the nature of the gauge face damage and the physical configuration of the wheels and axles, the flange may strike the gauge face anytime the two are adjacent, be it either in the first

half or downward portion of the arc, or much less frequently, on the upward swing when the flange is exiting the contact zone. Even if the flange does maintain contact with the gauge face, the actual contact patch may change continuously as different asperities become the "high points" of the dynamic contact zone. Damage scars are most prevalent as downward sweeping arcs which coincide with the leading edge of the flanges' motion. The prevalence of arcing in one direction and the intermittent damage is evidence supporting the concept that most wheel flange/rail contact is on the leading edge of the flange.

The grooves and prows or mounds of material suggest that the contact is one of an asperity between the rail and the wheel. Another way to view this is as a third body abrasion wear type. If a suitable piece of debris is positioned appropriately, either on the rail or wheel, and introduced into the contact zone, it becomes the high point and produces the characteristic damage. Curves are often littered with this type of debris rejected from the contact zone.

This naturally leads to the question, however, where did the first piece of debris come from and how was it generated? In a rail situation it would be impossible to assemble a consist completely free of these potential abrasive particles. In an Amsler test starting with new roller surfaces the answer is not as obvious and is addressed later.

Another factor that supports the similarities between a high slide/roll Amsler test and the rail gauge face can be found in cross section surface damage. In particular, section views of a groove and associated mound from both laboratory specimens and actual rail contain many common features. Directly preceding the grooves in the rail are

areas of relatively undisturbed material. Farther into the groove sub-surface layers become more and more disturbed. The adjacent prow is usually made up of layers of parallel pearlite lamellae that have been displaced from the groove to the mound. Cracks in both situations are normally associated with the downstream side of the mound (opposite from the groove), and are not true, sharp, growing cracks, but more properly cold laps or seams due to the re-deposition of the material. Like the cracks found in the rail, the Amsler cracks extended through approximately 3/4 of the depth of the deformed material.

In general, the damage on the rail gauge face was more intermittent than that found on the Amsler rollers. That is, the roller surfaces had no areas of completely undisturbed material, which is due to the fact that the rollers are smaller and no location can, over the course of a 1500 revolution test, entirely escape interacting with the mating roller.

Although duplicating wear mechanisms is certainly an important aspect of field simulation, the final test was how accurately can relative rail resistances be predicted. With the four FAST rails differing from the laboratory relative wear resistance rankings by a maximum of .55 for weight loss and .33 for diameter loss, a significant amount of confidence can be placed in the relative wear resistance predictions. These figures are in fact, surprisingly accurate given the wide variety of uncontrollable parameters present in the field that are either non-existent or purposely held constant in the laboratory.

To complete the comparison between the laboratory and field tests the differences between the two situations should be listed. The first

and most obvious is size. Railroad wheel diameters are approximately 25 times larger than the Amsler rollers. And, as mentioned earlier, the size of the surface damage features are also scaled down in the Amsler rollers.

A second difference can be found in one of the conversions of the wear data. Most rail wear is conveyed in terms of gauge face material lost per accumulated gross tonnage carried by the rail, i.e., inches per million gross tons (in/MGT). If the relative wear resistance and mechanisms are similar, the next step would be a conversion of the laboratory wear rates, in this case a weight loss per rolling distance (μgrams/meter rolled), to that of in/MGT. The conversion of Amsler wear data to in/MGT, however, does not lend itself to this comparison. While operating rail systems experience real gauge face wear rates in the range of up to .01 in/MGT [50], a conversion of the Amsler data results in approximately one half million in/MGT.

The most obvious source of the difference in this comparison would be the method of conversion. For example, if the conversion had been based on the volume loss rather than profile loss, the results may have been more comparable. The way the accumulated load is treated could also change the final figures. There are many possible variations of the conversion process, any number of which may produce a better correlation.

Factors other than the conversion itself may also influence the final comparison. Already considered as a major difference is the size of each system. Although the contact pressures are approximately comparable, there is still the 25 times difference in diameter between

wheel and Amsler roller. The most difficult parameter to quantify, however, is the nature of the contact zone between the wheel flange and gauge face. While several studies have attempted to model the contact patch [51-53], intuitively one would conclude that an enormously wide array of conditions exist, from an instantaneous brush in a tangent track to a constant crushing with both large and small contact patches in curves. Other factors, such as weather, are also excluded from laboratory tests. Overall, the relative wear resistances and the types and degrees of damage produced in the laboratory are encouragingly close to the data from FAST.

This project illustrated the need to exercise caution in making comparisons between the pin-on-disk work that produced two sets of wear rates with a slight modification of the test rig. Another example of the dangers of direct comparison is the relationships of the pearlite interlamellar spacings and hardness versus wear rates. The relationships were originally calculated in terms of Rockwell hardness units, but then converted to Brinell. Due to the difference in the hardness measuring principles of Rockwell and Brinell, however, the relationship between the two is not linear, and, if the spacing/hardness relationship is regressed in terms of Brinell instead of Rockwell, the exponent is halved. This is further evidence that a seemingly simple relationship between hardness and spacing, for example, cannot be cited or utilized without closely examining ostensibly insignificant experimental details.

Though not pivotal for the rail wear environment, the three types of wear encountered in the initial Amsler matrix have now been documented by two wear laboratories. [54] In the wear world this duplication of

what appear to be identical wear characteristics is indeed a noteworthy occurrence. Type I, primarily oxide flaking, does not appear to be unusual and follows along Welsh's explanation that a strong enough substrate will support an oxide, reducing the overall wear rate by limiting metallic debris removal [34]. Type III is also not difficult to rationalize with a third body abrasive explanation. Type II, however, defies easy interpretation. Though Type II wear rates are in between Type I and III, it is difficult to say if Type II is a transition or completely separate wear mechanism. The absence of both oxide and large metallic debris indicates that it is unrelated to either I or III. The fact that some heat treatments experience a transition into or out of Type II at different loads than other materials also lends credence to a completely new mechanism. But enough plastic deformation to produce the distinctive ripples may be the first stages of the plastic damage required for the beginning of Type III debris generation. This amount of deformation may also be preventing the formation of an oxide. Some of the harder materials never did wear by the Type II mode and alternated between Type I and III. All things considered, the uniqueness of the types of damage seem to be the overriding factor in deciding the three modes are separate and not mere perturbations of one another. As suggested by the original authors [49], however, the entire discussion may be one of semantics until such time that the wear process is controlled and, for example, rail wear is kept in Type II instead of Type III.

Another idiosyncrasy of the Amsler test that deserves mention is the tendency of the smaller roller to experience a higher wear rate. This effect has been noted but not explained by at least three laboratories [49, 54]. The most obvious explanation would be one of damage per unit area. If a single encounter produces equal damage on both rollers, the smaller roller, having a shorter circumference, must absorb equal damage in less material. Both rollers, however, do not necessarily experience equal sliding distance contacts. Since the upper roller is revolving at a slower rate than the lower roller by a factor of .909, the length of each encounter for the upper roller will be reduced by that much with respect to the lower roller. For 35 mm diameter upper and 45.2 mm diameter lower rollers, a 22% difference, this peripheral velocity factor only accounts for approximately half of the wear difference. Extended, this would mean that given identical materials for both the upper and lower rollers, the wear rates would be equal with an upper roller diameter of 35 mm and a lower roller diameter of 31.8, or approximately .3% slide/roll ratio. The closest this project came to verifying that prediction, however, was the old standard carbon rail (X21) on the Class U wheel (W1) at 1% slide/roll. This resulted in equal wear rates (within the accuracy of the test) for both rollers at two of the three contact pressures, and the rail (the larger roller) wearing faster at the remaining pressure. This comparison is not conclusive, though, due to the uncertain accuracy of the test at those low wear rates.

AMSLER REPEATABILITY

The need to perform the repeatability series arose after the W1 wheel steel had been expended. The repeat tests were run with the new W2 wheel to determine if the wear rates of rail steel running against the two different wheel steels could be considered to be from the same population. The data has provided a basis for comparison of the results from this project and from those of other laboratories. The variance has been used to make judgments not only about the inherent spread of Amsler test data but also on the effects of altering wheel steel and rail steel chemistries and hardnesses.

In addition, work performed at different centers has been used to evaluate the relevance of the data. [55] In comparison with all the other testing methods, the Amsler test ranks quite well. Where this project found standard deviations to be approximately 20%, other projects often experienced 4 to 10 times greater variations. [56]

The variability in the data may be caused by a couple factors. The random arrangement of the materials on the atomic scale (grain and lamellae orientation) probably contributes greatly to the random nature of the wearing process, along with the action of debris and contact patch mechanics. Test machine aberrations are less likely to produce such an arbitrary pattern, and the laboratory environment eliminates other variables by controlling such parameters as temperature and relative humidity. It is also possible that the variations seen in the wear data can be attributed to that all encompassing "statistical nature of wear."

PIN/DISK

The pin/disk test rig was selected as a possible candidate for rail simulation testing because several of its features were attractive. First it is easy to justify the use of a 100% sliding condition because a strong argument can be made that the rail gauge face/wheel flange interface is 100% sliding, despite the sliding/rolling nature of the running surfaces. [57] In addition, the pin/disk can be configured in a variety of ways by changing such factors as sliding speed, wear path diameter, pin diameter, pin length, specimen cooling, lubrication, materials and microstructures. Once debris has formed and is present, a third body wear mechanism would exist with debris being re-introduced into the contact zone.

Disadvantages with a pin/disk simulation of a wheel/rail system would include, first and foremost, the continuous nature of the contact on the pin face. While an area on the wheel contacts once per revolution, the pin sliding on a disk is always contacting the mating surface. Here the pin diameter and subsequent contact patch are variables that would be difficult to characterize. If the debris is indeed swept into the contact zone, it is likely that the distance over which it is trapped would have an influence on the wear rates.

A constantly contacting surface would also have a tendency to exacerbate any frictional heating effects. And, while cooling systems are possible, it is almost impossible to insure that the contact zone is free from flash temperature influences that may or may not be present in a sliding/rolling intermittent type of contact.

During the course of testing with the pin/disk machine, there arose several questions that complicated the situation. At first the only variable was the applied load. A CrMo chemistry was then introduced as a second variable. But during the testing it was noticed that some applied loads appeared to produce more vibration and subsequent loss of contact at the pin/disk interface. After it was established that there was a relationship between the vibration and wear rates the machine was modified to reduce some possible sources of vibration. Not only did the vibration change, but so did the wear rates. The pin/disk's strength, its ability to provide a wide variety of testing parameters, became a liability in the form of a maze of test variables with no economic way to resolve them. In fact, since this program discarded the pin/disk machine as a possible candidate, more extensive in-house investigations have shown that the other variables have more influence on the final wear rates than previously imagined. In particular, the sliding velocity, even with the presence of forced-air cooling, influences the wear rate drastically. The investigations also demonstrated that much of the work done here and previously [8] was dwelling on the edge of major wear rate transitions. [58]

The pin/disk modifications improved the machine's operating characteristics significantly. Exclusive of the vibration analysis, visual observations alone show that contact between the pin and the disk was much more constant, with more uniform sliding motion and decreased overall vibration. Future test results should more closely reflect the wear environment being tested and less the machine characteristics.

The vibration analysis was a different problem. Originally vibration values were recorded mid-way through each test. The question was asked, however, does one mid-test value accurately reflect the vibration state throughout the entire test? Consequently, the peak-to-peak voltages were recorded every second for one entire test. It was found that the magnitude of vibration decreases as the test progresses, dropping to less than one fourth of the initial value. This is an indication that the pin and disk wear into conformity as more deformation and material removal takes place. Although it was not experienced in this test series, it is possible that the vibration could increase if, for example, corrugations develop on the disk as sometimes happens during pin/disk testing. The vibration data for the reconstructed machine do indicate slightly higher vibration in the mid-load region at lower wear rates. There is enough variability of the vibration data in just one test, however, to make it difficult to conclude that the overall vibration in that load range is consistently higher. A more reasonable conclusion is that there is a need to carefully document seemingly insignificant test procedures and to exercise caution when comparing test results obtained from supposedly similar machinery.

Instrumentation

The disk revolution counter, LVDT and accelerometer generated good data. The Apple IIe also performed well, providing a real time plot of pin loss and sliding distance that was useful in determining test lengths. In addition, the calculations of weight loss, sliding distance, and ultimately wear rate in volume loss per unit sliding

distance were accurate, as checked by pin weights before and after the test. The source of greatest error was the disk groove depth which appeared to the LVDT as additional pin height loss. By recording the pin weight and length before and after the test, the groove depth contribution to the apparent wear was eliminated from the calculations. This groove depth effect can also be negated by increasing the diameter of the wear path and reducing the amount of wear at any one location in the wear path if disk materials permit.

The accelerometer used to assess the pin vibration also supplied useful data in determining the slip/stick nature of the contact zone for both pre and post drive line modification conditions. What the accelerometer could not directly display was the instantaneous load between the pin and disk.

The only vibration still present appeared to involve the machine as a unit, rather than of one component. This is an indication that the specimen securing components now match the overall machine rigidity.

DEFORMATION TESTING

Deformation testing was conducted to investigate the possibility that the various microstructural conditions may possess indirectly related resistances of wear and deformation. There would be no advantage to good wear resistance if excessive plastic flow renders the material useless. The tests were conducted in the fully lubricated state to avoid the dry wear rates. The rate of deformation was characterized by contact width increase and roller diameter decrease

per cycle. The best use of the information can be found in the comparison of the wear resistance to the deformation resistance. This comparison should indicate if any of the materials were more susceptible to one form of degradation or the other.

There were no cases, however, where the two parameters did not rank the materials in the same order. Those microstructures that were relatively wear resistant also possessed good deformation resistance. The softest heat treatment, B5, with a hardness of 91 Rb (BHN 190), provided an interesting example in this comparison. B5 was a partially spheroidized CrMo that wore at an unexpectedly low rate relative to the other heat treatments, based on hardness and pearlite spacing. Although the deformation test did indicate slightly more deformation for the hardness, it was not enough to explain the extraordinarily low wear rate in terms of material displacement instead of loss.

Initially the B5 heat treatment was particularly attractive in terms of wear mechanisms, because it performed as well as much harder rails without an immediately obvious explanation. One of the first possibilities considered was an inconsistency in the experimental process, either material, heat treatment, wear testing or final wear rate calculations. The experimental sequence, however, did not lend itself to a chance error, because the various steps were conducted on all heat treatments in series, precluding the occurrence of a random error each and every time the B5 rollers were handled. The next possible cause of the low wear rates, discussed previously, was that the deformation resistance was disproportionately low relative to the wear resistance for the material hardness. A third possibility was

that a different wear mechanism was operating. A second heat treatment was conducted (B6) and the microstructure of B5 duplicated as closely as possible. The wear properties of B6, however, did not confirm those of B5, even though the hardnesses were similar. The microstructures were also similar, though B6 was slightly less spheroidized. Wear tests conducted on the second heat treatment produced wear rates that coincided with the relationships established by the other materials and thus much higher than that of B5. If indeed the B5 microstructure does hold some advantage, it would be necessary to first reproduce the wear rates with another test series, and second, to determine the reason why that particular structure performs as it does.

WEAR MECHANISMS

Visual observation during Amsler testing at high contact pressures and higher slide roll ratios provide strong evidence for a third body abrasive mechanism. Similar rail gauge face damage suggests that the rail damage is also due primarily to a third body abrasive wear, with the third bodies consisting of debris from previous encounters. Richardson [27-28] did extensive work on wear by relatively soft abrasives and concluded that soft abrasives caused much the same type of damage as hard abrasives, modified only slightly by the size of the abrasive and the relative strengths of the abrasive and the parent material. He also noted that in heterogeneous materials that contain hard phases, the abrasive wear resistance is heavily dependent on grit size. Given the wide variety of abrasion scar size on the Amsler and gauge face surfaces, it is reasonable to believe that there is a wide

population of debris sizes and because all sizes are present, they will be effective as an abrasive grit.

The discussion of debris as a significant factor in the wear process immediately leads to such questions as where does the first piece of debris come from and what factors control the wear process? The first piece of debris is an interesting question, about which several theories exist. The delamination theory [22] would suggest that the surface strain is sufficient to cause dislocation motion and entanglements until a crack is formed and propagated releasing a chip of material from the surface. The adhesive wear concept would contend that some adhesion of the two surfaces occurred and when the junction was stressed at surface separation, debris was released.

The three wear "Types", I, II, and III, [49] might be included to explain initial debris by contending that the surface undergoes all three wear types sequentially as more damage is accumulated by the surface. Then, with ductility exhausted, continued deformation is not possible and regions with favorable (weakest) atomic arrangements (grain size, orientation, composition) rupture and debris is generated. After the first piece of debris is released it can escape the interface environment and take no further part in the process, or it can be recycled back through another contact zone. If recycled, it becomes a controlling factor in removing more debris because, compared to the local debris generating sites, a third body is much more significant.

This debris controlled environment leads to the next obvious observation, that more or less debris will determine the overall wear rates. If the system is relatively closed and debris cannot escape

readily, the wear rates would be expected to be maximized. Alternatively, if an effort is successfully made to remove loose particles from the components, one would expect lower wear rates. This would also suggest the possibility of a "debris saturated environment," where further increases in debris population will have no effect on the wear rates and a reduction will only decrease wear rates if the number of debris is lowered below some critical level of saturation. There have been efforts to determine the effect of "levels of debris population," though in a rail environment it may be of little value. Applied to the real world, it is hard to imagine that scraping train wheels to remove imbedded debris would actually reduce wear of the components. It seems equally unlikely that the rail/wheel situation is saturated, given the distance a generated particle needs to travel to be recycled through another contact zone due to the size of the components. The discussion then leads to the possibility that the wear in the case of the rail and wheel is controlled by debris population and controlling the debris may be as beneficial as controlling microstructures.

For the Amsler, the air cooling jet may have some influence in this "debris saturation." Initially, the air was provided to minimize temperature effects. It may be that the constant introduction of air removed enough debris from the surfaces to affect the wear rates by reducing third body encounters between the rollers, but limited work done without the cooling jet suggest that in the Type III mode, the wear rates will not be altered significantly. However, two factors should be kept in mind. One is that the test repeatability data scatter may mask a wear rate change as was seen previously, and two, it

could be that the Amsler roller interface is indeed already above the "saturated" level and that more debris than that removed by the air must be removed to significantly reduce roller wear rates.

The question of the first piece of debris warrants another volume. Indeed much has been written regarding the "breaking in" of tribological surfaces. Although an interesting aspect of this work, it was not a major factor in designing the experimental program. Using the analogy of a fatigue process that can be broken down into initiation and steady state growth stages, the wear process experienced by the rails is always in the second stage of deterioration. The "initiation" phase, in this case the generation of the first piece of debris, for all practical purposes does not exist and the situation is always one of steady state wear.

The initial or "running in" wear rates experienced by the machined Amsler roller surfaces coincides well with the amount of surface area contributing to Type III wear debris generation. The wear rates increased at an increasing rate until 100% of the roller surface was in the Type III mode. As another indication of the role of debris, two informal experiments were conducted by dropping debris into the contact zone before the surfaces had started to break down. In all attempts, Type III wear was immediately started once debris had been successfully introduced.

In some cases the roller surfaces regressed from a steady state Type III mode to Type I. This only occurred on the hardest microstructures tested. This transition could be a part of the advantages of finer pearlitic spacings. That is finer spacings provide more dislocation

barriers and therefore exhaust the soft sources more rapidly than a courser structure. This activates the harder sources producing a harder, stronger worked material near the surface. If the debris is no longer able to penetrate the surface and an oxide layer is given the opportunity to form, the material provides for a self shielding surface layer.

The reversion to Type I could also be explained by the saturated debris concept if the debris population decreased to a point that the oxide layer was permitted to form. This is not a likely scenario because the transition from Type III to Type I only occurred with harder materials at lower contact pressures, indicating that the transition is a result of material strength rather than debris population which had no reason to change.

WEAR/MICROSTRUCTURE RELATIONSHIP

At the risk of making comparisons warned against previously, it is still necessary to examine correlations between this and prior programs. Clayton's work [8] with a pin/disk machine produced an interlamellar spacing/wear rate relationship exponent of .97, compared to the range of .47 to 1.51 for the five contact pressures used in these experiments. Because the relationship between hardness and interlamellar spacing has been established, it is possible to consider past work that did not measure spacing but instead used hardness as an independent variable. Mutton [57] found wear rates decreased by a factor of two when hardness increased from 22 to 36 Rc (235 - 333 BHN) when testing on the large scale rig. A correlation between interlamellar spacing and yield strength [59] of $S_{-}^{-.5}$ to $S_{-}^{1.5}$, is similar to the interlamellar spacing and hardness indicated by the present data of $S_{-}^{-.42}$. As far as can be ascertained, therefore, the relations derived here are in general agreement with those from previous work.

Very little difference was found in mechanical properties as a result of compositional changes in the steels. This indicates that heat treating a standard carbon rail and a CrMo rail produces little to no differences in wear properties provided they have similar interlamellar spacing. Evidence [60] suggests that this is true only up to approximately 35 Rc hardness, where the microstructure of the standard carbon cannot be refined significantly further, leading to superior properties of the

CrMo only. The current program is continuing in this area and will involve the production and wear testing of finer structures of both CrMo and standard carbon.

Kalousek and Fegredo et.al. tried to establish, among other things, whether steels greater than 35 Rc (325 BHN) hardness exhibited an advantage over the present premium rail metallurgies. [61-65] They worked with several steel chemistries, one similar to a typical CrMo and another with increased vanadium. Microstructures ranging from refined pearlites to bainites and tempered martensites were investigated. The wear testing involved a sequence of lubricated and dry segments on a 1/8 scale rail/wheel wear testing machine. Most of the tests with steels of hardness greater than 38 Rc (352 BHN), however, were lubricated with completely dry segments being run only with steels less that 38 Rc (352 BHN). [60]

For the conditions employed the authors concluded that there was no advantage to increasing the hardness of the steels above 35 Rc (325 BHN) and that pearlite was superior to either bainite or martensite.

Masumoto et. al. [66] also did work comparing pearlites, bainites and martensites and came to the same conclusions that Kalousek et.al. had. Masumoto's pearlite hardness was about 40 Rc (360 BHN), and performed better than bainites or martensitic rails in dry twin roller tests. Pearlite spacings were not measured in these experiments. Another difference between Masumoto's testing and the current project was the loading, since he used 490 N on an 8 mm wide roller, approximately 550 N/mm^2, with 9% slide/roll ratio. If the two test machines are truly comparable, most of the wear generated by Masumoto's equipment

would be classified as Type I which could not be considered the best approximation of gauge face wear. Still, it is interesting to note that refined pearlite does possess greater wear resistance over harder microstructures in many applications and test conditions.

The present project has laid the ground work for testing microstructures with hardness values greater than 38 Rc (352 BHN). Heat treatments have been performed on CrMo and standard carbon rail resulting not in a traditional pearlite, but a "transitional" pearlite, which can easily be differentiated from bainite, and include hardnesses into the upper Rc 40's (450 BHN). Since this project has not completed that investigation, there is no information available to support the notion that increasing the hardness of the rail above 35 Rc (325 BHN) would be detrimental.

Heat Treatments

Heat treating eutectoid steel can be included among those tasks that all there is to know has long ago been documented and is common knowledge. There are innumerable charts, tables and plots that provide foolproof recipes to obtain any microstructure desired. Unfortunately, it appears, like pearlite, heat treating is an activity that contains many hidden variables that are seldom discussed in references.

Several sources exist that provide good heat treating background information, however. They include standard heat treating references [48], those articles written by or within the railroad industry regarding heat treated rail materials [4, 67], and other ferrous product manufacturers. Wire manufacturers have for decades been drawn to strong yet ductile steels that not only will perform well in final

product form, but can also be formed to smaller and smaller diameters.

A most ingenious piece of work was reported by Cahill and James. [68-70] The authors set out to find the relationship between patenting parameters and resultant microstructures and mechanical properties. Patenting is a term applied to the continuous heat treatment of wire which involves austenitizing, usually in multiple zone furnaces, followed by a rapid quenching, in past times in lead baths, today in less innocuous salt solutions, where transformation took place. Cahill and James were able to imbed thermocouples in wire less than .5 inches (12 mm) in diameter and feed the thermocouple laden wire through the patenting process while recording temperatures and times. They altered austenitizing temperatures, wire sizes, wire chemistry, wire surface condition, quench bath temperatures, and wire speeds.

There were several conclusions regarding the effects of austenitizing time and temperature. Although quenching from a lower austenitizing temperature produced more consistent microstructures due to the fact that there is less heat to withdraw, lower austenitizing temperatures required uneconomically long soak times. And, even though rapid transformation to pearlite was desirable with respect to final interlamellar spacings, the transformation speed increase due to inhomogeneous austenite also caused reduced final mechanical properties. Like temperature, austenitizing time also appears to have an influence on the final microstructure, with shorter times producing finer pearlitic spacings.

The authors found that transformation takes place at a temperature that is anywhere from 25 to 60 °C higher than the actual bath temperature,

and that by the time the specimen reaches the bath temperature, transformation is complete.

As discussed by Cahill and James (68-70), there are three considerations in controlling the austenitizing temperature. The first is the time required to produce 100% austenite prior to the isothermal treatment. The higher the temperature, the less time is required. At low austenitizing temperatures the transformation is inconveniently and expensively slow. The second consideration is the uniformity or homogeneity of the austenite. Non-homogeneous austenite, containing undissolved carbides or even non-uniform carbon distributions around locations of previous carbides, can cause the austenite-to-pearlite reaction to be accelerated or otherwise altered from that of a homogeneous structure. And, if the aim is the finest pearlite spacing possible, accelerated transformation may be advantageous. This non-uniformity is difficult to control, however, and, at least for the wire drawing community, is undesirable. The third consideration is the amount of heat to be withdrawn from a part required to lower it below the transformation temperature. Since precise control of the transformation is needed, the closer one stabilizes at a temperature near the transformation temperature, the more control one will have over the transformation rate. This requirement necessitates using the lowest possible austenitizing temperature.

Taking all three requirements into account results theoretically in a two step, or double austenitizing process. The first would be used to raise the part to a temperature high enough in the austenite region to obtain uniform austenite in the shortest possible time. The second step lowers the temperature to the minimum feasible, while still

remaining within the austenite range. After equilibrium has been achieved at that lower austenite temperature, the salt bath quench is performed. If the finest possible spacing is desired, the isothermal quench should be carried out with a salt bath temperature lower than that at which the transformation is required. This two step process was used in the current project with no discernible effect. Limitations of the heat treating equipment restricted the accuracy of the heat treating parameters.

Other groups have also made statements about austenitizing time and final microstructure. The contention that shorter times and lower temperatures enhance transformation kinetics has been supported by more than one research group including wire drawing [71], pearlite kinetics research [15], and more recently, the rail manufacturing industry [72]. The explanation put forth to explain the phenomenon says that although transformation from the parent microstructure to austenite is very rapid once the critical temperature is exceeded, full homogenization of all components residing in the steel is much slower, and that regions rich or lean in the various alloying or tramp elements can trigger faster transformations to pearlite due to constitutional supercooling or localized stresses.

Climax Molybdenum Corporation has had the opportunity to conduct extensive pearlite research, especially with respect to the effects of alloy additions and heat treatments. [71, 73-75] Their goal has usually been defined in terms of tensile strength, with rail quality categories including conventional rail with tensile strengths less than 100 ksi (690 MPa), high strength rail with strengths between 100 and

Fletcher and his associates, however, have not had the opportunity to conduct the relevant wear testing.

The advantages of pearlite have also been supported by Heller and Schweitzer [76], specifically they consider that increasing hardness improves wear resistance of pearlite and that pearlite possesses better wear resistance than either bainite or martensite.

Although the heat treatments required to obtain hardnesses greater than 35 Rc have been performed in this project, the wear testing of rollers has not. The structures obtained in the 35 to 48 Rc range are significantly different from traditional pearlite. In addition, the

remaining within the austenite range. After equilibrium has been achieved at that lower austenite temperature, the salt bath quench is performed. If the finest possible spacing is desired, the isothermal quench should be carried out with a salt bath temperature lower than that at which the transformation is required. This two step process was used in the current project with no discernible effect. Limitations of the heat treating equipment restricted the accuracy of the heat treating parameters.

Other groups have also made statements about austenitizing time and final microstructure. The contention that shorter times and lower temperatures enhance transformation kinetics has been supported by more than one research group including wire drawing [71], pearlite kinetics research [15], and more recently, the rail manufacturing industry [72]. The explanation put forth to explain the phenomenon says that although transformation from the parent microstructure to austenite is very rapid once the critical temperature is exceeded, full homogenization of all components residing in the steel is much slower, and that regions rich or lean in the various alloying or tramp elements can trigger faster transformations to pearlite due to constitutional supercooling or localized stresses.

Climax Molybdenum Corporation has had the opportunity to conduct extensive pearlite research, especially with respect to the effects of alloy additions and heat treatments. [71, 73-75] Their goal has usually been defined in terms of tensile strength, with rail quality categories including conventional rail with tensile strengths less than 100 ksi (690 MPa), high strength rail with strengths between 100 and

120 ksi (830 to 1030 MPa), and extra high strength rail with strengths greater than 120 ksi. Fletcher et. al. have shown that the limiting strength of traditional pearlite is approximately 100 ksi, which corresponds to pearlite interlamellar spacings of 100 nm. To obtain higher strengths and lower spacings they say that the transitional pearlite must be obtained, with transitional pearlite defined as that whose lamellae become very short and twisted with spacings in the 75 nm range. The hardness at this point would exceed 42 Rc (390 BHN). Fletcher and his associates, however, have not had the opportunity to conduct the relevant wear testing.

The advantages of pearlite have also been supported by Heller and Schweitzer [76], specifically they consider that increasing hardness improves wear resistance of pearlite and that pearlite possesses better wear resistance than either bainite or martensite.

Although the heat treatments required to obtain hardnesses greater than 35 Rc have been performed in this project, the wear testing of rollers has not. The structures obtained in the 35 to 48 Rc range are significantly different from traditional pearlite. In addition, the information generated by this program indicates that traditional pearlite cannot be obtained with interlamellar spacing less that 120 nm. It is not known, however, what method Fletcher and Pegredo et. al. used to measure pearlite spacings, and a difference of 20 nm is certainly within comparison accuracies given two separate measurement techniques. At any rate, there appears to be an initial coarsening of the carbides in the transitional region compared to the traditional pearlite. With further hardness increases, however, there is a renewed

refining of the carbides and spacings within the transitional pearlite. (Fig. 48) The first true bainite begins to appear in the 48 - 50 Rc range, though depending on one's definitions, the transitional pearlite range can be called a mix of bainite and pearlite with the lamellae shortening and losing its uniformly parallel form.

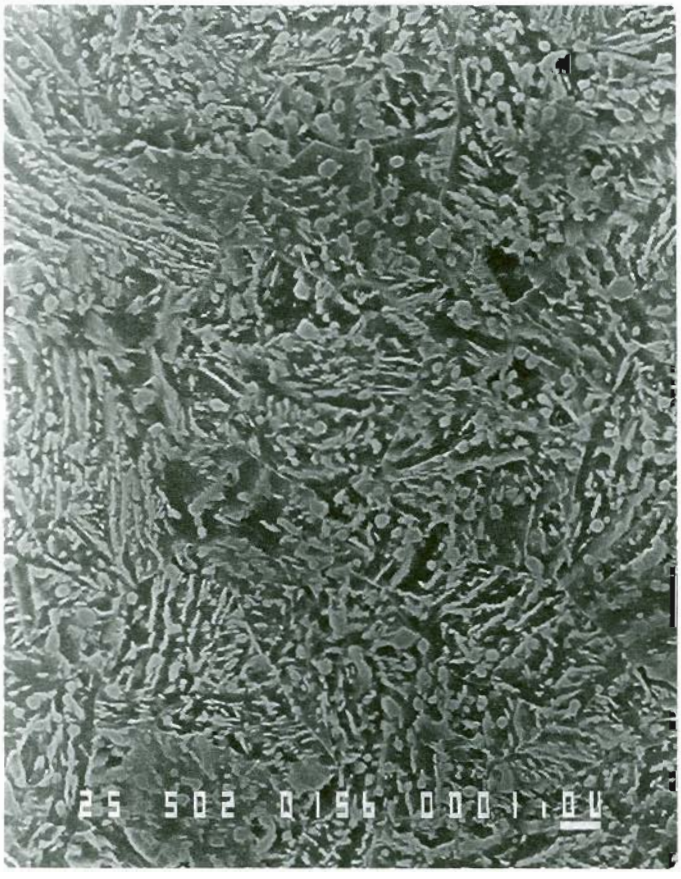

Figure 54. Transitional pearlite microstructure.

In the end, the isothermal heat treatments were successful in producing a wide variety of pearlitic microstructures. The equipment utilized, however, was somewhat restrictive in terms of heat removal capacity. Consequently, to obtain microstructures that reportedly form in the 600 to 700 °C (1110 to 1300 °F) range, it was necessary to "isothermally quench" to less than 200 °C (400 °F). This super cooling procedure provided the heat removal to produce the required transformations for the finer pearlitic spacings. In retrospect, the actual quench temperature is not critical, so long as the resultant microstructure is suitable. Consequently, the quench temperatures were adjusted according to experience with the equipment idiosyncrasies to obtain the desired microstructure regardless of the true isothermal transformation products at that temperature.

Later work in the project lead to a refinement of the heat treating process and improved control of the final microstructure. The major improvements centered around increasing salt bath agitation and surface area to volume ratios of the heat treated part. Both methods maximized the heat removal rates at the given isothermal quench within the restraints of the heat treating equipment.

The greatest disparity or anomaly in the heat treatments was the difference between the salt bath temperature and the temperature of transformation. Temperatures that according to the literature should generate martensite were used to obtain the finer spaced pearlites. This is undoubtedly due to the temperature difference between the material at transformation and the quench temperature and can be attributed to the physical capacities of the heat treating equipment.

The quench temperature is therefore irrelevant with respect to the final microstructure and only holds importance for possible future duplications of the heat treatments.

OLD STANDARD VS. NEW

In recent years rail manufacturers have been producing an Improved Standard (IS) rail. The rail is still classified as a standard carbon and uses similar chemical composition specifications to the old standard carbon, except that there are tighter tolerances on the some of the elements and about .2% Cr is added. The result is an improved rail with higher hardness and smaller interlamellar spacings. Because the rail is relatively new, actual wear performance improvements have yet to be documented.

This program used both an old and an improved standard carbon rails during the course of testing. The Amsler wear tests that enable comparison of the two standards, however, do not illustrate a decisive advantage for the IS rail. In four of the five contact pressures the old standard carbon rail actually had lower wear rates. Only at 900 N/mm^2 did the IS rail (X35) prove to be more wear resistant than the old standard carbon rail (X21). In all cases, however, the wear rates were within 20% of each other, an indication that the wear rates cannot be definitely labelled different, due to the accuracy of the Amsler wear test.

More interesting were the wear rates of the wheel rollers that were run against the two rail steels. In both cases the mating rollers were Class C wheel, with a hardness of 32 Rc (297 BHN). Also in both cases the wheel roller wore at a higher rate against the IS rail than against the old standard. This comparison is similar to the one discussed earlier with the standard carbon rail run against the two wheels. As before, wheel wear rate increases were very significant at

most contact pressures. At all contact pressures the wheel wore at least twice as quickly, and at one contact pressure 2.5 times, against IS (harder) than the softer old standard rail. While the repeatability data indicate no greater than 20% experimental variations, these wheel wear rates in all cases exceeded ten times that difference. This type of interrelated wear behavior is the type of response in a wear system that warrants reconsideration of supposedly simple solutions.

WHEEL STEEL HARDNESS EFFECTS ON RAIL WEAR RATES

It might be intuitively thought that increasing the hardness of one component in a two component system would not only reduce the wear of the harder part, but also increase the wear rate of the mating element. This position is maintained by Jamison [77] who found that increasing the hardness of either rail or wheel will increase the wear rate of the other component. All past work in this area, however, has not always supported this notion. Previous researchers [49] have found that changing the hardness of one roller in Amsler tests did not alter the behavior of the other roller.

This program, with its wide array of rail microstructures, provided an excellent opportunity to compare the effects of mating rollers. There were actually three opportunities to make this comparison. The first, of course, was to compare the wear rate of the old standard carbon rail (X21) against the two types of wheel steels, Class U (W1) and Class C (W2). This provided a means to directly compare wear rates with only one variation in the experiment, the type of wheel. The data is this case is not conclusive. Not only were the wear rates of the rail different against the two wheels, but they were higher in three of the five contact pressures against the softer wheel. In the cases where they were higher, they were less than the standard deviation of the repeatability data. When the rail wear rates were lower against the softer wheel, the differences were greater than the variance found in the repeatability data.

The two dissimilar wheels did not present such a muddled picture.

At all five contact pressures Class U wheel (W1) wore approximately twice as quickly as the Class C (W2) wheel. This comparison indicates that increasing the hardness of one component without changing the other will improve the wear properties of the hardened component. Whether or not the mating component does in fact experience an increase in wear rate, however, it cannot be proven with this data.

The second set of data available for comparison was that of Class U wheel (W1) against the standard carbon rail (X21), and the four FAST rails (X29, 30, 31, 32). This data set, too, is inconclusive. At all contact pressures there was no change in wheel wear rates until the rail reached a hardness of 34 Rc (322 BHN) where the wheel wear rate jumped almost by a factor of two. The only two rails that caused the significantly higher wheel wear rates were both CrMo.

A more complete picture can be obtained by looking at the third set of data, the wear rate of one wheel (Class C, W2) run against 2 rail steels in 14 microstructural conditions. This actually reverses the question, that is, does changing the rail hardness modify wear rates of the wheel.

There was a definite trend of increasing wheel wear rates as the rail hardness was increased. The effect was most pronounced at higher contact pressures, and decreased as the contact pressure was reduced. Contrary to the second comparison involving Class U wheel (W1), the rail that most often caused the higher wheel wear rates was the standard carbon, not the CrMo. In all three comparisons, the increase in wheel wear rates did not change as the rail hardness approached that of the wheel hardness as predicted by Rabinowicz [78]. The adhesive

wear theory predicts that increasing rail hardness will decrease the rail wear and increase the wheel wear until the two hardnesses are equal. At that point the wheel wear rate will not change with further rail hardness increases while the rail will continue to experience decreasing wear rates. In the second data set the wheel wear rate increase occurred at a rail hardness of 34 Rc (322 BHN) when the wheel itself was only 22 Rc (236 BHN). In the third comparison the wheel (hardness 32 Rc, 300 BHN) wear rate increases were continuous from the lowest hardness rail, 10 Rc (190 BHN), all the way up to the hardest rail, approximately 35 Rc (328 BHN), with no discernable anomaly when the rail hardness reached that of the wheel.

The wide variety of evidence presented in the literature and the conflicting findings in this project indicate that the effect of hardness of component on the wear rate of the other is more complex than appears at first glance. It may be necessary to design an experimental sequence that addresses the question directly using materials with greater differences than those of standard carbon and CrMo rails.

RECOMMENDATIONS FOR FUTURE WORK

Most research efforts generate as many if not more questions than they answer. This chapter is intended to address those issues that could not be resolved within the confines of this project.

The lack of precision in the final predictive relationships prompts further investigation. Is the spread in the wear data indeed attributable to the random nature of the wear process, or are limitations of the quantitative relationships related to the material properties - hardness and interlamellar spacing? The data generated in this project do not provide conclusive evidence for either case. If the limitation is due to using hardness or spacing as a basis for material wear response, another more pertinent characteristic would need to be found. On the other hand, future programs might address directly the repeatability of wear processes and the statistical nature of wear in an attempt to quantify what degree of precision can be expected for this type of material and wear system.

An accurate description of the wear rate/microstructure relationship is a second item of uncertainty. The ideal resolution would be the generation of an abundance of data, but until that data is produced, several questions remain. What is the precise nature of the curve? A linear relationship, bi-linear, or power? Is the accelerating effect on wear rate with changes in interlamellar spacing limited to pearlitic

microstructures, or can the relationship be utilized with other microstructures or even materials? Why is the relationship different for each contact pressure? Is it primarily a function of the abrasive wear and debris, or is more properly related to the material responding to varying stresses?

Another item is the question of the effect of rail hardness on the wear rates of wheels. As previously noted, a few projects have attempted to provide an answer, resulting in a wide range of conclusions. The fact that this project, despite a variety of wheel/rail combinations, also lacked conclusive evidence to support either opinion, suggests that the problem may be more complex than first appears. This leads to a program designed and conducted to specifically answer this question.

One approach to a positive resolution of the effects of chemistry would involve a test matrix that utilizes rail steels with even greater differences in chemical compositions. With more distinct chemical compositions, the effect of spacing and other microstructural parameters, for example secondary carbides, would also be more distinct.

Because this project was more concerned with steady state wear rates and test procedures and relationships, the phenomenon of the break-in or first abrasive groove received only cursory attention. But this initiation of a high wear condition is not only important from a practical viewpoint, but also interesting as basic materials science. Here, too, there is justification for a completely self contained project directed toward the elucidation of the original surface deterioration.

Finally, the performance of the old standard carbon rail with

respect to the Improved Strength standard carbon rail needs to be addressed more thoroughly. Though this project provided an opportunity to compare the two, the results were not conclusive and a more exhaustive test sequence may provide more decisive results.

CONCLUSIONS

1. The relationship between Type III sliding/rolling wear rate and pearlite interlamellar spacing of rail steels relationship are:

$$[\text{Wear Rate } (\mu g/m) = a(S_t)^b]$$

Po	a	b	r
1220	10431	0.47	0.64
1080	2138	0.70	0.73
900	788	0.80	0.67
700	7.97	1.51	0.79
500	5.51	1.33	0.81

2. The wear between rail gauge face and wheel flange is one of third body abrasion with the abrasion particles consisting of rail and wheel debris generated in previous encounters.

3. Changing the hardness of either the wheel or rail appears to affect the wear performance of both components.

4. This project produced no evidence to suggest that the wear resistance of improved standard carbon rail is superior to the old standard.

5. The Amsler wear machine provides a good simulation of wheel flange/gauge face wear at slide/roll ratios greater than 25% and contact pressures higher than 500 N/mm^2.

6. The Amsler is capable of providing reasonably accurate and reproducible wear data.

7. It is more difficult to obtain data relevant to the rail system from a pin-on-disk machine than the Amsler.

8. Direct comparison of wear data is dangerous due to the wide array of experimental variables that significantly alter the wearing system. The wear rates are extremely system dependent.

9. Heat treating steels and resultant microstructures are also very system dependent. Similar microstructures may be produced by temperatures profoundly different depending on the equipment utilized.

SUMMARY

One of the original designs of this project was the prediction of rail steel wear rates based on laboratory tests. In the strictest sense of the word, this objective was only partially realized. To say without categorization that the pearlite interlamellar spacing equations presented here can be applied without error to any operating rail system is optimistic. An argument may be made that relative wear resistances did not agree precisely with those of the FAST experiments, but neither were there magnitudes of difference [56] as is often the case with laboratory testing. Certainly the relationships might be refined with more information or even more thorough analysis of this project's data. Only future use of the relationships developed here, however, can adequately judge their accuracy.

The development of the accurate laboratory test was a matter of considering many possible alternatives and sifting through the maze of parameters and results complicating and concealing the most appropriate conditions. The test is simple enough that it can be conducted by any appropriately equipped laboratory, though the initial equipment cost is significant.

Despite the lack of wear data for steels harder than 35 Rc, much of the work to obtain that data has been completed. The ability to produce the full range of microstructures is of major consequence. It is anticipated that the work continuing will indeed provide definitive answers to these lingering questions.

Sometimes secondary or ancillary issues that are answered in the

course of investigations provide more than their share of interest. Along these lines were the matters of old versus improved standard carbon rail and the effects of increasing rail hardness on wheel wear performance. The evidence produced herein is not conclusive with regards to the first question, but the very fact that the data could not differentiate between the performance of the two standard carbon chemistries is a statement in itself. With respect to the latter issue, the procedures used in this undertaking provided strong evidence that altering one component will indeed affect the other's performance, though the precise relationship is more complex than simple hardness comparisons can define.

Finally, contributions to the assessment of third body wear mechanisms and debris have been made which hopefully will provide impetus to solve related problems and to investigate the break-in period of Type III sliding/rolling wear.

References

1. Rail Defect Manual, Sperry Rail Service, 1964.

2. The Making, Shaping and Treating of Steel, McGannon, H.E., Ed., United States Steel Corporation, 1971.

3. Heller, W., Koerfer, E., Schmedders, H., Production of Special Grade Naturally Hard Rails and Experience Gained in Operation, Proceedings of the Second International Heavy Haul Conference, Colorado Springs, Colorado, September 1982, pp. 170-177.

4. Hodgson, W.H., Yate, J.K., Preston, R.R., The Development of a Second Generation of Alloy Steel Rails for Heavy Haul Applications, Proceedings of the Second International Heavy Haul Conference, Colorado Springs, Colorado, September 1982, pp. 207-215.

5. Dearden, J., The Centenary of the Steel Rail, Railway Steel Topics, 4:1, (1957), pp. 11-24.

6. Amsler, A.J., Abnutzungsmaschine fur Metalle (A Wear Machine for Metals), Zeitschrift des Vereins Deutscher Ingenieure (Z-VDI), 66 (1922), pp. 377-378.

7. Kalousek, J., Development of a 1/8 Scale Dual Disc-on-Disc Rail/Wheel Wear Testing Facility, Canadian Metallurgical Quarterly, 21:1 (1982), pp. 67-72.

8. Clayton, P., The Relations Between Wear Behaviour and Basic Material Properties for Pearlitic Steels, Wear, 60 (1980), pp. 75-93.

9. Unpublished correspondence, Yawata Research and Development Laboratory, Kitakyushu City, 805, Japan.

10. Steele, R.K., Reiff, R.P., Rail: Its Behavior and Relationship to Total System Wear, Proceedings of the Second International Heavy Haul Conference, Colorado Springs, Colorado, 1982, pp. 115-164.

11. Welsh, N.C., Frictional Heating and Its Influence on the Wear of Steel, Journal of Applied Physics, 28:9 (1957) pp. 960-968.

12. Marcol, J., Mikulec, Z., Trends in the Patenting of Steel Wire, Wire World International, 28 (1986) pp. 22-27.

13. Sorby, H.C., On the Application of Very High Powers to the Study of the Microscopical Structure of Steel, Journal of the Iron and Steel Institute, 1, (1886), pp. 140-147.

14. Mehl, R.F., Hagel, W.C., The Austenite:Pearlite Reaction, Prog. Metal Physics., 6, (1956) pp. 74-134.

15. Puls, M.P., Kirkaldy, J.S., The Pearlite Reaction, Metallurgical Transactions, 3 (1972) pp. 2777-2796.

16. Zener, C., Kinetics of the Decomposition of Austenite, Trans. AIME, 167, (1946) pp. 550-583.

17. Shapiro, J.M., Kirkaldy, Theory of Decomposition of Eutectoids Assuming Local Equalibrium and Phase Boundary Diffusion, Acta Met., 16 (1968) pp. 579-585.

18. Brown, D, Ridley, N., Rates of Nucleation and Growth and Interlamellar Spacing of Pearlite in a Low Alloy Eutectoid Steel, Journal or the Iron and Steel Institute, Vol. 204 (1966), pp. 812-816.

19. Ridley, N., A Review of the Data on the Interlamellar Spacing of Pearlite, Met. Trans. A, Vol. 15A, June (1984), pp. 1019-1036.

20. Seetharaman, V., Trivedi, R., Eutectic Growth: Selection of Interlamellar Spacing, Metallurgical Transactions A, Vol. 19A, Dec. (1988), pp. 2955-2964.

21. Principles of Tribology, Halling, J., ed. MacMillam Press, London, 1978.

22. Suh, N.P., The Delamination Theory of Wear, Wear, 25 (1973), pp. 111-124.

23. Archard, J.F., Hirst, W., An Examination of a Mild Wear Process, Proceedings of the Royal Society A, 238 (1956), pp. 515-531.

24. Archard, J.F., Hirst, W., The Wear of Metals Under Unlubricated Conditions, Proceedings of the Royal Society A, 236, Aug. 2, (1956), pp. 397-410.

25. Kerridge, M., Lancaster, J.K., The Stages in a Process of Severe Metallic Wear, Proceedings of the Royal Society A, 236, Aug. 2, (1956), pp. 250-264.

26. Sheasby, J.S., Attainment of Debris Free Dry Wear Conditions, Wear of Materials (1981), pp. 75-81.

27. Richardson, R.C.D., The Wear of Metals by Relatively Soft Abrasives, Wear, 11 (1968), pp. 245-275.

28. Richardson, R.C.D., Wear of Metals by Hard Abrasives, Wear, 10 (1967), pp. 291-309.

29. Lanford, G., Deformation of Pearlite, Met. Trans. A, Vol. 8A, June (1977), pp. 861-875.

30. Billinghurst, P.R., Brookes, C.A., Tabor, D., The Sliding Process as a Fracture-Inducing Mechanism, Physical Basis of Yield and Fracture, pp. 253-258.

31. Rao, C.M., Kosel, T.H., An X-Ray and TEM Study of Subsurface Recovery During Abrasion, International Wear of Materials 1985, Ludema, K.C. ed. Vancouver, British Columbia, Canada, pp. 363-372.

32. Salesky, W.J., On Fundamentals of Sliding Wear in Steels, Doctorate Dissertation, University of California, Berkeley 1983.

33. Welsh, N.C., The Dry Wear of Steels Part I. The General Pattern of Behaviour, 257 (1965), pp. 31-50.

34. Welsh, N.C., The Dry Wear of Steels Part II. Interpretation and Special Features, 257 (1965), pp. 51-70.

35. Archard, J.F., Contact and Rubbing of Flat Surfaces, Journal of Applied Physics, 24:8 (1953), pp. 981-988.

36. Rosenfield, A.R., Votava, E., Hahn, G.T., Slip Induced Crack Formation in Mild Steel, Transactions of the ASM, Vol. 61 (1968) pp. 807-815.

37. Gensamer, M., Pearsall, E.B., Pellini, W.S., and Low, J.R.Jr., The Tensile Properties of Pearlite, Bainite, and Spherodite, Transactions of the American Society for Metals, 12 (1942), pp. 983-1020.

38. Pickering, F.B., Some Aspects of the Relationship Between Microstructure and Mechanical Properties, Iron and Steel, March 1965, pp. 110-117.

39. Puttick, K.E., The Structure, Deformation, and Fracture of Pearlite, Part I. Structure, Journal of the Iron and Steel Institute, 2 (1957), pp. 161-176.

40. Alexander, D.J., Bernstein, I.M., Microstructural Control of Flow and Fracture in Pearlitic Steels, Phase Transformations in Ferrous Alloys, Marder, A.R., Goldstein, J.I., eds., AIME, (1984), pp. 243-257.

41. Pickering, F.B., Garbarz, B., The Effect of Transformation Temperature and Prior Austenite Grain Size on the Pearlite Colony Size in Vanadium Treated Pearlitic Steels, Scripta Metallurgica, 21 (1987), pp. 249-253.

42. Shen, D., Friction and Wear of Eutectoid and Hypoeutectoid Steels, International Wear of Materials 1985, Ludema, K.C. ed. Vancouver, British Columbia, Canada, pp. 194-204.

43. Beagley, T.M., McEwen, I.J., Pritchard, C., Wheel/Rail Adhesion - The Influence of Railhead Debris, Wear, 33 (1975), pp. 141-152.

44. Bhattacharyya, S., Wear and Friction in Steel, Aluminum, and Magnesium Alloys. Part I. Pearlitic and Spheroidized Steels, Wear, 61 (1980), pp. 133-141.

45. Isothermal Transformation Diagrams, United States Steel Corporation, 1963, Pittsburg, Pennsylvania, U.S.A.

46. VanderVoort, G.F., Roosz, A., Measurement of the Interlamellar Spacing of Pearlite, Metallography, Vol. 17, (1984), pp. 1-7.

47. Reiff, R.P., Defect and Wear Studies on Premium and Standard Rails, Rail Experiment RME IV, Transportation Test Center Technical Note, June 1985.

48. Brooks, C.R., Heat Treatment of Ferrous Alloys, Hemisphere Publishing Corp., Washington, 1979.

49. Bolton, P.J., Clayton, P., Rolling-Sliding Wear Damage in Rail and Tyre Steels, Wear, 93 (1984), pp. 146-165.

50. Steele, R.K., A Perspectival Review of Rail Behavior at the Facility for Accelerated Service Testing, Canadian Metallurgical Quarterly, Vol. 22, (1983), pp. 353-367.

51. Krause, H., Scholten, J., Factors Influencing the Frictional and Wear Behaviour of the Wheel/Rail Systems, Proc. of the 5th International Wheelset Congress, Tokyo, October 1975, Paper 7.

52. Kalousek, J., Ghonem, H., The Effect of Lubrication and Steering on Rail/Wheel Wear and Contact Fatigue, Proc. of the Conference on the Economics and Performance of Freight Car Trucks, Montreal, Canada, October (1983), p. 45.

53. Ghonem, H., Kalousek, J., Stone, D.H., Dibble, D.W., Observations of Rail Wear on Heavy Haul Railway Lines, Proc. of the International Symposium of Contact Mechanics and Wear of Rail/Wheel Systems, Unviersity of British Columbia, Vancouver, July (1982), p. 249.

54. Unpublished correspondence, British Rail Research Laboratory.

55. Danks, D., Clayton, P., Comparison of the Wear Process for Eutectoid Rail Steels: Field and Laboratory Tests, Wear, 120 (1987) pp. 233-250.

56. Wallbridge, M.C., Dowson, D., Distribution of Wear Rate Data and a Statistical Approach to Sliding Wear Theory, Wear of Materials 1987, Ludema, K.C., editor, pp. 101-110.

57. Unpublished work, Oregon Graduate Center, Beaverton, Oregon.

58. Mutton, P.J., The Influence of Microstructure on the Wear Behaviour of Rail and Wheel Materials, Master of Applied Science Thesis, University of Melbourne, 1985.

59. Alexander, D.J., Berstein, I.M., "Microstructural Control of Flow and Fracture in Pearlitic Steels," Proc. Phase Transformations in Ferrous Alloys, eds. Mardo, A.R., Goldstein, J.I., AIME, New York 1984.

60. Kalousek, J., D.M. Fegredo, and E.E. Laufer, The Wear Resistance and Worn Metallography of Pearlite, Bainite, and Tempered Martensite Rail Steel Microstructures of High Hardness, International Wear of Materials 1985, Ludema, K.C. ed. Vancouver, British Columbia, Canada, pp. 212-231.

61. Fegredo, D.M., Pritchard, D.,A Metallographic Examination of Rollers Subjected to Wear Under Rolling Sliding Conditions, Wear, 49 (1978), pp. 67-78.

62. Fegredo, D.M., M.T. Shahata, Palmer, A., Kalousek, J., The Effect of Inclusion Type and Control on the Wear of an Alloy Rail Steel, Report MRP/PMRL 85-2(OP-J), (1985), pp. 1-9.

63. Fegredo, D.M., Kalousek, J., The Effect of Spheroidization of the Dry Wear Rates of Standard C-Mn and Cr-Mo Alloy Rail Steels, Wear of Materials 1987, pp. 121-132.

64. Fegredo, D.M., Parsons, D.E., Pollard, W.A., Ng-Yelim, J., The Development of Very Hard and Strong Premium Rails by Controlled Cooling Procedures, Canadian Metallurgical Quarterly 22:3 (1987), pp. 385-395.

65. Fegredo, D.M., Kalousek, J., The Effects of Mixed Microstructures of Wear, Contact Mechanisms and Wear of Rail/Wheel Systems II, Gladwell, G.M.L., Ghonem, H., Kalousek, J., eds., (1986), pp. 289-313.

66. Masumoto, H., Sugino, K., Hayashida, H., Development of Wear Resistant and Antishelling High Strength Rails in Japan, 1st International Heavy Haul Conference, 1978, Australia.

67. Heller, W., Schweitzer, R., Hardness, Microstructure and Wear Behavior of Steel Rails, Heavy Haul Conference, (1982), pp. 282-286.

68. Cahill, T., James, B.A.J., The Effect of Patenting Variables on the Structures and Properties of Patented Rod, Part I. Wire and Wire Products 43:2 (1968), pp. 65-71.

69. Cahill, T., James, B.A.J., The Effect of Patenting Variables on the Structures and Properties of Patented Rod, Part II. Wire and Wire Products 43:3 (1968), pp. 72-79.

70. Cahill, T., James, B.A.J., The Effect of Patenting Variables on the Structures and Properties of Patented Rod, Part III. Wire and Wire Products 43:4 (1968), pp. 82-87, 139.

71. Smith, Y. E., & Fletcher, F. B. Alloy Steels for High Strength As Rolled Rails, D. H. Stone & G. G. Knupp (Eds.), Rail Steels - Developments, Processing and Use, ASTM STP 644, 1978.

72. Gossman, A.A., Bondar, L.A., Kuznetsova, V.A., Austenite Decomposition Kenetics in Experimentaly Alloyed Rail Steel, Izvestia VUZ, 8 (1983), pp. 57-58.

73. Fletcher, F.B., Smith, Y.E., Development of High Strength Chromium Molybdenum Rail Steel with Improved Weldability, Proc. of the 1st International Heavy Haul Conference, Perth, Australia, 1978.

74. Fletcher, F.B., Smith, Y.E., Biss, V.A., Fast-Welding Chromium Molybdenum Vanadium Extra High Strength Rail Steels. Proc. of the First International Heavy Haul Conference, Perth, Australia, (1978), pp. 41-47.

75. Heller, W., & Schweitzer, R. High-Strength Pearlitic Steel Does Well in Comparative Tests of Alloy Rails. Railway Gazette International, 136;10 (1980), pp. 855-857.

76. Heller, W., Schweitzer, R., Weber, L., Modern Developments in Rail Steel Metallurgy and Production, Canadian Metallurgical Quarterly, 2:21 (1981), pp. 3-15.

77. Jamison, W. E. Wear of Steel in Combined Rolling and Sliding. ASLE Transactions, 25:1 (1980), pp. 71-78.

78. Rabinowicz, E., The Scope of the Rail and Wheel Wear Problem - An Introduction, Rail and Wheel Lubrication Symposium, Memphis, TN., December 1-2, 1981, pp. 1-10.

72. Gossman, A.A., Bondar, L.A., Kuznetsova, V.A., Austenite Decomposition Kenetics in Experimentaly Alloyed Rail Steel, Izvestia VUZ, 8 (1983), pp. 57-58.

73. Fletcher, F.B., Smith, Y.E., Development of High Strength Chromium Molybdenum Rail Steel with Improved Weldability, Proc. of the 1st International Heavy Haul Conference, Perth, Australia, 1978.

74. Fletcher, F.B., Smith, Y.E., Biss, V.A., Fast-Welding Chromium Molybdenum Vanadium Extra High Strength Rail Steels. Proc. of the First International Heavy Haul Conference, Perth, Australia, (1978), pp. 41-47.

75. Heller, W., & Schweitzer, R. High-Strength Pearlitic Steel Does Well in Comparative Tests of Alloy Rails. Railway Gazette International, 136;10 (1980), pp. 855-857.

76. Heller, W., Schweitzer, R., Weber, L., Modern Developments in Rail Steel Metallurgy and Production, Canadian Metallurgical Quarterly, 2:21 (1981), pp. 3-15.

77. Jamison, W. E. Wear of Steel in Combined Rolling and Sliding. ASLE Transactions, 25:1 (1980), pp. 71-78.

78. Rabinowicz, E., The Scope of the Rail and Wheel Wear Problem - An Introduction, Rail and Wheel Lubrication Symposium, Memphis, TN., December 1-2, 1981, pp. 1-10.

Appendix I

AS RECEIVED AND HEAT TREATED

RAIL AND WHEEL MICROSTRUCTURES

1000X

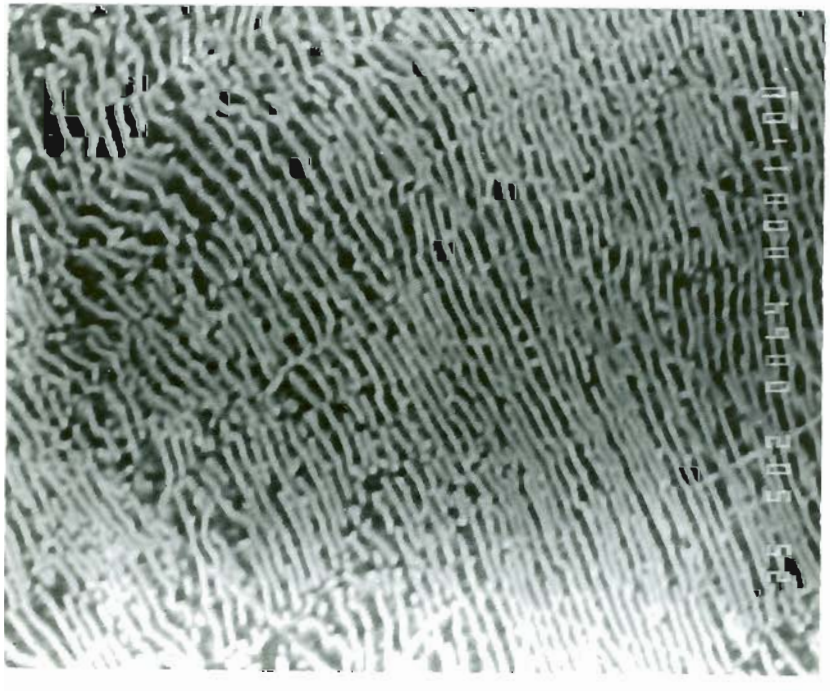

5000X

Figure 55. Microstructure of Class U wheel (W1), interlamellar spacing 214 nm.

1000X

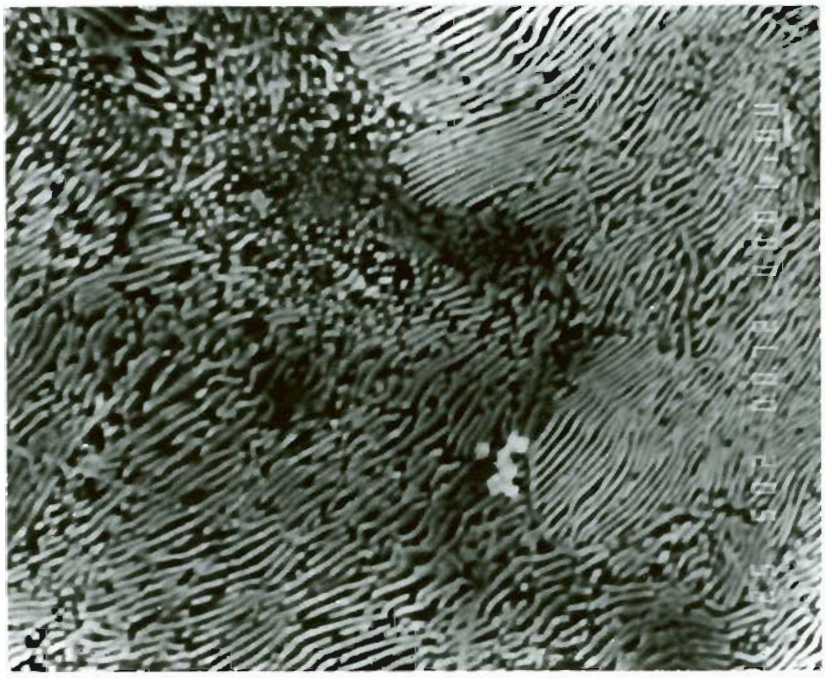

5000X

Figure 56. Microstructure of Class C wheel (W2), interlamellar spacing 162 nm.

1000X

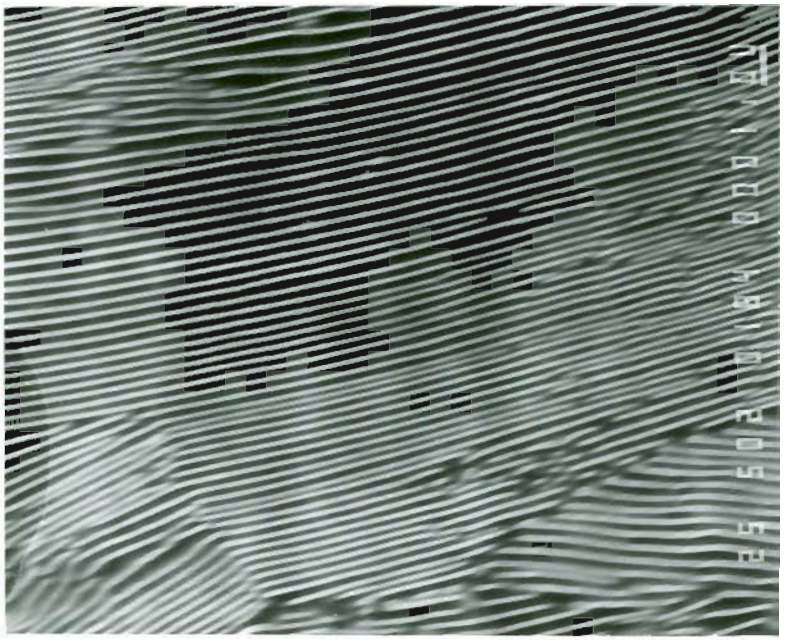

5000X

Figure 57. Microstructure of standard carbon rail from FAST, (X29), interlamellar spacing 255 nm.

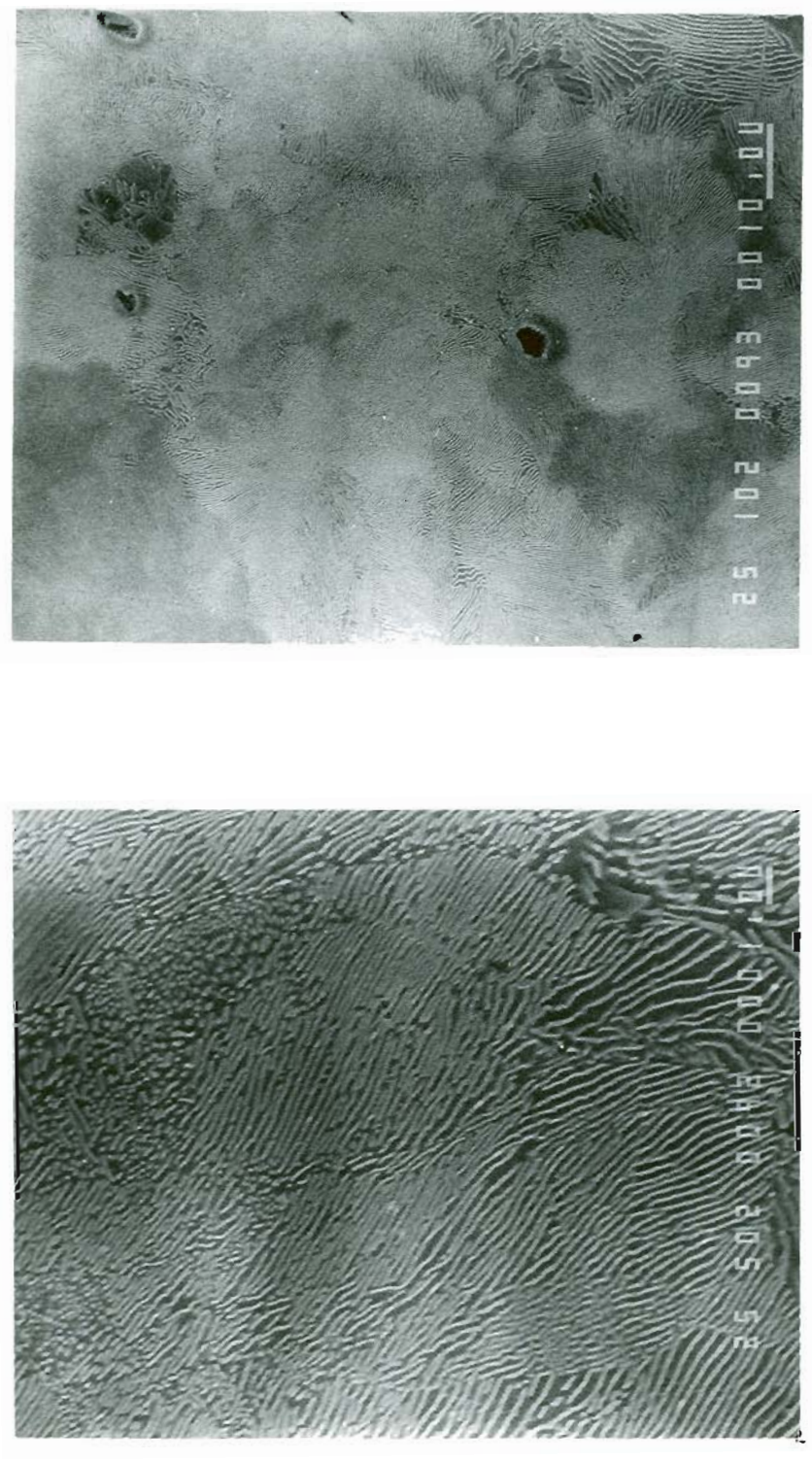

1000X

5000X

Figure 58. Microstructure of CrMnSiV FAST rail, (X30), interlamellar spacing 151 nm.

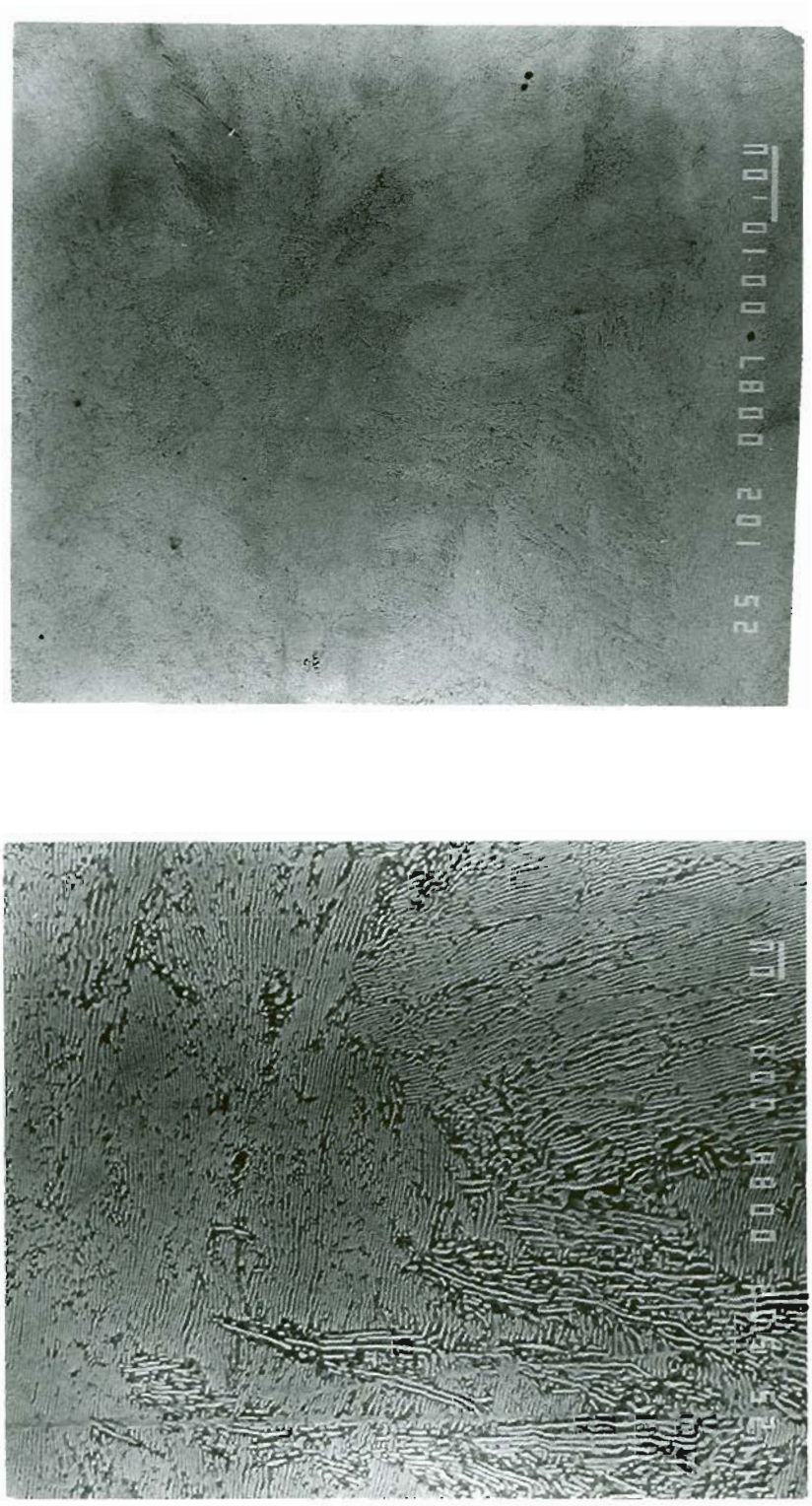

1000X

5000X

Figure 59. Microstructure of CrMo #1 FAST rail (X31), interlamellar spacing 137 nm.

1000X

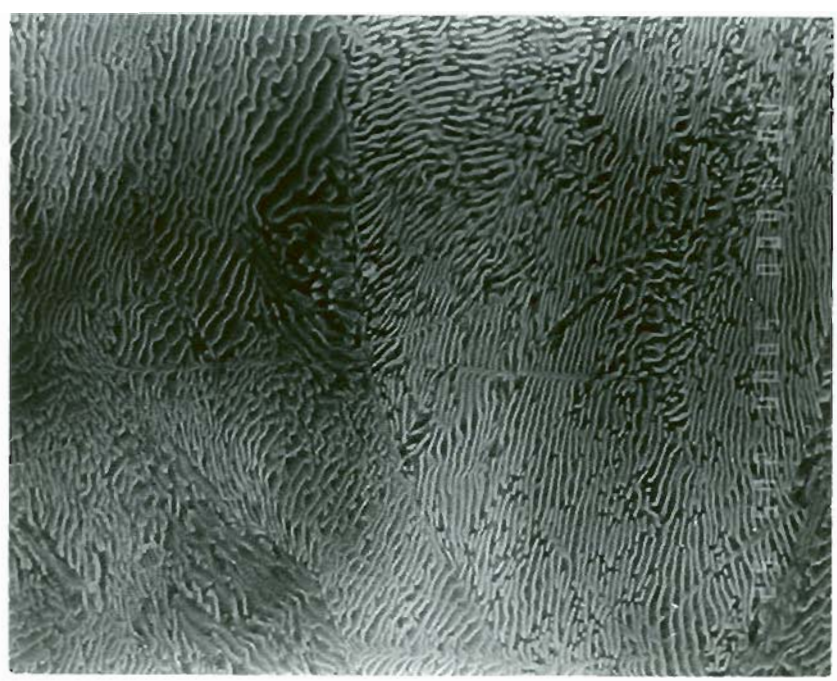

5000X

Figure 60. Microstructure of CrMo #2 FAST rail (X32), interlamellar spacing 156 nm.

1000X

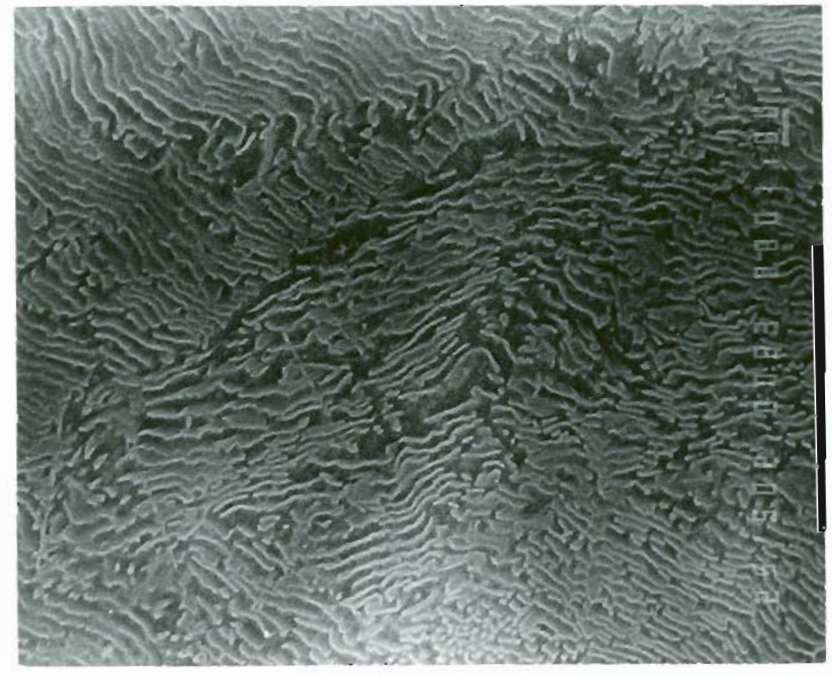

5000X

Figure 61. Microstructure of improved standard carbon rail (X35), as received, interlamellar spacing 186 nm.

1000X

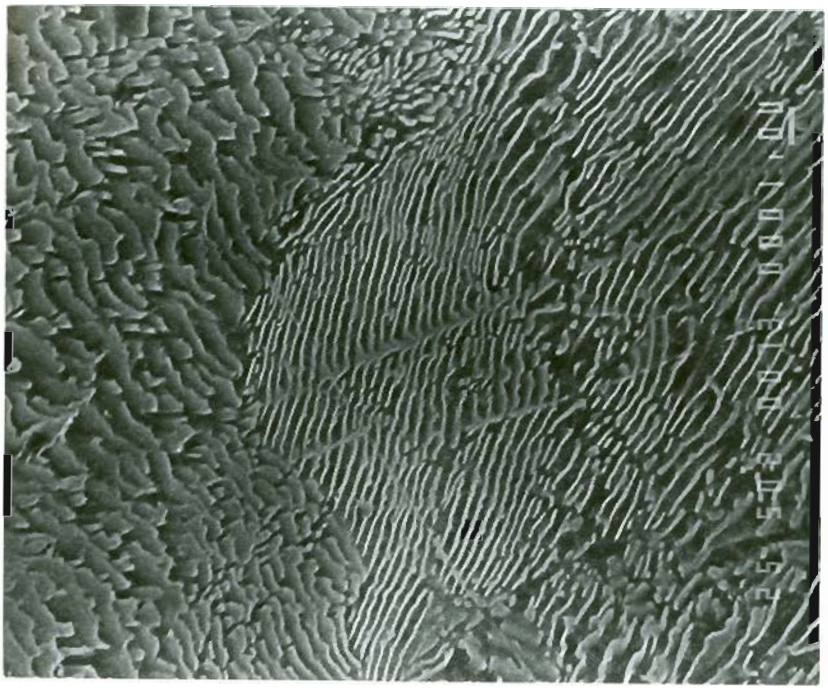

5000X

Figure 62. Microstructure of heat treated standard carbon rail, 604 °C (1120 °F) isothermal quench (A3), interlamellar spacing 216 nm.

1000X

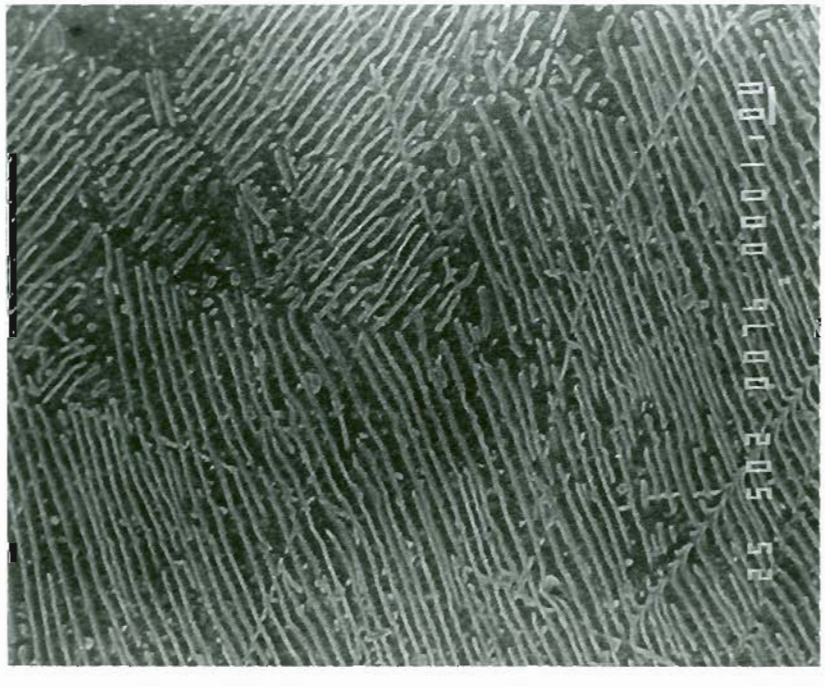

5000X

Figure 63. Microstructure of heat treated standard carbon rail, 626 °C (1158° F) isothermal quench (A4), interlamellar spacing 220 nm.

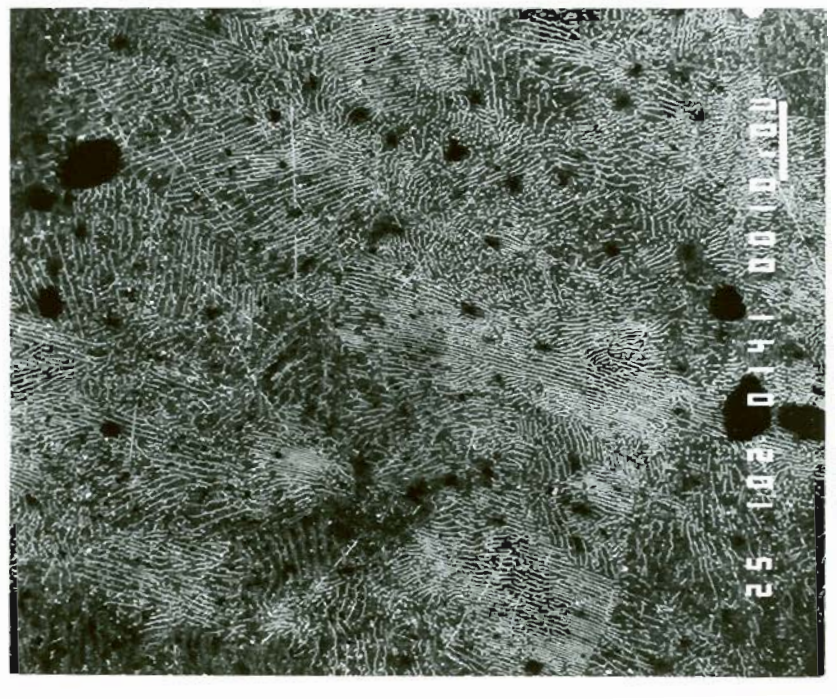

1000X

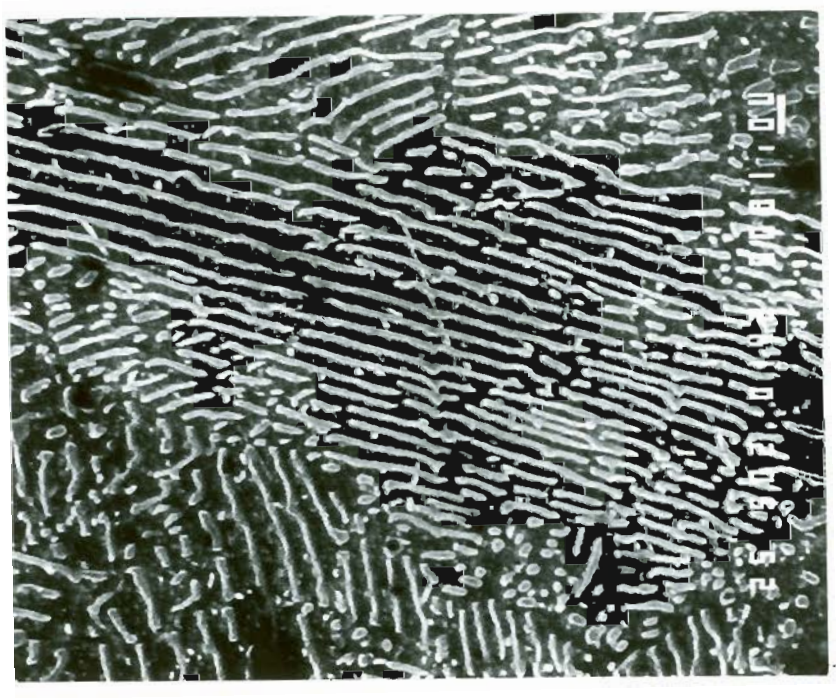

5000X

Figure 64. Microstructure of heat treated standard carbon rail, 669 °C (1237 °F) isothermal quench (A5), interlamellar spacing 452 nm.

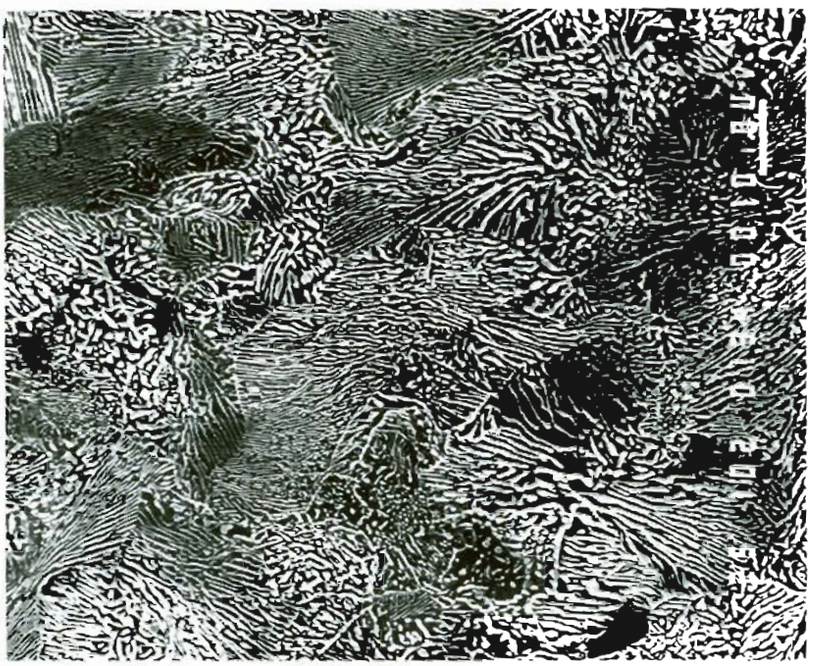

1000X

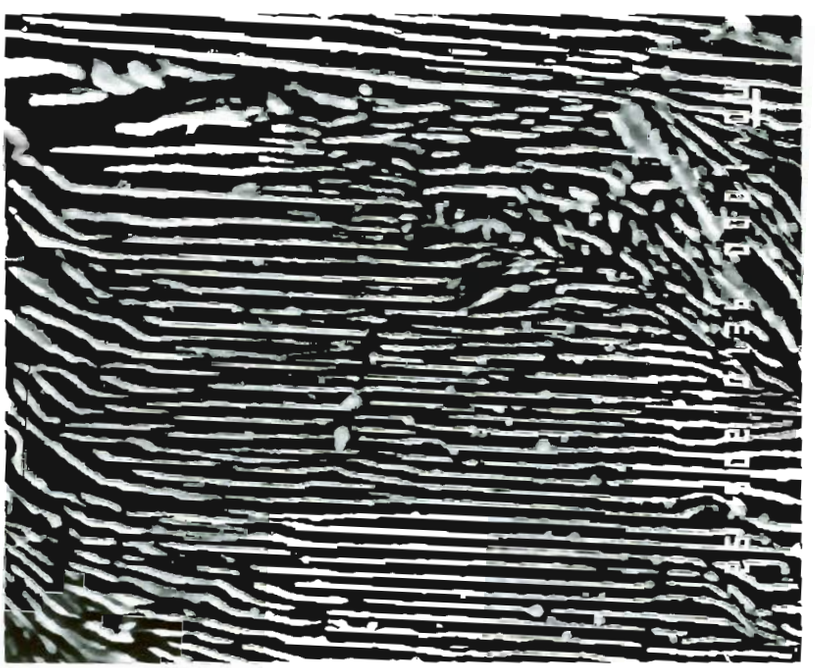

5000X

Figure 65. Microstructure of heat treated standard carbon rail, 655°C (1211 °F) isothermal quench (A6), interlamellar spacing 352 nm.

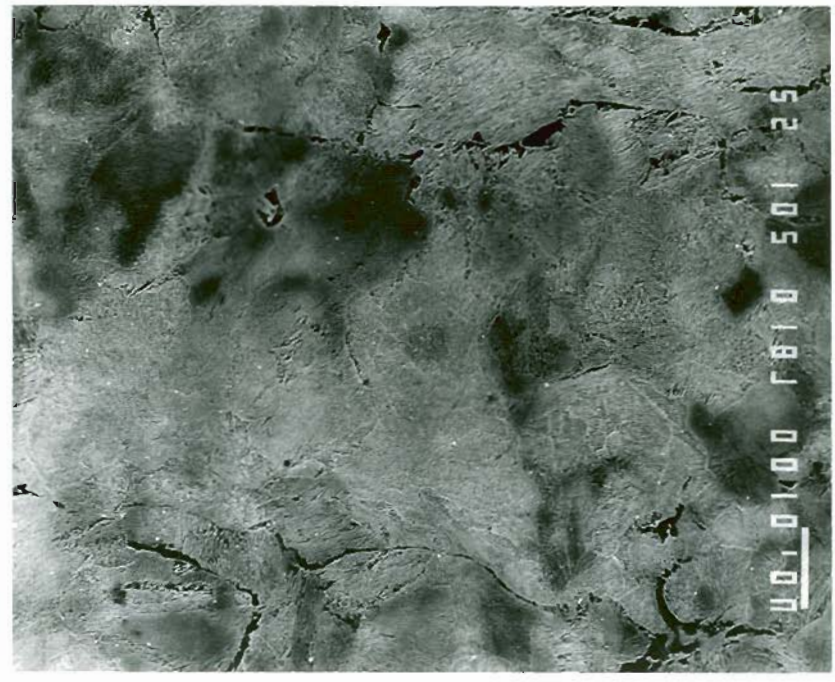

1000X

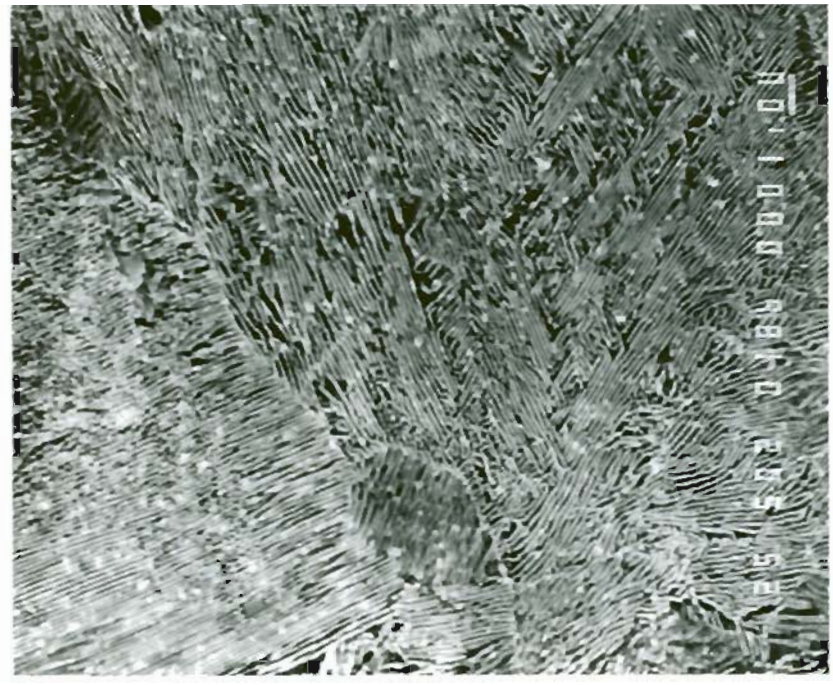

5000X

Figure 66. Microstructure of heat treated standard carbon rail, 196°C (385 °F) isothermal quench (A7), interlamellar spacing 118 nm.

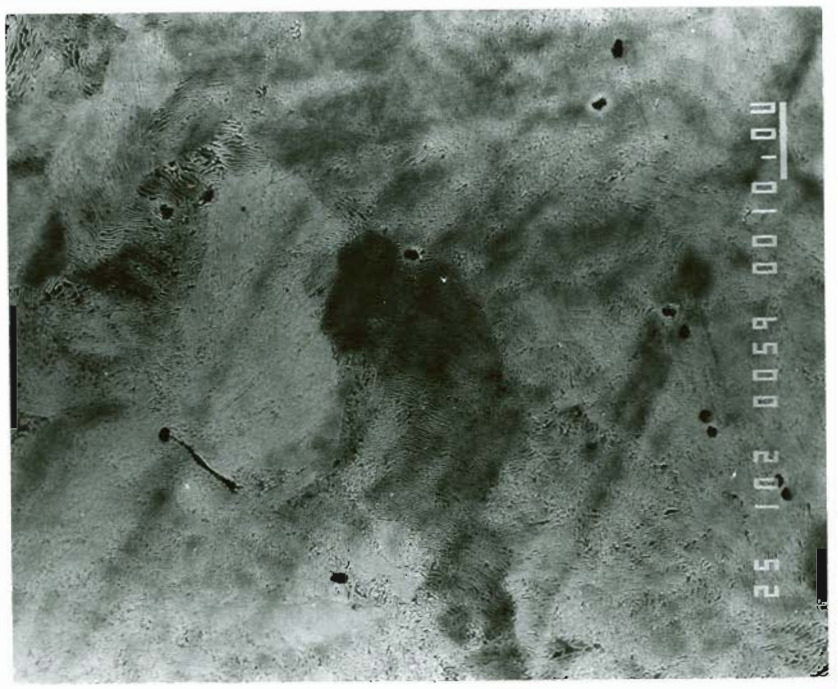

1000X

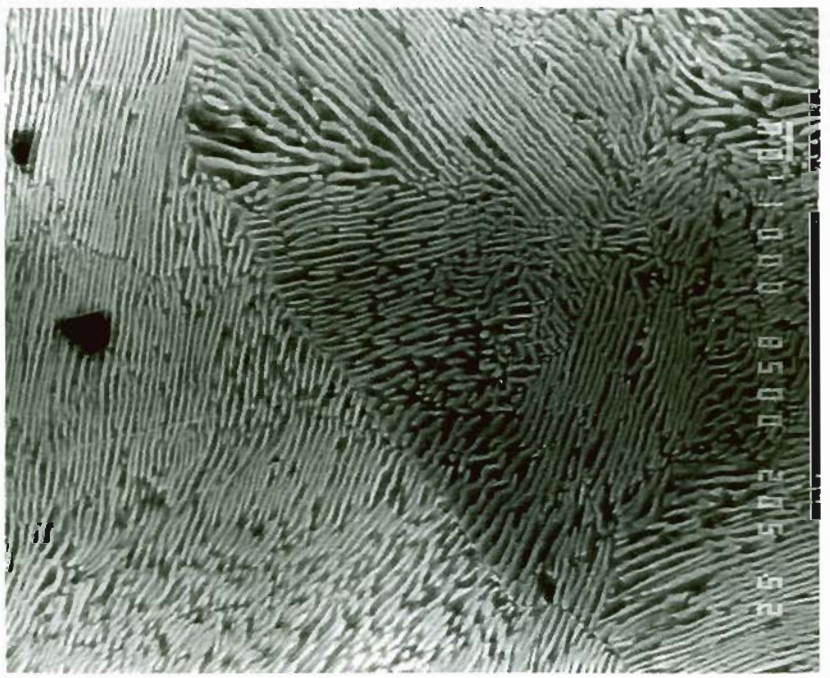

5000X

Figure 67. Microstructure of CrMo rail (X34) as received, interlamellar spacing 166 nm.

1000X

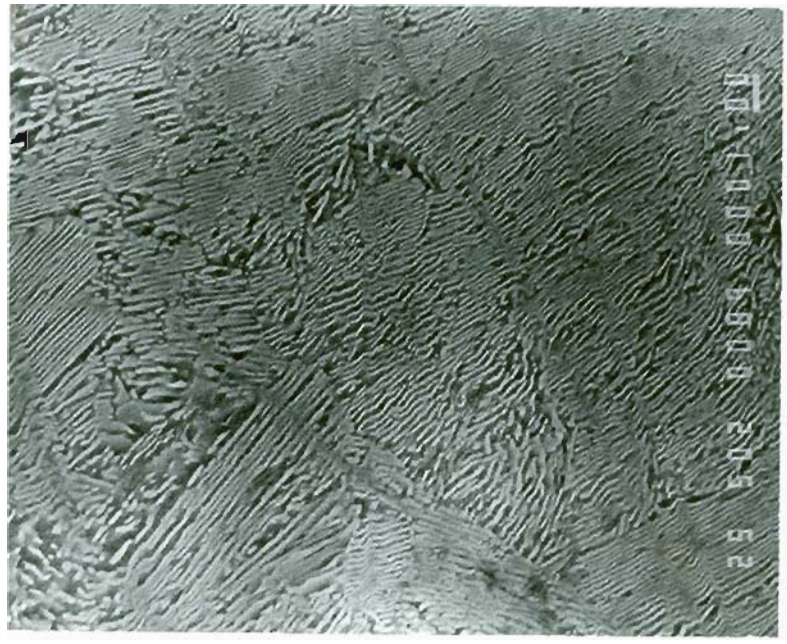

5000X

Figure 68. Microstructure of heat treated CrMo rail, 485 °C (905 °F) isothermal quench (B1), interlamellar spacing 135 nm.

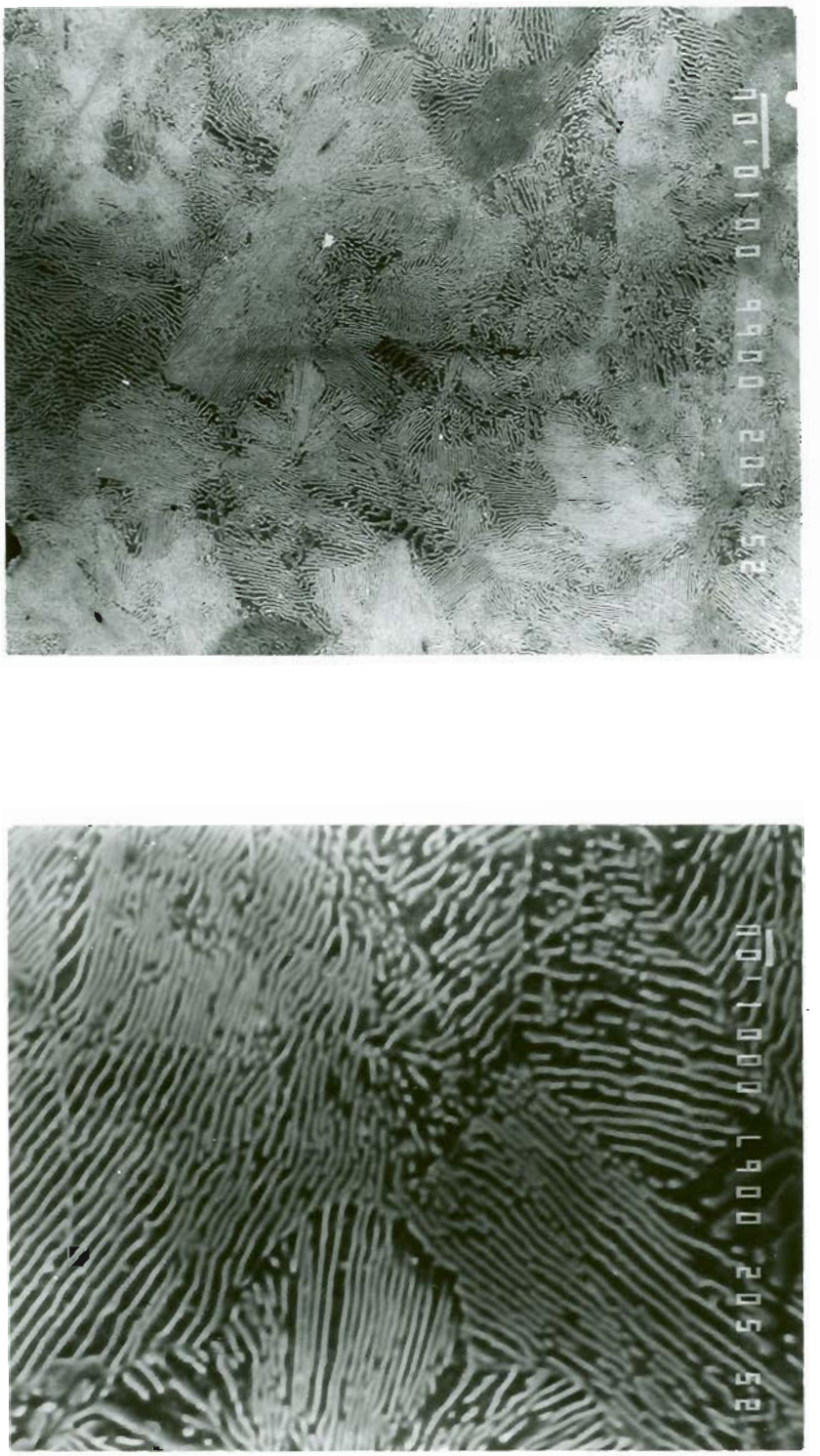

1000X

5000X

Figure 69. Microstructure of heat treated CrMo rail, 597 °C (1106 °F) isothermal quench (B3), interlamellar spacing 171 nm.

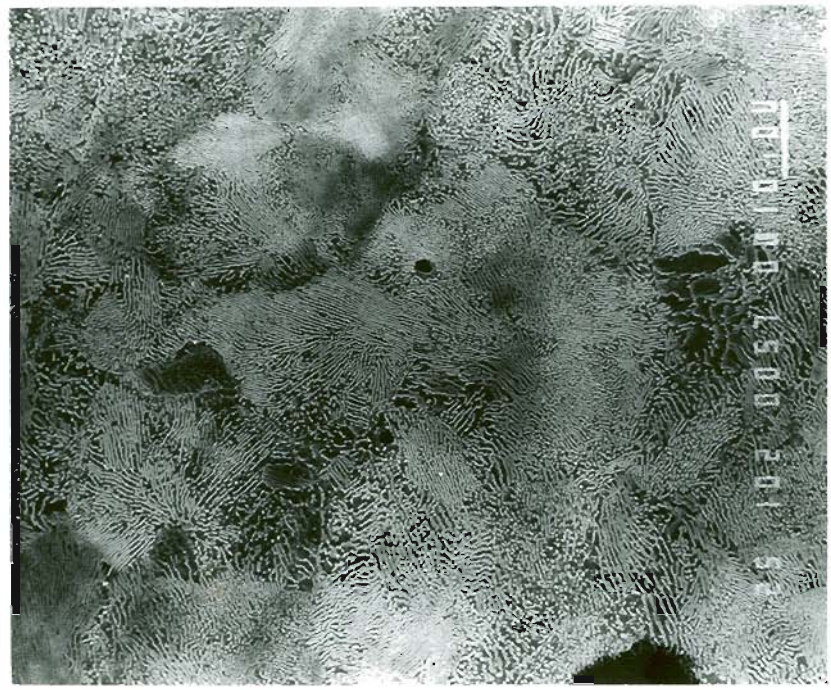

1000X

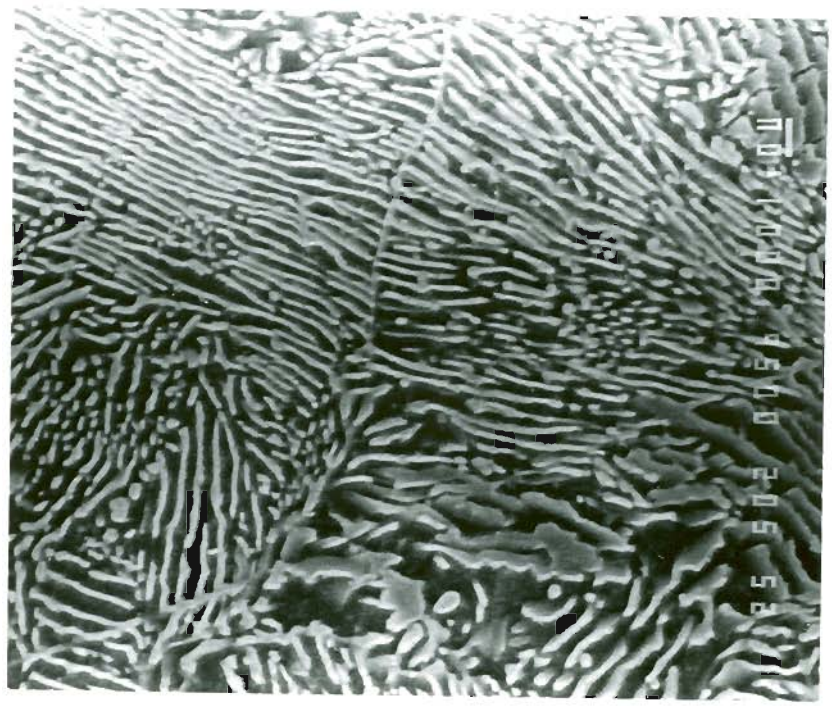

5000X

Figure 70. Microstructure of heat treated CrMo rail, 659 °C (1218 °F) isothermal quench (B4), interlamellar spacing 231 nm.

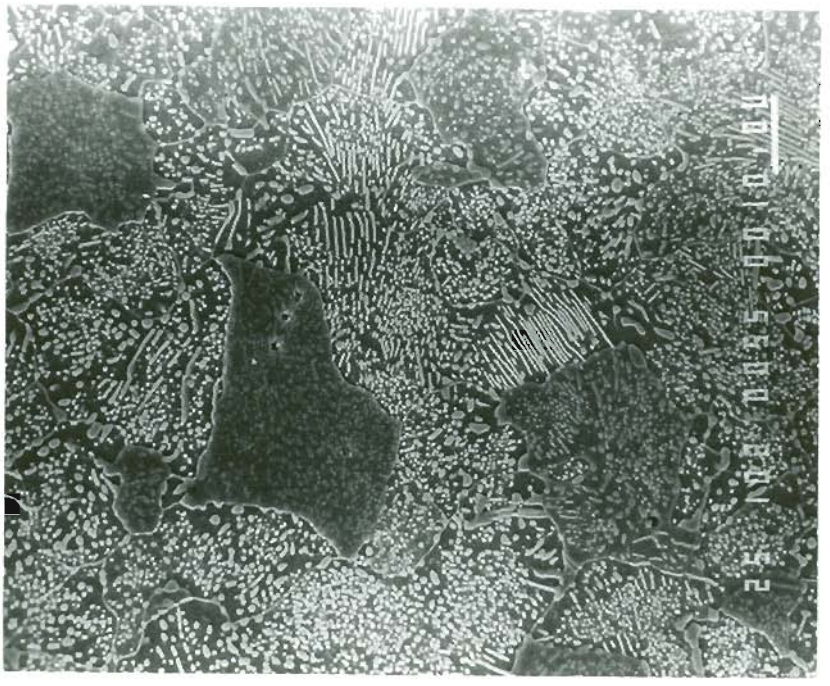

1000X

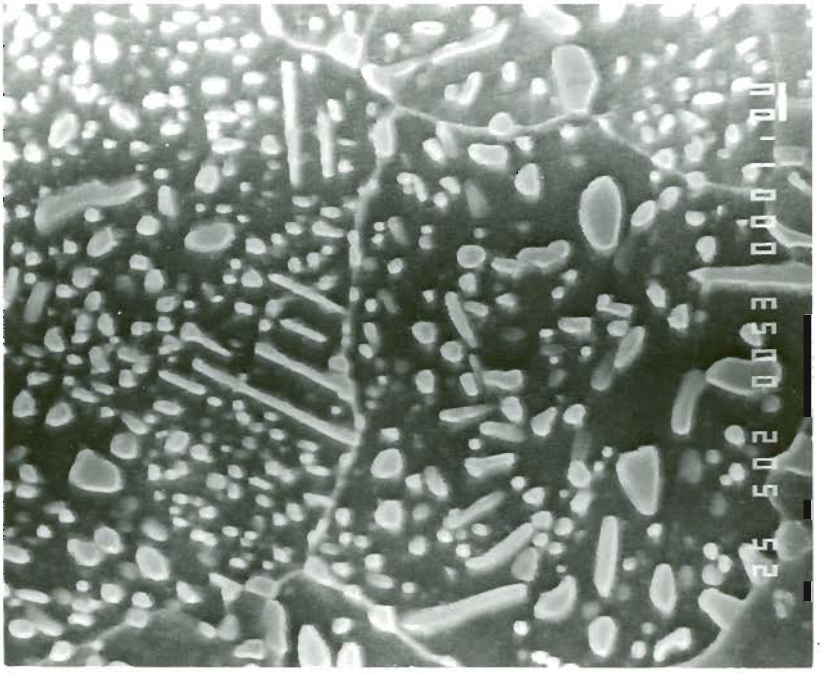

5000X

Figure 71. Microstructure of heat treated CrMo rail, 715 °C (1319 °F) isothermal quench (B5), interlamellar spacing 391 nm.

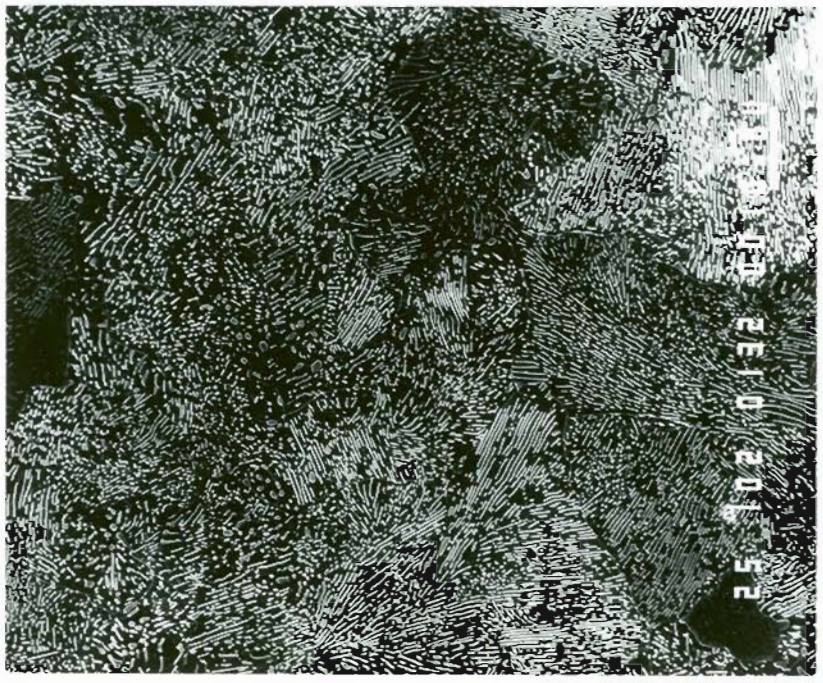

1000X

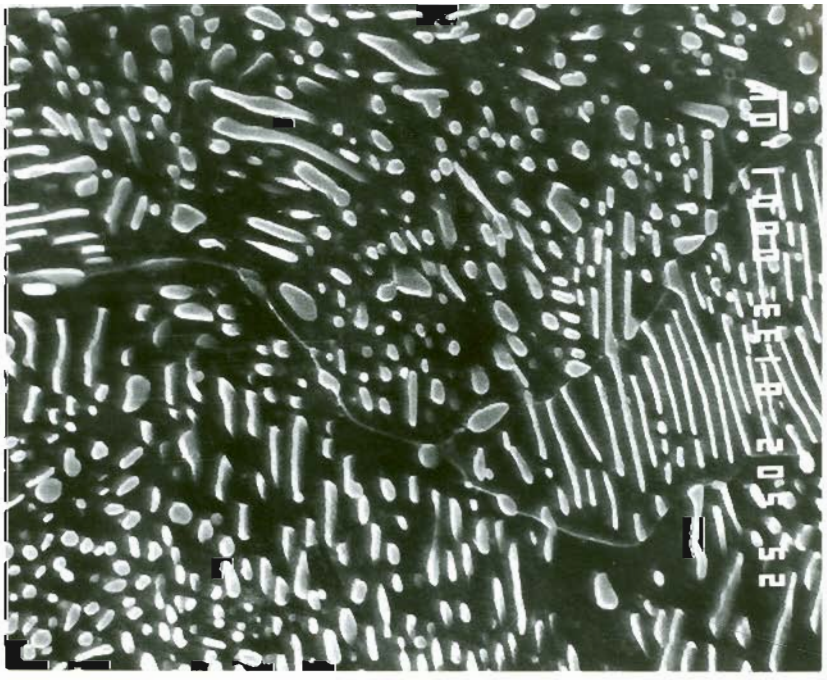

5000X

Figure 72. Microstructure of heat treated standard carbon rail, 704 °C (1300 °F) isothermal quench (B6), interlamellar spacing 472 nm.

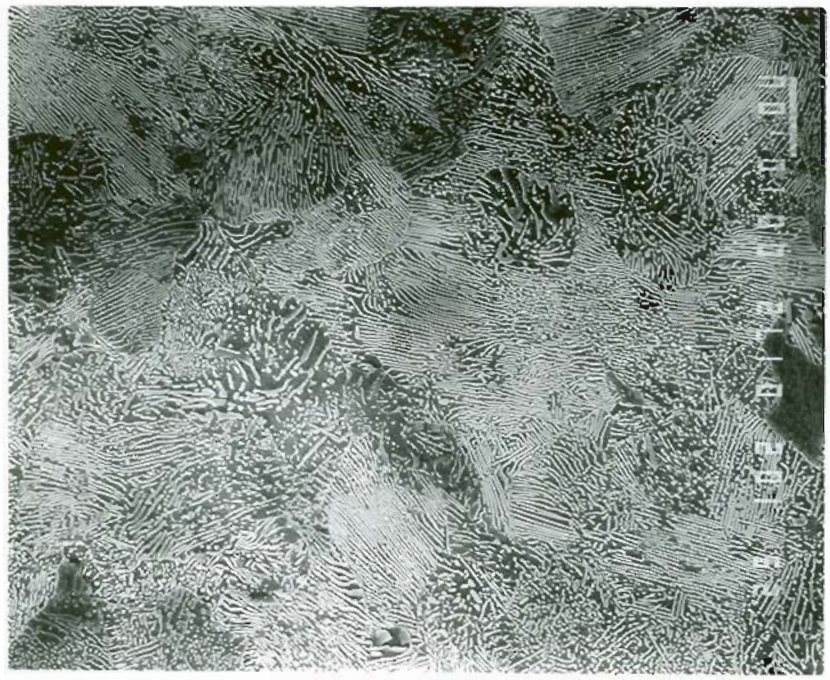

1000X

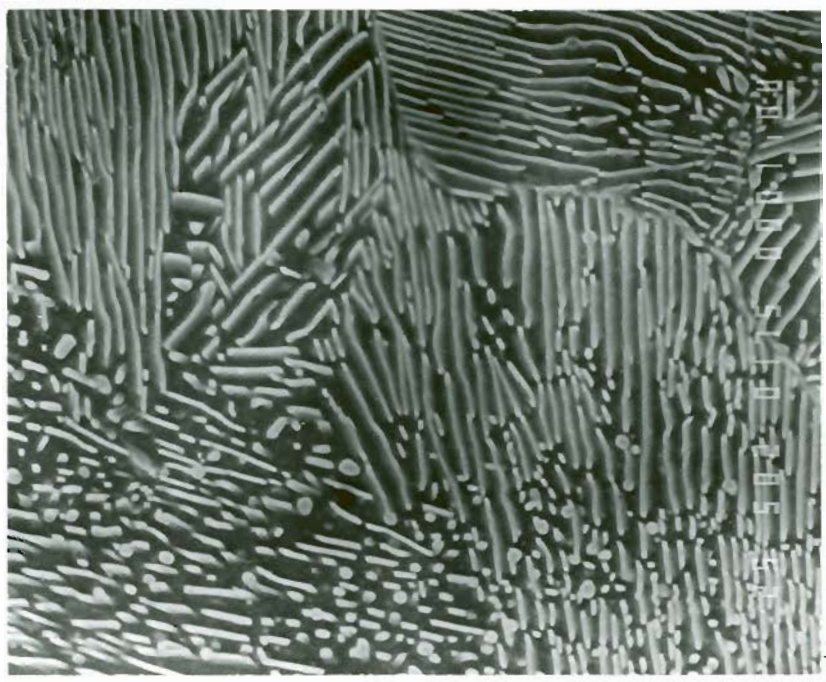

5000X

Figure 73. Microstructure of heat treated standard carbon rail, 650 °C (1202 °F) isothermal quench (B7), interlamellar spacing 315 nm.

Appendix II

GLOSSARY OF TERMS AND SYMBOLS

Amsler: a twin disk wear and lubrication test machine

bainite: a metastable steel microstructure consisting of ferrite and cementite transformed from austenite at temperatures below the pearlite range but above the martensite start (Ms) temperature

BHN: Brinell hardness number

cementite: a hard intermetallic compound of iron and carbon, designated Fe_3C

consist: all the vehicles that make up an operating train

CrMo: Chromium Molybdenum rail

eutectoid: an alloy of two or more solids formed from a solid solution

ferrite: a solid solution of iron and carbon

FAST: Facility for Accelerated Service Testing, a 5 mile loop of test track located at the Transportation Test Center in Pueblo, Colorado

gauge face: inside verical edge of a rail

δ: slide roll ratio

in/MGT: inches of rail profile, either running surface or gauge face, loss per accumulated Million Gross Ton of traffic

interlamellar spacing: mean distance between the iron carbide plates in a pearlitic microstructure

IS: Improved Strength standard carbon rail

OM: Optical Microscopy

pearlite: iron and steel composite in the form of ferrite and iron carbide plates

Po: Contact pressure in N/mm^2

Rc: Rockwell hardness value, C scale

running surface: top horizontal surface of rail

S: mean interlamellar spacing of carbide plates in pearlite

precision cross sectioning: cross sectioning of a specimen through a precise location or feature

SEM: Scanning Electron Microscopy

snap gauge: a device used to measure rail profile

Std C: standard carbon rail

TEM: Transmission Electron Microscopy

Type I: wear mechanism type produced in an Amsler wear test characterized by an oxidative surface, relative low wear rates, originally defined by Bolton and Clayton [8]

Type II: wear mechanism type, characterized by a rippled surface and metallic debris, intermediate wear rates, orginally defined by Bolton and Clayton, [8]

Type III: type of wear mechanism, defined as third body abrasive wear, high wear rates, originally defined by Bolton and Clayton [8]

WR or W: Wear rate

wheel flange: the outside vertical face of the wheel extending beyond the running surface

Vita

Dan was born in Sheboygan, Wisconsin on August 9, 1954. He was raised in Springfield, Illinois. He served in the U.S. Navy nuclear submarine forces for six years before attending California Polytechnic State University in San Luis Obispo. After receiving his B.S. in Metallurgical Engineering, he attended the Oregon Graduate Center in Beaverton, Oregon.